

HOLOCENE HISTORY OF SEDIMENT DEPOSITION AND
STRATIGRAPHY ON THE HANAIEI COASTAL PLAIN,
KAUAI, HAWAII

A THESIS SUBMITTED TO THE GRADUATE DIVISION OF THE UNIVERSITY
OF HAWAII IN PARTIAL FULFILLMENT OF THE
REQUIREMENTS FOR THE DEGREE OF

MASTER OF SCIENCE
IN
GEOLOGY AND GEOPHYSICS
MAY 1996

By

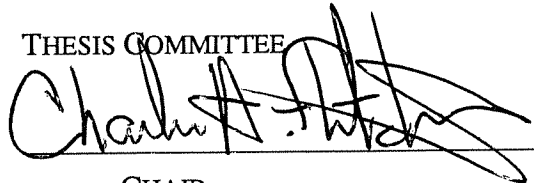
R. Scott Calhoun

Thesis Committee:

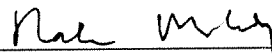
Charles Fletcher, Chair
Ralph Moberly
Craig Glenn
Ross Sutherland

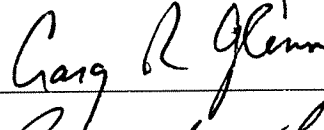
We certify that we have read this thesis and that, in our opinion, it is satisfactory in scope and quality as a thesis for the degree of Master of Science in Geology and Geophysics.

THESIS COMMITTEE



CHAIR







ACKNOWLEDGEMENTS

I would like to thank Troy Rosenbush, Alex Ress, Doug Neal, and Eric Grossman for their help and suggestions in the field; Bruce Richmond, Tony Jones, Clark Sherman, Floyd McCoy, and Rob Mullane for their discussions and insights; Gary McMurtry and Max Cremer for their assistance in measuring the lead-210 and cesium-137 radioactivity levels; and the landowners and farmers around the town of Hanalei who permitted me to core on their land and who continue to wave as they drive by. A special thanks to my advisor Chip Fletcher for his suggestions on my fieldwork and his guidance when it came time to write.

My research was supported by grants from the State of Hawaii Department of Land and Natural Resources (DLNR-POC92119), National Science Foundation (EAR-9317328), and the U.S. Geological Survey (No. 1434-94-A-1029).

ABSTRACT

Fluvial, marine, and mixed fluvial-marine sediment deposition on the Hanalei coastal plain on the north shore of Kauai, Hawaii records a middle- to late-Holocene regression. Approximately 4000 yr. B.P., the present Hanalei coastal plain was largely covered by a shallow marine bay. Fourteen radiocarbon dates from the regressive boundary in 67 gouge auger cores show a seaward progradation of the shoreline from 4800 - 4580 cal. yr. B.P. to at least 2160 - 1940 cal. yr. B.P. and probably later. During regression, marine sands were stranded as beach accretion ridges, and then buried by fluvial floodplain sand and mud. River channel scouring locally eroded the surface of the marine lithosome, exposed older marine sands, and created a stratigraphic disconformity at the contact of fluvial and marine sediments. Elsewhere, mixed basalt and carbonate sand deposition records past positions of the marine-influenced Hanalei River channel.

Long-term sediment accumulation rates of fluvial sediments were calculated using regressive boundary radiocarbon dates, while lead-210 and cesium-137 were used to calculate short-term sedimentation rates. Rates derived from lead and carbon closely agree, ranging from 2.32 ± 0.77 mm/yr to 0.94 ± 0.12 mm/yr and from 2.91 ± 0.15 mm/yr to 0.14 ± 0.03 mm/yr, respectively ($\pm = 1$ standard deviation). Sedimentation rates using cesium-137 were approximately an order of magnitude greater, ranging between 26.1 ± 2.9 mm/yr and 15.1 ± 0.5 mm/yr. The disparity between the cesium-based rates and the lead and radiocarbon rates is probably due to downward migration of cesium-137 in near surface sediments.

Numerous researchers have interpreted elevated marine deposits throughout the Pacific and Indian Oceans as evidence of relative sea-level highstands. The coastal plain at Hanalei Bay is an example of such evidence. Additionally, since abundant marine production cannot have solely caused the described beach progradation, the regression on

the Hanalei coastal plain is best explained by sea-level fall from a middle- to late-Holocene relative highstand predicted by geophysical models of whole Earth lithospheric deformation related to deglaciation.

TABLE OF CONTENTS

ACKNOWLEDGEMENTS.....	iii
ABSTRACT.....	iv
INTRODUCTION.....	1
CHAPTER 1: REVIEW OF DATING TECHNIQUES.....	3
CARBON-14.....	3
LEAD-210.....	9
CESIUM-137.....	12
CHAPTER 2: COASTAL CARBONATE DEPOSITS.....	16
BACKGROUND.....	17
CAUSES OF SEA-LEVEL VARIATION.....	19
<i>Climate Change and Rapid Ice Sheet Decay</i>	19
<i>Geoidal Migration</i>	21
<i>Hydroisostasy</i>	22
<i>Tectonism and Lithospheric Flexure</i>	22
<i>Storms and Tsunamis</i>	24
MARINE CARBONATES AS EVIDENCE.....	25
Pacific Ocean.....	25
<i>Marshall Islands</i>	25
<i>Hawaii</i>	25
<i>French Polynesia</i>	27
<i>Cook Islands</i>	27
<i>Western Samoa</i>	28
<i>Tonga</i>	28
<i>Fiji</i>	28
<i>New Caledonia</i>	29
<i>Mariana Islands</i>	29
Indian Ocean.....	30
<i>Cocos Keeling Islands</i>	30
<i>Thai Peninsula</i>	30
CONCLUSION.....	30
CHAPTER 3: HOLOCENE HISTORY OF SEDIMENT DEPOSITION AND STRATIGRAPHY ON THE HANAIEI COASTAL PLAIN, KAUAI, HAWAII.....	32
GEOLOGIC SETTING.....	32
<i>Topography</i>	32
<i>Tectonics</i>	34
METHODS.....	35
DESCRIPTION.....	41
<i>Core Descriptions</i>	42
<i>Noncored Regions</i>	45
<i>Regressive Overlap Boundary</i>	45

<i>Rates of Sediment Deposition</i>	46
DISCUSSION.....	49
<i>Sediment Accumulation Rates</i>	49
<i>Sedimentation Rates</i>	53
<i>Paleoshorelines</i>	58
4000 yr.....	61
3000 yr.....	62
2000 yr.....	62
<i>Terrigenous and Marine Lithosomes</i>	63
<i>Barrier Reef Complex</i>	64
<i>Hanalei River Meander</i>	65
<i>Age Anomalies</i>	67
<i>Region Dominated by the Hanalei River</i>	68
<i>Sea-Level Highstand</i>	68
<i>Sediment Production</i>	72
CONCLUSION.....	74
Appendix A: Map of labelled cores on Hanalei coastal plain used in this research....	76
Appendix B: Bearings from core sites to reference points.....	77
Appendix C: Stratigraphic columns of cores taken from Hanalei coastal plain.....	85
REFERENCES.....	154

LIST OF TABLES

TABLE 1 - Radiocarbon dates and sediment accumulation rates.....39

LIST OF FIGURES

Figure 1 - Uranium-238 decay series.....	10
Figure 2 - Location map of the Hawaii Islands, the island of Kauai, and the Hanalei coastal plain.....	33
Figure 3 - Facies underlying surface fluvial deposits on the Hanalei coastal plain.....	37
Figure 4 - Four cores showing typical stratigraphy found on the Hanalei coastal plain.....	43
Figure 5 - Sediment accumulation rate map.....	48
Figure 6 - Cesium and lead radioactivity profiles of three short cores.....	50
Figure 7a - Fluvial sediment thickness map.....	51
Figure 7b - Elevation of surface of marine and fluvialmarine facies.....	51
Figure 8 - Isochrons of top of the marine lithosome.....	54
Figure 9 - 4000 yr. paleoshoreline.....	55
Figure 10 - 3000 yr. paleoshoreline.....	56
Figure 11 - 2000 yr. paleoshoreline.....	60
Figure 12 - Fence diagram of the stratigraphy inside the large meander of the Hanalei River.....	66
Figure 13 - Subfacies profiles of Hanalei coastal plain.....	70
Figure 14 - Plot of age and elevation of carbonate sands found on the Hanalei coastal plain.....	71

INTRODUCTION

Numerous studies around the world have documented geologic indicators recording past sea-levels that differ from the modern level (Pirazzoli, 1991). Recently, geophysical models (Nakada, 1986; Lambeck, 1990; Mitrovica and Peltier, 1991; Tushingham and Peltier, 1991) have begun to explain these diverse data found on many oceanic islands. Far from the direct influence of melting continental ice sheets and the associated crustal instability, tectonically stable islands appeared to be good candidates for recording eustatic sea-level changes following the last glacial maximum. However, the various timings and magnitudes of sea-level indicators studied on several seemingly stable islands demonstrated that finding a single eustatic sea-level history for the post-glacial and Holocene period would not be as easy as once believed (Kidson, 1982).

Researchers are now documenting local relative sea-levels and comparing them to the predictions of the geophysical models and relative sea-levels from other islands both near and far. On the subtropical high volcanic Hawaiian islands, sea-level indicators are relatively common; however, interpreting their causes and significance is problematic. On Oahu, Easton and Olson (1976) disagreed with Stearns (1935) when they concluded that no middle to late-Holocene highstand of the sea occurred in Hawaii. Bryan and Stephens (1993) also broke with Stearns (1977) and interpreted a pronounced bench around Hanauma Bay in terms of modern processes requiring no sea-level highstand. Researchers on Oahu (Athens and Ward, 1991) and the neighboring island of Kauai (Masumoto *et al.*, 1988; Jones, 1992) have interpreted marine stratigraphic layers as evidence of a middle- to late-Holocene relative sea-level highstand.

To test the geophysical models' predictions of a sea-level highstand in Hawaii, an investigation of the middle- to late-Holocene history of the Hanalei coastal plain was conducted. This coincides with the location and timing of Jones' conclusions. To

accomplish this, several different approaches were explored. Subsurface facies and facies contact analysis and radioisotope dating were the primary means of inquiry. Surface soil analysis and descriptions and a review of similar environments within and around the Pacific Basin completed the investigation.

CHAPTER 1: REVIEW OF DATING TECHNIQUES

The dating of geological formations is fundamental to understanding geologic history whether the dating technique is relative or absolute. Techniques such as stratigraphic position and amino-acid analysis are relative and can only show whether one formation is older or younger than another. Radioisotope techniques using such isotopes as uranium-238, thorium-230 and potassium/argon-40 will give an absolute age in terms of years before present; however, absolute dating techniques do have limitations. Since an individual isotope is useful for dating a limited range of ages, specific geochronologic questions are answerable through the use of only a few isotopic clocks. Additionally, a geologic formation is unlikely to contain more than a few datable isotopes. Even when the formation is the right age to date with an isotope it contains, there are assumptions made in dating procedures that must be understood before the resulting data may be properly interpreted.

Carbon-14, lead-210, and cesium-137 are particularly useful isotopes for dating young sediments. All three have relatively short isotopic half-lives and are reasonably common in certain types of comparatively recently deposited sediments. As outlined below, they all yield absolute dates, but, to properly interpret their intrinsic meaning, a researcher must understand their formation and deposition.

CARBON-14

The dating of organic material using carbon-14 has become a tremendously useful tool in many different scientific disciplines. Quaternary geologists commonly use it to determine when a specific layer of sediment was deposited; although because the radioactivity measured in radiocarbon dating cannot be reliably measured in material

older than 25,000 to 30,000 years, the technique is limited in its geologic application to recent Earth history. Even in younger samples, it has other limitations that must be understood before its full use can be realized in dating organic material.

The carbon atom is typically made up of six protons, six electrons, and six neutrons. The protons and neutrons give carbon an atomic weight of 12 (carbon-12 or ^{12}C). A carbon atom may have seven (^{13}C) or eight (^{14}C) neutrons. Carbon-14 is the only one of the three isotopes that is radioactive. Although all three carbon isotopes are found naturally on Earth, ^{12}C is by far the most common, comprising 98.9% of all carbon on Earth, followed by ^{13}C at 1.1%, and ^{14}C with only $1.18 \times 10^{-10}\%$ (Olsson, 1968).

Radiocarbon is continuously being produced in Earth's upper atmosphere by high energy subatomic particles that bombard Earth from space. Most of these subatomic particles are absorbed in the upper atmosphere, but some reach Earth's surface and add to the natural background radiation. The amount of cosmic radiation reaching Earth's atmosphere varies, owing to fluctuations in the radiation's sources and to the variations in the magnetic fields of the Sun and Earth. When the magnetic fields are strong, fewer cosmic rays reach the atmosphere than when the magnetic fields are weak (Bradley, 1985). Nitrogen-14 in the upper atmosphere may absorb incoming cosmic particles. When struck by an energetic neutron one proton is knocked out of the nitrogen-14 nucleus and replaced by a neutron. The resulting carbon atom contains 6 protons and 8 neutrons (^{14}C) (Lowe and Walker, 1984). This radioactive isotope will eventually decay by beta transformation producing a nitrogen-14 atom and a free electron.

Chemically, radiocarbon reacts like a carbon-12 atom. It readily oxidizes to produce carbon dioxide, which then quickly disperses throughout the atmosphere and biosphere (Lowe and Walker, 1984). New radiocarbon enters the food chain when carbon dioxide molecules diffuse to Earth's surface and are used by plants during

photosynthesis. Animals obtain the radioactive carbon by feeding on plants, or animals that have eaten plants. In this way, organisms are continuously resupplied with modern ^{14}C .

One early assumption of radiocarbon dating was that the quantities and ratios of all carbon isotopes are the same in the biosphere as they are in the atmosphere. This is not entirely valid. Terrestrial plants preferentially take up ^{12}C during photosynthesis, while oceanic water preferentially absorbs ^{14}C (Lowe and Walker, 1984). This fractionation of the atmospheric carbon isotope ratios can be corrected by measuring the $^{13}\text{C}:^{12}\text{C}$ ratio in addition to the $^{14}\text{C}:^{12}\text{C}$ ratio. The fractionation of the stable $^{13}\text{C}:^{12}\text{C}$ ratio is about half that of the radioactive $^{14}\text{C}:^{12}\text{C}$ ratio (Bradley, 1985).

The radiocarbon resupply system stops abruptly when an organism dies. From the moment of death, the amount of radiocarbon in an organism decreases at a constant decay rate. The amount of ^{14}C in an organism at death is assumed to reflect the amount of ^{14}C in the atmosphere at that time. The rate of decay of ^{14}C is constant and calculated to have a half-life of 5730 ± 40 years (Williams *et al.*, 1993). This means that after about 5730 years, half the original amount of radiocarbon is left in the organic tissue, and after about 11,460 years a quarter of the original radiocarbon remains.

If the original amount of ^{14}C in the organism is known and the quantity left in the fossil can be measured, then the length of time lapsed since the organism's death can be calculated. There are still several corrections required before making an accurate calculation of a specimen's age, and terrestrial and marine samples need separate consideration. Radiocarbon years are not of equal length to calendar years. This results from variations in radiocarbon production in the atmosphere due to changes in the rate of cosmic ray bombardment, fossil fuel consumption, and atmospheric nuclear testing (Lowe and Walker, 1984). The industrial burning of fossil fuel lowers the $^{14}\text{C}:^{12}\text{C}$ ratio

by flooding the atmosphere with ^{12}C . In the last 40 years, atmospheric detonation of nuclear weapons has increased atmospheric ^{14}C by almost 100% rendering ^{14}C useless for dating modern samples (Lowe and Walker, 1984). As a result, 1950 AD is used as the reference year for radiocarbon years before present (BP). Therefore, an organism that died in the year AD 550 should have a ^{14}C age of 1400 yr. B.P., even though calculations of age based upon radiocarbon abundance would suggest an age of approximately 1880 yr. B.P. (Talma and Vogel, 1993). To correct for this error in terrestrial samples, a calibration curve has been prepared (Talma and Vogel, 1993) showing the difference between the calendar year and the radiocarbon year. This curve was produced by ^{14}C dating of pieces of wood whose ages were precisely calculated using dendrochronology. Dendrochronology uses the annual growth rings of particularly long lived specimens of pine, oak, sequoia, and fir in Europe and North America to determine the yearly variation in atmospheric radiocarbon through time. Hundreds of samples were dated this way producing a calibration curve extending to 7,200 yr. B.P. (Stuiver, 1993; Stuiver and Becker, 1993). Until recently samples from earlier than 7,200 yr. B.P., and all marine samples, had to be corrected using other means that had not been independently verified. Now Bard *et al.* (1990b) have calibrated a uranium-thorium curve to the radiocarbon curve back to 30,000 yr. B.P. using corals from Barbados.

A second correction is only applied to marine samples. Because radiocarbon can take many years to diffuse from the atmosphere into the ocean, by the time it is incorporated into the marine environment it has already significantly decayed. As a result, the ocean water itself can be radiocarbon dated giving the water an apparent age. This apparent ^{14}C age of the water is transferred to living organisms within it (Lowe and Walker, 1984). Different regions of the ocean will give different ages. "Packages" of water, such as the North Atlantic Deep Water and the Antarctic Bottom Water, can be

traced as they move around the world in part by their ^{14}C radioactivity (Stuiver et al., 1983). This radiocarbon age of oceanic water is called the ΔR . In surface waters around Hawaii, $\Delta R = 115 \pm 50$ years (Stuiver and Reimer, 1987).

A final correction is needed for both terrestrial and marine samples. Different species take up and hold different amounts of carbon. To determine the amount of ^{14}C originally in a specimen, the $^{13}\text{C}:^{12}\text{C}$ ratio is also measured. Carbon-12 and carbon-13 are stable isotopes and will still be present in their original quantities. The original amount of ^{14}C can then be determined since ^{14}C and ^{13}C generally have a fractionation ratio of about 2 to 1 (Lowe and Walker, 1984). Various regions of the world also have slightly different fractionation ratios. The $^{13}\text{C}:^{12}\text{C}$ ratio of Hawaiian samples is particularly critical because Hawaiian species are very different from species in areas that are likely to have been extensively sampled. Also, carbon dioxide vented by Hawaiian volcanoes may have significantly altered the local carbon isotope ratios (C. Patrick, Beta Analytic, personal communication).

Corrections, such as the ones described, may be performed at a dating laboratory. However, the validity of several assumptions must be addressed in the field. If a specimen's age is being used to determine the age of a layer of sediment, then it must be assumed that the organism died soon before the layer of sediment was deposited. If the organism lies elsewhere for a period of time before being deposited, then the age will reflect the age of the organism and not the desired age of the sediment layer. Similarly, if the sediments have been deposited, eroded, and redeposited, the resulting ^{14}C age will be the organism's age and not the age of the target deposit.

Another assumption results from the so-called "old wood effect" (Talma and Vogel, 1993). If an organism such as a tree lives a long time, for example 300 years, and then dies and is buried for 400 years, what is the age of a sample taken from that tree? A

sample from the outside layer of the tree would give a date of 400 years while a sample from the center would give a date of 700 years. If the tree has been split up so it is impossible to tell where in the tree a sample came from, there would be a problem telling the age of death for that tree. Are the samples from two different trees; one that died 400 years ago and another that died 700 years ago? Or could they be from one tree that started growing 800 years ago and lived for 500 years? There is no way to tell simply from the ages of the samples. Without knowing the type of tree or where on the tree the sample came from, one must assume the sample is from a short-lived tree or the outside of the tree.

One error for which corrections cannot be made is called the "hard-water" error. This occurs in areas with underlying carbonate bedrock. Groundwater passing through the bedrock becomes enriched in dissolved carbonate. The dissolved carbonate can precipitate into a specimen and dilute its $^{14}\text{C}:^{12}\text{C}$ ratio with quantities of inert carbon-12 (Lowe and Walker, 1984). At the time of collection, the sample collector must determine the amount of likely contamination. Collectors generally avoid dating specimens collected from areas likely to have significant hard-water contamination and the resulting error.

Although the "hard-water" error is usually found in terrestrial environments, it has also been found in some marine carbonates around Hawaii. Marine mollusk shells collected offshore of Pleistocene limestone coasts were dated as much as 620 radiocarbon years older than similarly aged same-species mollusk shells located along volcanic coasts (Dye, 1994). The error is thought to be a result of groundwater passing through the limestone and absorbing radiocarbon-depleted carbon before flowing into the ocean where the depleted carbon is incorporated into the marine organisms living there.

Although most "hard-water" contamination is difficult to correct, if sample of a known age can be dated, this particular error may be compensated for (Dye, 1994).

Although radiocarbon dating techniques rely on corrections and assumptions, these can be compensated for in a laboratory and their validity estimated in the field. With a thorough understanding of the processes involved with radiocarbon dating, accurate and reproducible dates can be obtained.

LEAD-210

For measuring short-term sedimentation rates, the isotope lead-210 can be effective. A naturally occurring, short-lived isotope, lead-210 is the twelfth member of the fifteen isotope (fourteen transformation) ^{238}U decay series (Fig. 1). With a 22.2 year half-life, ^{210}Pb can only be used to date sediments deposited during the past 150 year. After 6 or 7 half-lives, the isotopic abundance is too low to measure accurately. Lead-210 has been used to calculate the snow accumulation rates on both alpine and continental glaciers and sedimentation rates in lacustrine and marine environments (e.g. Crozaz *et al.*, 1964; Krishnaswami *et al.*, 1971; Koide *et al.*, 1972). In any sediment type, the sampled sediment must be undisturbed. Bioturbation, wave agitation, and slope failure being three significant mechanisms of disturbance. The volumes of unsupported ^{210}Pb is much greater in marine sediments than in lacustrine or glacial deposits. Decay of radium 226 in the overlying seawater also appears to be in insignificant volumes (Koide *et al.* 1972).

An earlier uranium-238 decay series member, radium-226, decays into gaseous radon-222. Radon is released into the atmosphere where, with a half-life of just 3.8 days, it quickly decays through a series of four nuclides with half-lives just minutes long to ^{210}Pb (Friedlander *et al.*, 1964). Atmospheric ^{210}Pb rapidly attaches itself to aerosol

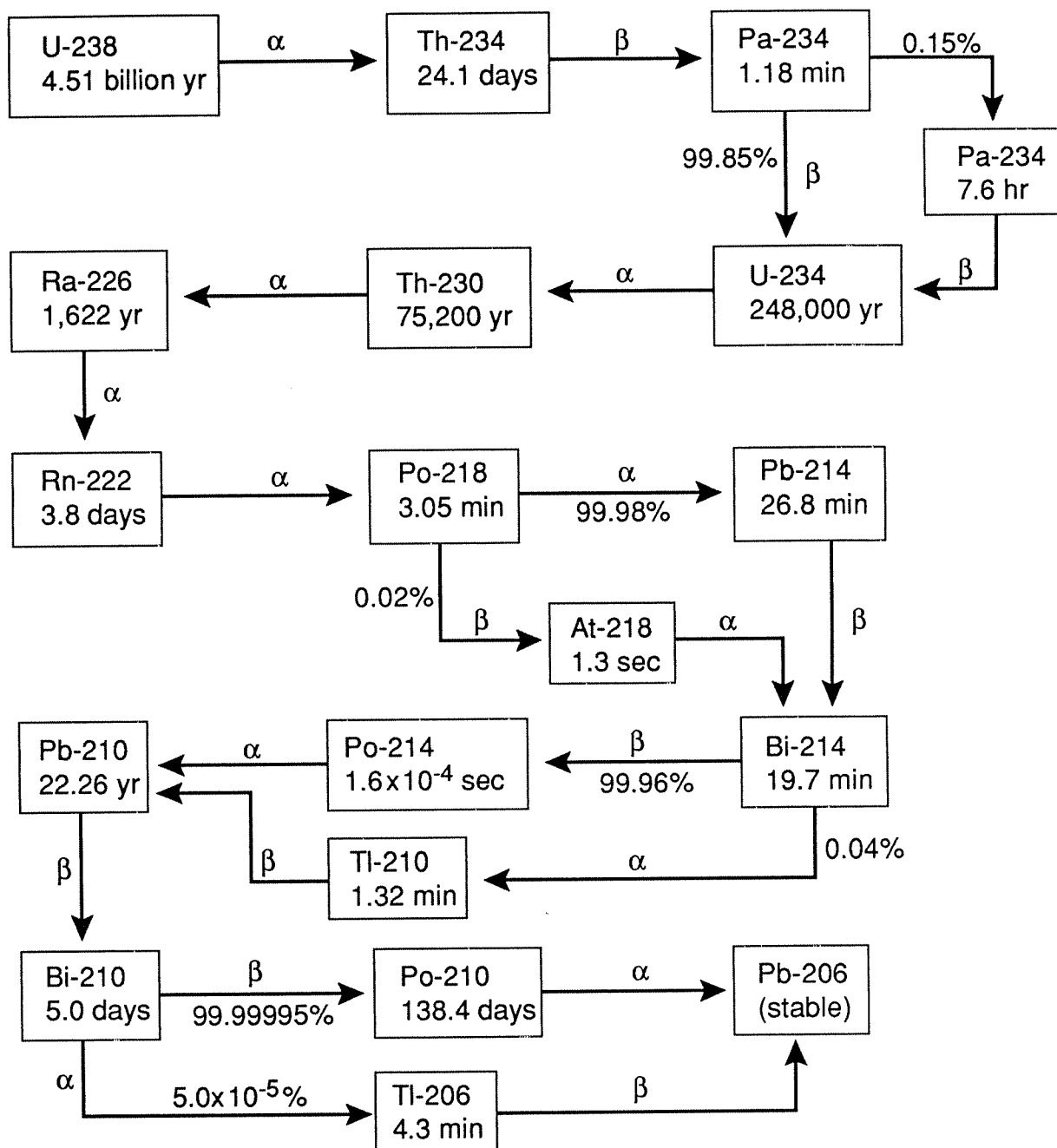


Figure 1: U-238 Decay Series. U = uranium, Th = thorium, Pa = protactinium, Ra = radium, Rn = radon, Po = polonium, Pb = lead, Bi = bismuth, At = astatin Tl = Thallium. Half-life intervals are shown in years (yr), days, hours (hr), minutes (min), or seconds (sec). α = an alpha particle emission, β = a beta particle emission. Eight alphas and 6 betas are emitted during this series. (After Friedlander *et al.*, 1964)

particles and returns to Earth with precipitation or as particulate fall-out. On the ground, it is incorporated into sediments, particularly aquatic sediments, and decays through bismuth-210 and either polonium-210 or thallium-206 to stable lead-206. Two principal assumptions are made in lead-210 dating: 1) the sediments must be part of a closed system where the only loss of ^{210}Pb is through radioactive decay; and, 2) the quantity of ^{210}Pb at the time of sediment deposition must be known. The reliability of lead-210 dates depends upon these assumptions or the accounting of them.

Although much of the radon produced by decaying radium is released into the atmosphere, some of it remains in Earth's crust. There it decays to ^{210}Pb in the surrounding rocks or sediments. The dating process is complicated if this earthbound ^{210}Pb mixes with ^{210}Pb formed in the atmosphere, since only atmospheric ^{210}Pb reflects sedimentation. To correct for this supported decay error, the amount of radium-226 in the sediment must be subtracted from the total amount of ^{210}Pb , allowing the calculation of the atmospheric ^{210}Pb . This can sometimes create the appearance of there being negative amounts of atmospheric ^{210}Pb . Ideally, only ^{210}Pb produced in the atmosphere, or unsupported ^{210}Pb , is found in the sediments being dated.

To calculate the time since lead was deposited, the decay rate of lead must be known and the original amount of lead must be known. Fortunately, the decay rate of ^{210}Pb has been measured to be 22.2 years, and the amount precipitating out of the atmosphere appears to be relatively constant (Crozas *et al.*, 1964). There has been some concern that the atmospheric testing of thermonuclear weapons added ^{210}Pb to the atmosphere. However, after investigating former test sites on Bikini and Eniwetok Atolls, Beasley (1969) found no evidence that significant quantities of ^{210}Pb were produced during nuclear explosions.

When the abundance of a daughter isotope is supported by the decay of its parent for a significant amount of time relative to the parent's half-life, the ratio of the two isotopes reach an equilibrium. This is caused when the decay rate of the daughter nuclide becomes equal to the production of the daughter nuclide by the decay of the parent nuclide. If such a system has been disturbed, it is possible to date the disturbance by measuring the degree to which the equilibrium has been restored (Bradley, 1985). Measuring the amount of equilibrium present in a system is another way to determine whether the ^{210}Pb is supported or unsupported.

The ^{238}U decay series can be used in several dating methods. Other ^{238}U decay series isotopes used in dating include ^{238}U , ^{230}Th , ^{234}U , and ^{226}Ra (Williams *et al.*, 1993). The dating methods using these isotopes have very high upper age limits compared with ^{210}Pb . Dating with the $^{234}\text{U}/^{238}\text{U}$ ratio is limited to sediments younger than 1.25 million years, while ^{230}Th dated sediments must be younger than 300,000 years. The datable time period of the $^{226}\text{Ra}/^{238}\text{U}$ ratio is closest to the datable time period of ^{210}Pb , but, with a 10,000 year old limit, it can still date much older sediments (Williams *et al.*, 1993). Lead-210 is one of a few dating techniques that can accurately date sediments on the time scale of 150 years.

CESIUM-137

Cesium-137, a byproduct of nuclear fission, is a purely artificial radionuclide. Although it was first released into local environments during atomic tests in 1945 (Carter and Moghissi, 1977), the global distribution of ^{137}Cs did not begin until high-yield thermonuclear tests in late 1952 (Perkins and Thomas, 1980). Measurements by the Health and Safety Laboratory in 1972 show global ^{137}Cs fallout began in 1952 ± 2 years. However, measurable quantities generally did not appear in sediments until 1954 (Wise,

1980; Longmore, 1982). Globally, periods of high ^{137}Cs fallout in 1958, 1963-1964, 1971, and 1974 correlate with above-ground nuclear testing (Carter and Moghissi, 1977). Since the 1963 Test Ban Treaty, global ^{137}Cs fallout has steadily declined with minor increases in 1971 and 1974 from atmospheric testing by non-treaty nations. By 1983, the deposition of ^{137}Cs in global sediments from fallout was no longer detectable (Cambray et al., 1985). However, in some regions of the world, the Chernobyl nuclear reactor accident in the Ukraine gives a final ^{137}Cs spike in the 1986 horizon (Ehlers *et al.* 1993).

Deposited ^{137}Cs is readily adsorbed onto cation exchange sites of clay and organic particles. This adsorption severely limits the mobility of ^{137}Cs owing to chemical and biological processes in soil (Schulz *et al.*, 1960; Tamura and Jacobs, 1960; Davis, 1963; Tamura, 1964a,b; Lomenick and Tamura, 1965; Schulz, 1965; Brisbin *et al.*, 1974; Eyman and Kevern, 1975; Wise, 1980; Campbell, 1982). Dahlman *et al.* (1975) do not consider uptake by vegetation a significant source of cesium loss.

To use ^{137}Cs to calculate sedimentation rates, the years represented by peaks in sedimentary cesium 137 must be known. By measuring the depth in the sediment of different ^{137}Cs peaks, the amount of sediment deposition per year can be calculated. Deposition of ^{137}Cs can occur by direct fallout from the atmosphere, washing of vegetation, decaying of vegetation containing ^{137}Cs , redeposition of eroded sediments, or settling from water on floodplains and coastal areas (Ritchie and McHenry, 1990). Most cesium-laden suspended sediment will be deposited fairly quickly, so sediments do reflect the levels of fallout (Ritchie and McHenry, 1990).

In the northern hemisphere, the 1954 and 1963-1964 sediment horizons can usually be identified with ^{137}Cs . The 1954 horizon is the deepest sediment layer containing ^{137}Cs , whereas the 1964 horizon has the highest concentration. A small ^{137}Cs spike can identify the 1958 horizon in some localities (Ritchie and McHenry, 1990).

Including the top of the sediments representing modern deposition, this gives a total of four datable horizons. With several sediment layers dated, a short-term comparison of sedimentation rates can be made.

The ^{137}Cs dating technique does have some limitations. As most sediment ^{137}Cs profiles will conclusively date only one or two layers, other techniques must be used if more detailed sedimentation rates are needed (Ritchie and McHenry, 1990). The identification of the deepest detectable levels of ^{137}Cs as the 1954 horizon can be incorrect. This horizon is marked by the earliest deposits of ^{137}Cs . Early ^{137}Cs deposits were usually quite small and sometimes near the level of detectability for ^{137}Cs . With a 30 year half-life, by 1984, only half the ^{137}Cs deposited in 1954 was left. In some areas, the levels of ^{137}Cs laid down in 1954 may now be too low to detect. In such a case, the deepest ^{137}Cs layer now represents a more recent horizon (Ritchie and McHenry, 1990). Also, a profile of the sediment size is necessary for a full interpretation of a ^{137}Cs profile. Since ^{137}Cs adheres more readily to finer grain sizes, an increase in the percentage of coarse grains causes a decrease in the ^{137}Cs concentration regardless of changes in the amount of atmospheric fallout. As a result, ^{137}Cs is of limited value in areas where sand dominates the sediments (Ritchie and McHenry, 1990). Finally, deposition of ^{137}Cs in sediments strongly correlates with precipitation (Davis, 1963).

Although ^{137}Cs concentrations in sediment layers generally reflect the amount of atmospheric fallout, there appear to be some inconsistencies. Some small watersheds have shown a 6 to 12 month lag time between atmospheric fallout and ^{137}Cs deposition in the sediment (Ritchie *et al.*, 1973). Furthermore, although chemical movement does not appear to be a problem for ^{137}Cs dating, physical disturbance by living organisms or other means can be a source of error. The reworking of sediments can reduce the maximum concentrations and broaden the ^{137}Cs peaks (Ritchie and McHenry, 1990).

Although such movement is not likely to change the depth of the major ^{137}Cs peaks (Krishnaswami *et al.*, 1971; Pennington *et al.*, 1973, 1976; Ritchie *et al.*, 1973; Robbins and Edgington, 1975; Wise, 1980; Campbell, 1982), physical movement of the 1954 horizon will cause it to appear shallower or deeper than it should. Movement may disperse this layer so that it can no longer be detected. In this case, the deepest detectable ^{137}Cs layer is shallower than the expected 1954 horizon. Physical movement may also displace detectable amounts of ^{137}Cs deeper into the sediments causing ^{137}Cs detection to occur deeper in the sediments than the 1954 horizon. In general, low ^{137}Cs concentrations will be more greatly affected by physical movement than high concentrations (Ritchie and McHenry, 1990). Diffusional movement of ^{137}Cs , while usually limited, can occur in certain soft-water lake environments (Davis, 1963; Tamura, 1964a,b; Lomenick and Tamura, 1965; Krishnaswami *et al.*, 1971; Aston and Duursma, 1973; Evans *et al.*, 1983; Davis *et al.*, 1984; Torgenson and Longmore, 1984).

The ^{137}Cs dating technique is limited to sediments deposited after atmospheric thermonuclear testing began producing measurable amounts of ^{137}Cs in 1954. The position of any 1954 layer will continue to become more and more difficult to locate as the quantity of 1954 vintage ^{137}Cs decreases from radioactive decay. The Test Ban Treaty of 1963 stopped most atmospheric nuclear testing, and since 1964, the level of ^{137}Cs deposited in global sediments has continually decreased until 1983 when it was no longer detectable. As a result, the 1964 sediment layer contains the last major spike of ^{137}Cs sediment levels (Ritchie and McHenry, 1990).

CHAPTER 2: COASTAL CARBONATE DEPOSITS

Abundant field evidence throughout the Pacific and Indian Oceans has given rise to questions about the stability of recent and modern sea-level. Much of this evidence is in the form of coastal carbonate deposits and erosion features interpreted as a fossil shoreline located above the modern shore and formed between 1,500 and 5,000 yr. B.P. Some recent geophysical predictions for a middle- to late-Holocene highstand of the sea are based primarily on numerical calculations of the viscoelastic response of Earth's lithosphere to the melting of glacial ice and subsequent redistribution of mass on Earth's surface (Nakada and Lambeck, 1989; Mitrovica and Peltier, 1991). The model predictions rely on field evidence that constrain the timing and magnitude of predicted sea-level rise and often prescribe values for elevation and timing to test the sensitivity of the models themselves. As a result, there is some circularity to the predictions based on the models. Hence, it is of vital interest to sea-level researchers and modelers alike to obtain precise field data with which to formulate an understanding of the interaction between Earth rheology, climate, and sea level within coastal areas during the recent past.

The recent calculation that global sea-levels are presently rising 1-4 mm/yr. (Peltier and Tushingham, 1989; Houghton *et al.*, 1990; Nerem, 1995) has led to interest in determining the rate, magnitude and timing of past relative sea-level rise. In addition, coastal environments that owe their existence to past and present climatic and sea-level conditions are highly susceptible to flooding and erosion under the rising sea-levels predicted by the Intergovernmental Panel on Climate Change (Houghton *et al.*, 1990). A possible middle- to late-Holocene highstand of relative sea-level has been used as an analog to identify areas susceptible to flooding and related hazards associated with rising sea-levels. Verification of the cause of the carbonate deposits and erosional features will

assist in the interpretation of sea-level trends from satellite altimetry (Nerem, 1995) and an expanding global tide-gauge database and contribute to an understanding of the processes responsible for shaping the coastal environments.

BACKGROUND

Studies of Quaternary sea-level change and recent post-glacial sea-level recovery have long been a focus for sea-level researchers and are reviewed in detail by Kidson (1982), van de Plassche (1986), and Devoy (1987). The concept of a post-glacial (Holocene) sea-level higher than present was introduced by Daly's (1920, 1934) study of emerged coral platforms in the Indian and Pacific Oceans. This sparked considerable debate among researchers who eventually divided among three schools of thought (Devoy, 1987).

The first group supported a rapid and oscillatory pattern of sea-level rise to a highstand +3 m above present sea level *c.* 5,000 yr. B.P. (Fairbridge, 1961) associated with the Holocene thermal maximum known as the hypsithermal. Proponents asserted that after this time, sea-level oscillated at an amplitude of 6 m around its present position in response to thermal expansion and contraction of sea-water and ice volume variations since the hypsithermal. Opponents questioned the accuracy of their results and argued that tectonic activity influenced their indicators. The second school led by the work of Shepard (1963, 1964) and Scholl and Stuiver (1967) supported sea-level rise at varying rates during the Holocene as envisioned by Fairbridge (1961) but found no evidence for a sea level higher than present. Data supporting this concept came primarily from low-lying depositional coastal environments. Bloom and Stuiver (1963), Jelgersma (1966), Bloom (1967), Thom *et al.* (1969), and Kidson and Heyworth (1973) found evidence to demonstrate a smooth gradual rise of sea-level but lacked evidence for any sea-level

higher than present. This promoted a third group which favored a sea-level that steadily rose to its present position between 5,000 and 3,600 yr. B.P. (Fisk, 1951; Godwin *et al.*, 1958; McFarlan, 1961) and stood still thereafter. While their evidence came primarily from the coast of the Gulf of Mexico, they received substantial criticism for amassing data from around the world regardless of data type, source, or accuracy as detailed by Devoy (1987).

The search to identify a single global "eustatic" signal of sea-level rise continued into the 1970s and 1980s under the International Geological Correlation Programme (IGCP) Project No. 61, which attempted to establish the trend of mean sea-level during the last 15,000 years (Bloom, 1977). However, errors introduced by inaccurately interpreting sea-level indicators, defining various sea-level datum and tide levels, and inconsistent corrections for tectonic and isostatic effects made comparisons of eustatic sea-level curves from around the world futile. Responding to these issues, Kidson (1982) and Devoy (1987) reviewed the history and concerns of Holocene sea-level research, and van de Plassche (1986) produced a manual for sea-level studies in hopes of standardizing research methodology and the evaluation of sea-level data.

Recognizing that regional differences in sea-levels are manifestations of changes in Earth's geoid and effected by climatic, eustatic, isostatic, and tectonic processes, researchers have since largely abandoned the quest for a eustatic sea-level curve in favor of constructing relative sea-level histories with regional validity. Pirazzoli's *World Atlas of Holocene Sea-Level Changes* (1991) summarized the existing field evidence of Holocene sea-level movements by compiling published sea-level curves for various regions. In the past few years, numerous studies from around the world have added to the database of Holocene sea-level histories and help clarify the middle- to late-Holocene highstand debate.

Opponents of higher than present Holocene sea-levels have most commonly argued that evidence in support of a Holocene highstand has been misinterpreted and/or skewed by tectonic and oceanographic (storms, tsunamis) processes. However, as the understanding of geologic processes and the precision of surveying and dating technology improves, so too does our ability to discern evidence of sea-level movements. It has only been since the 1950s, with the advent of radiocarbon dating, that significant Holocene sea-level studies have been published. Mörner (1980) showed how a representative sea-level curve for Fennoscandia could be produced by correcting for isostatic uplift, while Chappell and Polach (1991) and Edwards *et al.* (1993) constructed a detailed post-glacial sea-level history, including changes in the rate of sea-level movements, for tectonically unstable Papua New Guinea. The Holocene highstand debate continues to be reshaped by improvements in our ability to measure and understand influential geologic processes and our capacity to interpret them.

CAUSES OF SEA-LEVEL VARIATION

The dominant forces that influence Holocene sea-level movements are: 1) climate change and rapid ice sheet decay; 2) the variation in the geoid; 3) the glacio- and hydro-isostatic redistribution of Earth's mass in response to ice sheet advance and retreat; and, 4) the evolution of ocean basin morphology. It is readily apparent that these processes work on different time and spatial scales.

Climate Change and Rapid Ice Sheet Decay

Climate change appears to have played the greatest role in affecting early Holocene sea-levels, bringing about the collapse of most of the continental ice sheets and returning melt water to the ocean basins. Submerged shorelines offshore of Barbados

indicate that global sea-level rose approximately 120 m to its present level from a low stand *c.* 21,000 yr. B.P. (Bard *et al.*, 1990a). However, because it is thought that the retreat of the ice sheets terminated *c.* 6,000 yr. B.P., sea-level researchers disagree on whether or not the contribution to sea-level fluctuations by climate change in the late Holocene was slight and relatively less than geophysical forces.

Warming global climate influences sea-level in two ways. The first is by melting of the world's glaciers. Melting the continental ice sheets is the primary factor in raising world sea-level, but alpine glaciers do contribute a small amount. The second factor is through expansion owing to the thermal properties of water. In general, water is considered incompressible, but spread out over the vast amounts of water in the ocean, warmer ocean water will have a slightly greater volume. This greater volume will manifest itself as a higher sea-level; however, with projections of ~6 cm rise in sea level per 0.8° C increase in global temperatures (Wigley and Raper, 1978), the difference in sea-level due to temperature induced volume variation is quite small and can easily be over shadowed by other sea-level controls.

Recent evidence from the Antarctic continental shelf and drowned *Acropora palmata* reef frameworks in the Caribbean indicates that eustatic sea-level rise since the last glacial maximum has been episodic owing to catastrophic collapses of various continental ice sheets (Anderson and Thomas, 1991; Blanchon and Shaw, 1995). The gradual rise in sea-level resulting from glacial melting floated parts of the ice sheets grounded on the continental shelves. The ice sheets became unstable and collapsed, causing rapid rises in eustatic sea-level (*i.e.*, >45 mm/yr in <300 yrs; Blanchon and Shaw, 1995).

Glacial ice volumes are generally considered to have been at their minimum about 6,000 yr. B.P. Only the Greenland and Antarctic continental ice sheets remained, and

they and the world's alpine glaciers are thought to have been at a minimum. As a result, the oceans held more water during that time than at any other period during the Holocene. This time coincides with the hypsithermal measured by pollen distribution (COHMAP, 1988), treeline fluctuations (LaMarche, 1973; Luckman, 1988), dendrochronology (Feng and Epstein, 1994), and oxygen isotope records from ice cores (Paterson *et al.*, 1977; Shackleton, 1987; Bender *et al.*, 1994). These separate studies indicate a warm period ending after 6,000 yr. B.P. The measurements were taken from a range of latitudes, including the White Mountains of California (LaMarche, 1973; Feng and Epstein, 1994), the Athabasca Glacier in Alberta, Canada (Luckman, 1988), and the Devon Island ice cap in the Canadian High Arctic (Paterson *et al.*, 1977). The coincidence of the hypsithermal and the global glacial minimum may have had a pronounced effect on sea-level.

Geoidal Migration

Changes of sea level in response to geoidal variations have, until recently, been considered theoretical. Mörner (1976) showed that the geodetic sea level or 'equipotential surface of the geoid' varies with respect to Earth's center by as much as 180 m. He also showed the present geoid configuration is not stable and must have changed with variations in gravity and other controlling factors. Although not unrelated to crustal instability of tectonic or isostatic origin, the geoid in the oceans coincides with the sea surface and hence its instability is distinct from instability of the ocean bottom. Mörner argued that short-term geoidal variation meant that sea-level changes could no longer be interpreted exclusively as evidence of glacial ice volume changes. Highs and lows in the sea surface modeled by Walcott (1972) and Farrell and Clark (1976) have since been surveyed, and are believed to migrate over time.

Mitrovica and Peltier (1991) predicted higher than present sea levels for 18 small islands in the Pacific Ocean during the Holocene. They attributed the highstand to the migration of the mantle away from equatorial bulges towards the oceanic portion of a rebounding moat encircling previously glaciated regions following maximum glaciation. This equatorial ocean siphoning mechanism is now thought by some to have influenced relative sea-level variation in oceans far from ice sheets during the past 4000 years, when ice volumes are believed to have remained relatively static.

Hydroisostasy

Islands far from glaciated regions may be influenced by the isostatic response of Earth's lithosphere to the increase in mass of glacial meltwater added to the oceans. Clark *et al.* (1978), following the work of Walcott (1972) and Chappell (1974), proposed sea-level curves for different regions based on numerical models of the spherical viscoelastic response of Earth's lithosphere to the decay of the most recent continental ice sheets. Nakada (1986) and Lambeck (1990) have further refined these models, and predicted emerged Holocene shorelines on islands larger than 10 km in radius far from glaciated regions. It is thought that a hydroisostatic adjustment caused by an increased load on the ocean floors inducing the upper mantle to flow from under the oceanic portion of the lithosphere towards an island will lift the island relative to sea level, leaving a shoreline stranded above present day sea-level.

Tectonism and Lithospheric Flexure

Acting on a much longer time scale and at a far slower rate, the gradual spreading of the sea floors driven by plate tectonics have altered the shape and storage volume of the world's oceans. The exact contribution of ocean basin volume change to sea-level

movements remains unknown but is often assumed slight for Holocene-scale studies. However, some localized episodic tectonic events have been examined (Chappell and Polach, 1991) and their contribution isolated to produce a relative sea-level history closely resembling that from other locations (Fairbanks, 1989). Our limited understanding of ocean basin volume changes continues to improve as advancements in remote sensing and surveying afford more detailed observation and analysis of geologic processes acting on various spatial and temporal scales.

Vertical displacement of islands because of lithospheric flexure in the Pacific has been observed in Hawaii and Tahiti, where the horizontal movement of the Pacific Plate over a mantle plume has created an island chain by volcanic eruptions. Loading of Earth's crust and mantle at the hotspot creates a zone of subsidence proximal to the loading point, and a rising distal arch that circumscribes the region of greatest subsidence (Watts and ten Brink, 1989). Uplift, followed by subsidence, is associated with the movement of an island across the arch. In Hawaii, it has been estimated that the arch should be uplifting the island of Oahu at 0.01-0.03 times the maximum subsidence rate (P. Wessel, personal communication; Watts and ten Brink, 1989). This could account for an 18 cm middle- to late-Holocene sea-level highstand on Oahu.

Despite model limitations and the use of unknown parameters (i.e., the exact elasticity of Earth's rheological structure, rate of ice melt, and maximum ice sheet thickness), it is now clear that no part of the crust can be considered completely stable. As a result, there is as much to be learned about Earth's rheology, as well as glacial history, from observations of sea-level change as there is of sea-level history from studies of Earth's rheology.

Storms and Tsunamis

Even with geophysical models appearing to account for sea-level highstand evidence, it is possible for many pieces of evidence to have been emplaced by catastrophic events, such as large storms or tsunamis. Interpreting intertidal features such as notches as sea-level indicators assumes that daily waves and intertidal communities of bioeroding organisms are the primary agents in their formation. However, it is possible that rare events, 5-10 m storm waves or tsunamis, could be an important element in forming shoreline features. Also, sand, coral, and algal rubble can be deposited well above mean sea-level by these waves. The tremendous force of such events is enough to account for even some of the coral which appears to be in growth position. In Indonesia, a coral reef block 6 m high and estimated to weigh more than 540 metric tons was moved more than 100 m inland from the shoreline by a tsunami in the 1880s (McCredie, 1994). Without knowing this block's history, it would be possible to mistake its coral as being *in situ*, particularly if the block were later partially buried. The Hawaiian Islands of Molokai and Lanai have lithified outcrops of carbonate sand, gravel and rubble mixed with basalt rubble at elevations of above 60 and 300 m respectively that have been interpreted as tsunami deposits (Moore and Moore, 1984; Moore *et al.*, 1994). The north shore of the Hawaiian island of Oahu has several locations with examples of boulders of fossilized coralline algae reef deposited 2 to 4 m above sea-level, apparently by storm or tsunami waves. The major axes of the largest such boulder measures 4 m, 6 m, and 10 m. Half-buried in unconsolidated sediments and with a few coral growths, these boulders could appear to be bedrock with coral in growth position. As a result, it is difficult to discount tsunamis or storm waves as a cause of sea-level indicators simply because a feature is too large or too high.

MARINE CARBONATES AS EVIDENCE

Coastal marine carbonate deposits and erosional features from islands throughout the Pacific and Indian Oceans have been used as evidence of a middle- to late-Holocene sea-level highstand. Although this evidence appears to support geophysical and climate model predictions of a sea-level highstand, the presence of such evidence alone does not prove the existence of a highstand of the sea. Sea-level indicators of various types are reviewed by van de Plassche (1986) and Pirazzoli (1991) and include both geological and biological features. Emerged beaches and floodplains (Athens and Ward, 1991), wave-cut platforms and notches (Pirazzoli and Montaggioni, 1988), stranded coral reefs (Jones, 1992), and estuarine swamps (Ellison, 1994) have all been used to decipher the timing and magnitude of relative sea-level highstands in the Holocene.

Pacific Ocean

Marshall Islands

Few studies have documented Holocene sea-level evidence in the central Pacific Ocean. In the Marshall Islands, however, Buddmeier *et al.* (1975) concluded sea-level stood at least +1 m between 3,500 and 2,000 yr. B.P. from analysis of emerged reef flats overlaying carbonate material that gave radiocarbon dates between 5,000 and 3,500 yr. B.P. This conclusion relies on the assumption that Enewetok Atoll has continuously subsided at 0.02 to 0.04 mm/yr (Menard, 1964) throughout the late Holocene.

Hawaii

In the Hawaiian Islands, deciphering the history of Holocene sea-level change is complicated by local tectonics and lithospheric flexure associated with the Hawaiian hotspot. The only existing curve, a reef-accretion curve (Easton and Olson, 1976)

inadequately represents Holocene sea-level movements for several reasons. It assumes that reef growth kept pace with the rise of mean lower low water (mllw) following the last glaciation. In Hawaii, no coral species have been identified whose growth range is restricted to the upper 10 m of the water column. As a result, the coral dated in the study was not necessarily growing within 10 m of sea-level. In addition, Davies and Hopley (1983) and Neumann and Macintyre (1985) showed that reef growth can often lag significantly behind sea-level rise. Most importantly, their reef-accretion curve documents the subtidal stratigraphy, hence it does little to record sea-level movements.

In a comment on the work of Easton and Olson (1976), Stearns (1977) criticized their conclusion that there was no middle-Holocene highstand, arguing their research ignored a small but important outcrop of beachrock level with the prominent +2 m bench found in another part of Hanauma Bay and numerous other locations around Hawaii and throughout the Pacific. Bryan and Stevens (1993) propose that salt-weathering is responsible for the bench at Hanauma Bay but do not exclude a highstand as a contributing factor in its development. Unfortunately, the debate over Hanauma Bay has led to mistaken conclusions regarding the history of sea-level in Hawaii in general (Peltier *et al.*, 1978) and confusion regarding its nature (Nakada, 1986).

Nevertheless, more and more coastal carbonate deposits in Hawaii continue to be described. Jones (1992) reported *in situ* stranded coral (*Porites compressa*) standing +1.8 ± 0.3 m (mean sea-level) within the Hanalei River, Kauai dating between 3,000 and 4,500 yr. B.P. Near the mouth of Kapaa Stream on Kauai, Yonekura (1988) found both marine and terrestrial mollusks along a marine contact between 1.1 and 1.3 m above present mean sea level, dating to 3,800 to 4,000 yr. B.P. On the island of Oahu, Athens and Ward (1991) found evidence the sea inundated Kawainui Marsh between 1,500 and 4,000 yr. B.P., although they did not determine the height of the inundation. Radiocarbon dates

from an emerged intertidal notch on south Mokulua Island and a possible stranded beach on Kapapa Islet (Fletcher and Jones, in press) suggest a 1.4 ± 0.25 to 1.6 ± 0.45 m higher sea-level stand between 2,000 and 4,000 yr. B.P. These coastal carbonates provide important evidence for creating a possible sea-level curve for Hawaii. Tide gauge data on both Kauai and Oahu show that these islands are currently experiencing a relative rise in sea-level (1.5-2 mm/yr; N.O.S., tide gauge records).

French Polynesia

Throughout French Polynesia, Pirazzoli and Montaggioni (1988) found marine carbonates between 0.8 to 1.0 m above present sea-level with an age of 1,250 and 5,000 yr. B.P. Dated samples consisted of exposed corals, abandoned algal ridges, reef frameworks in growth position, emerged tidal notches, and skeletal reef conglomerates in which the position of the former low water level at the time of cementation has been determined by petrological analysis. Furthermore, they have shown with numerous dated samples that between 1,250 and 4,500 yr. B.P. relative sea level could not have dropped below +0.7 m for any appreciable length of time without affecting coral growth. The gradual drop in sea level since 1,500 yr. B.P. however, is not explained by global isostatic model results which predict a highstand in this region during the middle Holocene. Pirazzoli and Montaggioni (1988) propose that a gradual cooling of deep water in the region may explain the observed sea-level fall better than geoidal migration.

Cook Islands

In the Cook Islands, Ellison (1994) interpreted her analysis of pollen and charcoal sampled from five coastal clay-filled swamps as evidence of a relative sea-level highstand. Radiocarbon dates from samples of *Cyperaceae* and *Rhizophora* indicate that

between 4,500 and 6,500 yr. B.P. these swamps (+1.1 m, msl) were coastal lagoons inundated by the sea. Yonekura (1988) obtained radiocarbon dates from raised microatolls +1.3 to +1.7 m (msl) between 3,400 and 5,000 yr. B.P. with a maximum elevation corresponding to an age between 3,400 and 4,000 yr. B.P. Scoffin *et al.* (1985) found evidence for a possible short-lived sea-level peak between 1,000 and 2,000 yr. B.P. from an emerged and slightly eroded algal ridge on Suvarrow Atoll.

Western Samoa

Sugimura *et al.* (1988) and Rodda (1988) found beachrock on the islands of Upolu and Savai'i between +0.8 and +0.95 m (msl) and a wave-cut notch at +2.3 m (msl) on Savai'i dating to the late-Holocene.

Tonga

In Tonga, Dickinson *et al.* (1994) obtained radiocarbon dates of *c.* 3,000 to 6,000 yr. B.P. from charcoal excavated from a buried, abandoned late-Holocene coastal archaeological site. Accretion of the coastal plain seaward of the site appears to indicate that progradation of the beach has left a late-Holocene shoreline 1-2 m above msl.

Fiji

Several workers in Fiji have found coastal carbonates of middle- to late-Holocene age. Nunn (1990) distinguished carbonates of +1-2 m (msl) height with the maximum elevation dated between 2,000 and 3,000 yr. B.P. on Vanua Levu. Dates and elevations from beaches (Nunn, 1990), coastal terraces (Berryman, 1979), notches (Berryman, 1979; Miyata *et al.*, 1988) and fossil corals in growth position (Miyata *et al.*, 1988) on various islands throughout Fiji of middle- to late-Holocene age have also been described.

New Caledonia

Baltzer (1970) established middle- to late-Holocene radiocarbon dates for samples of *Rizophora* peat, an indicator of the higher part of the intertidal zone. Cabioch *et al.* (1989) obtained elevations and dates of corals from 39 cores drilled into the fringing reef which support a relative higher sea-level in New Caledonia from *c.* 6,000 yr. B.P. until about 3,000 yr. B.P. Coudray and Delibrias (1972) proposed that sea-level in New Caledonia stood 1 m higher than present between 3,000 and 4,400 and stayed above 0.7 m until 770 yr. B.P.

Mariana Islands

Kayanne *et al.* (1993) documented 54 radiocarbon dates from notches and reefs that suggest relative sea-level may have risen gradually to a maximum of +1.8 m (msl) between 6,000 and 4,200 yr. B.P. After 4,200 yr. B.P., abrupt uplift is thought to have caused emergence of the reef. Subtracting out tectonic uplift, they have created a sea-level curve that records a slight transgression from 6,000 to 4,200 yr. B.P., and stabilization after 4,200 yr. B.P. in support of the model predictions of Nakada and Lambeck (1989). Because the contribution of relative sea-level change resulting from tectonic activity is not exactly known, Kayanne *et al.* (1993) contend that part of the apparent emergence found from their data may correspond to the sea-level highstand predicted by Mitrovica and Peltier (1991).

Indian Ocean

Cocos Keeling Islands

In the Cocos Keeling Islands, Woodroffe *et al.* (1990) have found consistent radiocarbon dates for corals from the surface and shallow subsurface of a conglomerate platform which indicate they grew or were emplaced on the reef flat *c.* 3,000 yr. B.P. under a sea-level regime 0.5-1.5 m higher than at present. Fossil microatolls, consisting of heads of branching *Porites* stripped off on their tops, also have been dated to approximately 3,000 yr. B.P. Finally, intertidal beachrock overlying microatoll and conglomerate platforms postdate both landforms and are found as high as +2 m (msl), but no dates have been measured for the beachrock.

Thai Peninsula

Although not an island, the west coast of the Thai peninsula contains sea-level indications from *in situ* fossil massive reef-front *Porites* corals exposed on reef flats. From radiocarbon dates and leveling data, Tudhope and Scoffin (1994) concluded sea-level was at least 0.8 m higher than present from 5,200 to 3,000 yr. B.P.

CONCLUSION

Abundant evidence in the form of marine carbonates and erosional features has been documented on islands throughout the Pacific and Indian Oceans. These data appear consistent with some geophysical model predictions for recent emergence of island shorelines far from the influence of continental boundaries due to both geoidal migration (Mitrovica and Peltier, 1991) and hydroisostasy (Nakada and Lambeck, 1989); however, because of the varied nature of coastal processes affecting sea-level indicators,

these data are not entirely conclusive. From this growing database of evidence, a better understanding of both the sea-level response to deglaciation and Earth's lithospheric response to changes in ice-ocean water volume changes will emerge.

CHAPTER 3: HOLOCENE HISTORY OF SEDIMENT DEPOSITION AND STRATIGRAPHY ON THE HANAELI COASTAL PLAIN, KAUAI, HAWAII

GEOLOGIC SETTING

The Hawaiian Islands, a linear chain of volcanic islands located 19° N to 28° N in the central Pacific Ocean, lie within the band of subtropical northeast tradewinds that control the general precipitation pattern. The larger islands have distinct wet and dry sides where the wet sides commonly receive rainfall exceeding 5 m/yr while the dry sides may receive less than 0.3 m/yr. Draining the northeastern slopes of Mt. Waialeale on the island of Kauai (Fig. 2), the headwaters of the Hanalei River receive some of the highest recorded rainfall on Earth (>10 m/yr). As a result, large quantities of sediment are eroded and floodplain deposition is an important sedimentary process.

The Hanalei River crosses a 1-2 km wide coastal plain before flowing into crescent-shaped Hanalei Bay on the north shore of Kauai. The bay opens slightly west of due north and receives two other minor rivers: the Waioli and the Waipa. The Hanalei River occupies the eastern section of the coastal plain, while the Waioli and Waipa share the western portion, separated by a low volcanic ridge extending nearly to Hanalei Bay. Intense mountain rains to the south can quickly swell these rivers to flood stage.

Topography

The areal extent of the flat Hanalei coastal plain is defined on maps by the 20 ft. (6 m) contour, which corresponds reasonably well with a sharp break in slope between steep basaltic highlands and the level coastal plain. Most of the coastal area lies between the 1 and 3 m levels, although near the mountains it exceeds 3 m as does the center of the

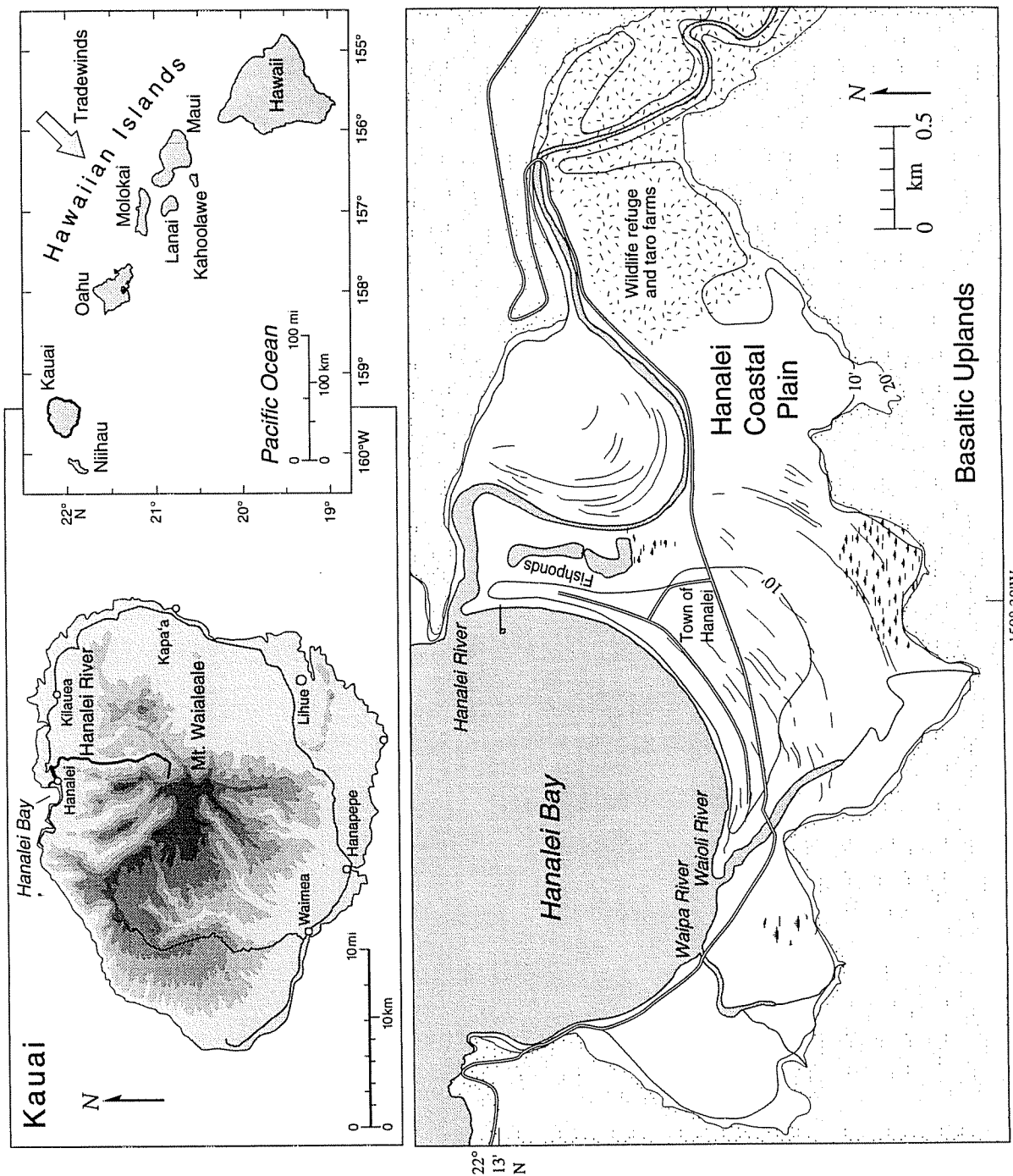


Figure 2: Map of the Hawaiian Islands, the island of Kauai, and the Hanalei coastal plain on the north shore of Kauai, Hawaii. Also shown are the town of Hanalei, the meander scars and beach ridges mapped by Moberly (1968), major roads, and the areas of disturbed stratigraphy associated with the waterfowl refuge and the Hawaiian fishponds. The 10 and 20 ft (3.0 and 6.1 m) contours were obtained from a set of U.S. Army Corps of Engineers contoured orthophotoquads (1:4800).

plain adjacent to the bay where the town of Hanalei sits and where it approaches 6 m (Fig 2).

South of the topographic high upon which the town was built, some freshwater wetlands abut the basaltic uplands. These marshes range in elevation from *c.* 2 to 3 m (above msl), and occur where upland runoff collects on the poorly-drained surface of the coastal plain. Another subtle feature on the coastal plain is a series of low relief lineations visible in aerial photographs interpreted by Moberly (1968) as "crescentic bayhead beach ridges....that show the advance of the land as well as the old meander scars of the rivers..." However, despite attempts, these features could not be positively identified in the field. Local agriculture has masked this landform even while following its form. The other important topographic features on the coastal plain are fishponds located near the mouth of the Hanalei River. The shape of the fishponds lend themselves to interpretation as an oxbow. However, the ponds have been modified by human activity, although the extent of modification is unclear.

The coastal plain's low lying features and juxtaposition to Hanalei Bay and Hanalei River leaves it susceptible to marine and fluvial sediment deposition and flooding. A combination of coastal and fluvial processes have and continue to shape these lowlands.

Tectonics

Located in the middle of the Pacific Plate, Kauai is in a low seismic area. The northwesternmost main island of the Hawaii Islands, Kauai lies 550 km from the seismically active Hawaiian hotspot under Kilauea volcano. Although tremors from three distant (>100 km) earthquakes have been felt on Kauai during historical times, little damage and no vertical displacement of the land surface was reported on the island

(Furumoto *et al.*, 1990). During this time, no seismic activity has been centered on the island or the surrounding seafloor. Long-term vertical movement of the island is believed to be downward because of lithospheric cooling as it moves away from the hotspot. Additionally, although models with an extremely thick (>40 km) elastic crust indicate that Kauai could be experiencing some uplift as it moves across the arch caused by the lithospheric flexural response to volcanic loading at the Big Island of Hawaii (Wessel, P., personal communication, 1994), any resulting uplift should be minimal (<20 cm) during the middle- to late-Holocene. Similarly elevated and dated evidence of a relative sea-level highstand of middle Holocene age is found on the southwest, east, and north sides of Kauai (Matsumoto *et al.*, 1988; Matsumoto, 1990; Jones, 1992), creating the need for a mechanism to account for the entire island's uplift rather than simply one side upthrusting or tilting. Because such a mechanism appears to be missing, co-seismic vertical movement is not considered likely on Kauai.

METHODS

To investigate the sedimentary history of the Hanalei coastal plain, 67 gouge auger cores, generally 3-7 m in length and 2.54 cm in diameter, and three shorter (<1 m) but larger diameter (6.5 cm) cores were obtained. Gouge auger core depth was limited by an inability to penetrate either thick carbonate sand or highly compacted fluvial sediments. Cored facies, facies contacts, and faunal and floral components of facies were sampled, described, and interpreted for paleoenvironmental analysis while in the field. Cores were wrapped in aluminum foil and stored in the University of Hawaii SOEST core laboratory (*c.* 4° C) for future reference. Grain size analysis was not conducted on the marine sediments found in the cores due to the limited penetration and recovered sample size. References to grain sizes are a result of field observations.

The short, thick cores were obtained with a clear plastic core liner sharpened at one end and driven vertically into the ground with a hammer and extracted by hand. Compaction of the core sample was corrected for by dividing the total penetration of the corer by the length of sample recovered. These cores were capped at both ends and returned to the laboratory for description and analysis. In the laboratory, the cores were cut in half with a core splitter, photographed, and their sediment grain size and color described. One half of the core was stored in the SOEST core laboratory and the other half had 5, 6, or 10 evenly spaced samples removed and tested for cesium and lead isotope levels. After cesium and lead testing, all five samples from short core CsPb 1 were examined with x-ray diffraction to determine mineral content.

Core locations were surveyed using hand-held digital compass triangulation ($\pm 0.5^\circ$) which closely-spaced cores indicated translated into a horizontal survey accuracy of *c.* ± 10 m (Fig. 3 and Appendixes A and B). These locations were then plotted on the U.S.G.S. 7.5' Hanalei quadrangle and a U.S. Army Corps of Engineers orthophotoquad (scale 1:4800). The elevations of the core tops were taken from the orthophotoquad, which reported spot elevation accuracy to ± 0.5 ft (0.15 m). The estimated core elevation accuracy (± 0.25 m) is determined from a consideration of orthophotoquad resolution, triangulation-survey accuracy, and core-measurement error.

Gouge auger cores were dated with radiocarbon and ^{137}Cs and ^{210}Pb techniques were used on the short cores. All radiocarbon samples consisted of carbonate sands, detrital wood, or woody plants, and were visually inspected for contamination by secondary carbon both before and after rinsing and drying on a 4 phi sieve. Samples showing contamination were not dated. Once at Beta Analytic, carbonate sand samples were washed in deionized water, crushed and dispersed, and repeatedly subjected to HCl etches to eliminate secondary carbonate components.

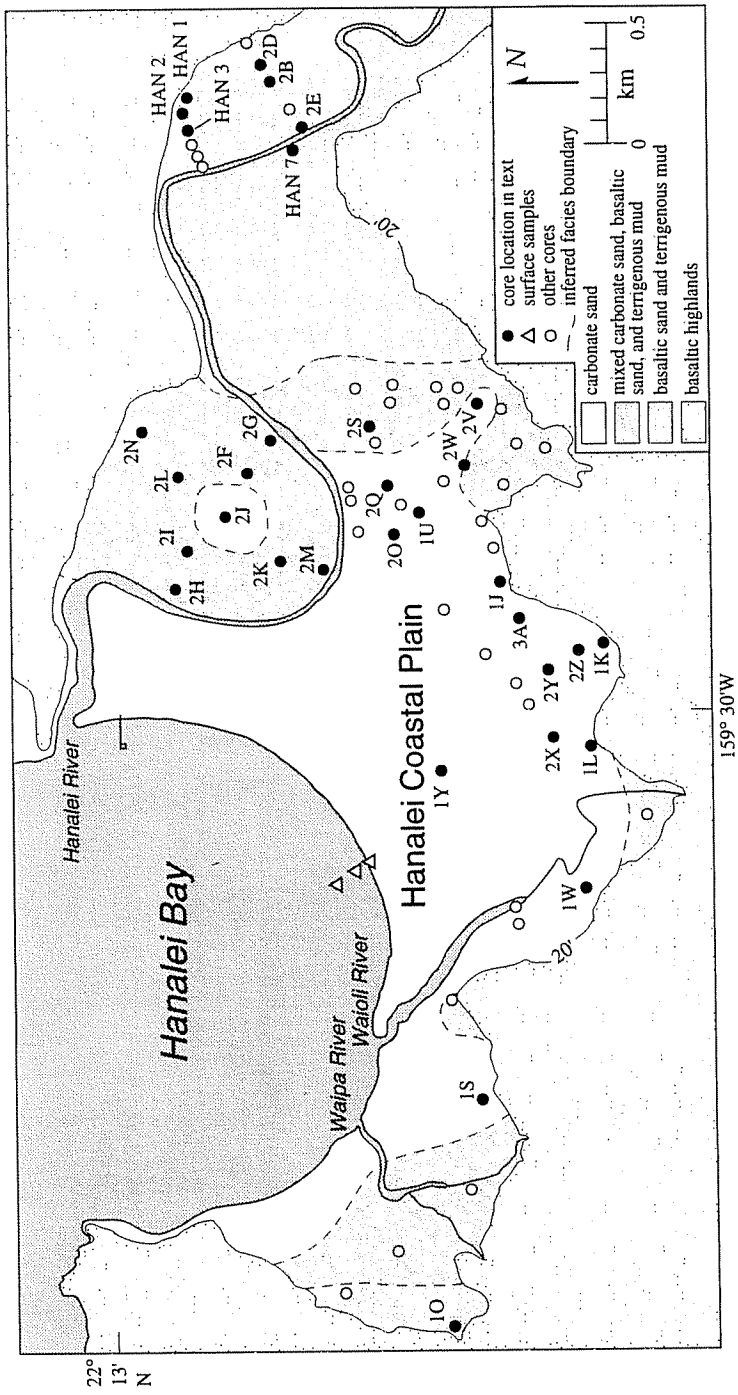


Figure 3: Facies underlying surface fluvial deposits on the Hanalei coastal plain. The location of each core is also shown.

Woody samples were gently crushed and dispersed in deionized water, and then given hot HCl washes to eliminate carbonates and alkali (NaOH) washes to remove secondary organic acids (written communication, Beta Analytic, 1994).

Each of the three short cores used for cesium-137 and lead-210 isotope dating had grass rooted in ~5 cm of grayish-brown silt at the ground surface. Below this, there was approximately 25 cm of grayish brown silt. Occasional clasts of fine and very-fine reddish brown sand were enclosed in the silt with the percentage of sand increasing with depth. The bottom 10-20 cm of each core was fine sand or very-fine silty sand. Samples for cesium and lead isotope levels measurement were removed from evenly spaced and measured layers of the three short cores. Wet samples ranged in mass from 3.5 to 5.5 g. Each sample's water percentage was measured by weighing before and after drying at 60° C. The samples were then ground into a fine powder with a mortar and pestle and dried again for 24 hours at 60° C. These were sealed in individual containers and set aside for three weeks of "gassing" (releasing radon gas into the container). At the end of three weeks, each sample spent two days in the gamma spectrometer in Gary McMurtry's laboratory at the University of Hawaii, Department of Oceanography, where Max Cremer recorded isotope levels.

Linear interpolation between radiocarbon dates was used to determine long-term sediment accumulation rates. When possible, multiple dates and depths were used, but if only one date was obtained from a specific core, the present ground surface was used as a second depth and date (Table 1). The range of sample depth and the first standard deviation range of the calibrated radiocarbon dates were used to determine the sediment accumulation rate error. The deepest layers containing cesium and lead were used as the AD 1954 and 150 year-old horizons respectively when calculating sedimentation rates.

TABLE 1: Radiocarbon dates and sediment accumulation rates. Samples dated by Beta Analytic.

Beta ID #	Core	Depth (cm)	Elev. (m) (above msl)	^{14}C B.P. (1 σ)	Material	Cal. yr. B.P.	Accum. Rate (mm/yr)
55542	Han 1	200-228	2.9	3540 \pm 100	Plant detritus	3970 - 3690	0.56 \pm 0.06
55543	Han 1	309-312		5390 \pm 60	Peat	6290 - 6110	0.42 \pm 0.11 (DI)
55539	Han 1	458		6170 \pm 120	Wood	7180 - 6850	0.50 \pm 0.01
55535	Han 2	195-200	2.7	3520 \pm 100	Peat	3870 - 3630	2.01 \pm 0.65 (DI)
55536	Han 2	427-436		4270 \pm 80	Wood	4860 - 4620	0.65 \pm 0.02
55534	Han 3*	380	2.7	4240 \pm 100	Wood	4860 - 4570	0.53 \pm 0.02
55537	Han 3*	578-600		4370 \pm 70	Organic soil	4980 - 4840	2.53 \pm 0.68 (DI)
55541	Han 7*	345-355	4.3	3690 \pm 100	Plant detritus	4140 - 3860	0.91 \pm 0.03
55538	Han 7*	389-400		3650 \pm 90	Wood	3960 - 3690	0.81 \pm 0.03
55540	Han 7*	649		3790 \pm 110	Wood	4280 - 3940	1.20 \pm 0.04
68764	1K	210	2.9	4160 \pm 60	Carbonate sand	4800 - 4580	0.88 \pm 0.04
68765	1O	385-400	5.8	4540 \pm 80	Wood	5310 - 5000	1.03 \pm 0.05
68766	1O	695-700		6090 \pm 90	Wood	6940 - 6740	1.58 \pm 0.07
68768	1S	330-340	2.9	3800 \pm 80	Carbonate sand	4260 - 3980	1.16 \pm 0.49
68769	1W*	211-217	2.3	3280 \pm 80	Carbonate sand	3550 - 3340	0.45 \pm 0.01
68770	1W*	310-318		2700 \pm 70	Carbonate sand	2770 - 2670	0.76 \pm 0.04
68771	1Y	37-42	4.1	2110 \pm 80	Carbonate sand	2160 - 1940	1.86 \pm 0.34 (DI)
68773	2B	482-485	3.7	4220 \pm 110	Wood	4840 - 4450	1.02 \pm 0.02
68774	2B	630-640		4790 \pm 70	Wood	5580 - 5320	0.81 \pm 0.04
68776	2D	331-334	3.4	4550 \pm 60	Wood	5290 - 4990	0.62 \pm 0.03
68777	2E	361-364	4.3	1440 \pm 70	Wood	1310 - 1190	1.15 \pm 0.04
68779	2G	217-220	2.6	1550 \pm 60	Wood	1410 - 1320	0.19 \pm 0.02
68781	2I	455-463	1.2	2970 \pm 60	Wood	3100 - 2940	1.04 \pm 0.05
68782	2J*	143-150	1.4	4100 \pm 60	Carbonate sand	4810 - 4620	2.29 \pm 1.01 (DI)
68783	2J*	165		2580 \pm 60	Wood	2730 - 2370	1.17 \pm 0.04
68784	2M	322-328	1.1	2530 \pm 80	Carbonate sand	2720 - 2410	0.65 \pm 0.05
68785	2N*	215-220	1.7	3650 \pm 130	Carbonate sand	4120 - 3700	1.27 \pm 0.09
68786	2N*	258-260		3130 \pm 110	Carbonate sand	2830 - 2630	0.56 \pm 0.04

68787	2O	129-142	2.3	2640 ± 80	Carbonate sand	2780 - 2620	0.50 ± 0.04
75908	2Q	26-38	2.4	2420 ± 60	Carbonate sand	2480 - 2310	0.14 ± 0.03
75909	2S	345-359	2.1	3240 ± 110	Carbonate sand	3680 - 3390	1.00 ± 0.06
75910	2V	107-110	2.1	1510 ± 60	Wood	1410 - 1310	0.80 ± 0.04
75911	2V	110-130		2930 ± 70	Carbonate sand	3110 - 2860	0.40 ± 0.05
75912	2V	157-167		3080 ± 70	Carbonate sand	3340 - 3120	0.50 ± 0.03
75913	2W	142	1.8	2930 ± 80	Carbonate silt	3160 - 2900	0.47 ± 0.02
75914	2X	188-195	2.9	modern	Wood	modern	-----
75915	2X	195-200		3600 ± 50	Carbonate sand	4100 - 3960	0.49 ± 0.01
75916	2Y	54-66	2.9	2970 ± 100	Carbonate sand	3250 - 2920	0.20 ± 0.03
75917	2Z	67-75	2.9	2920 ± 120	Carbonate sand	3320 - 2950	0.23 ± 0.03
75918	3A	133	2.9	modern	Wood	modern	-----
75919	3A	155-163		2750 ± 130	Carbonate sand	3120 - 2760	0.09 ± 0.02 (DI)
71400	beach surface			1820 ± 50	Carbonate sand	1300 - 1190	0.54 ± 0.05
71401	submerged in 1.5 m of water from surf zone bar			1680 ± 60	Carbonate sand	1200 - 1020	
71402	submerged in 3 m of water from nearshore			1560 ± 70	Carbonate sand	1070 - 910	

* = Cores with overlapping or inverted ages

DI = Sediment accumulation rate over dated interval between adjacent samples. All other accumulation rates are based on surface to depth interval.
core elevation error = ±0.25 m

DESCRIPTION

The stratigraphy of the coastal plain can be separated into three paleoenvironmental units: terrigenous sediment, marine carbonate sand, and mixed terrigenous and marine carbonate sediment. Terrigenous sediment consists of red-brown clay, red-brown silt, black silt, and black basaltic sand facies. The marine carbonate sand consists of whole and fragmented skeletal carbonate from foraminifera, mollusks, coralline algae, echinoids, and corals. The mixed terrigenous and marine carbonate sediment consists of black silt or black sand and fragments of carbonate marine organisms ranging in size from very fine to very coarse sand.

In most cores, the uppermost facies is red-brown mud, overlying black silt and black basaltic sand. The Soil Conservation Service (1972) described the red-brown silt and clay as containing clay minerals weathered from basalt; additionally, X-ray diffraction indicates the presence of augite and anorthite. As a result, red-brown mud is interpreted as fluvial deposits related to modern river overbank deposition during floods. Black silts, which are not always present in cores, are inferred to indicate marine wedge influenced relict oxbows and meander depressions that have been heavily vegetated, the decay of which has produced traces of iron sulfide. Black basaltic sand facies, with rounded sand and gravel, are interpreted to represent former river channels or channel-proximal flood deposits and show a history of channel meandering associated with the Hanalei, Waioli, and Waipa rivers. The content of the carbonate sands indicates they are typical of Hawaiian nearshore and littoral deposits (Moberly *et al.*, 1965), and are interpreted as representing former beach or nearshore marine environments. Mixed terrigenous and carbonate (fluvial-marine) sediment is inferred to represent the confluence of fluvial and marine environments (i.e., a river mouth bar or fluvial channel routinely invaded by a tidal marine front). Marine carbonate sand underlies the channel

and levee sands both conformably and unconformably. There are sites near the rivers, however, where no marine sand is found. In these cases, the fluvial-marine facies commonly underlie the fluvial unit (Fig. 3 and Appendixes A and C).

Core Descriptions

Figure 4 shows four representative cores from the Hanalei coastal plain. Core 1L is located next to the mountains ≥ 200 m east of the Waioli River at an elevation of 2.9 m (Fig. 3). The top 2.17 m of core 1L is a clay-rich terrigenous mud. At 2.17 m, the sediment becomes sand, and between 2.17 and 2.46 m of depth there is a gradual increase in the amount of carbonate sand. Below 2.46 m, the sand is carbonate, virtually identical in content to the carbonate sand found on the modern beach and littoral system of Hanalei Bay. From 2.46 to the bottom of the core at 4.0 m, the sediment is various shades of white and gray carbonate sand. The lowest 0.69 m of the core has coarse sand, and the lowest 0.10 m contains some gravel-size sediments and pieces of coral. Because of the core's elevation at 2.9 m (msl), the carbonate sand between depths 2.17 and 2.9 m is above modern mean sea level.

Core 1J is situated *c.* 0.75 km northeast of core 1L, and, like core 1L, is 10 to 30 m from the break in slope where the coastal plain meets the basaltic uplands (Fig. 3). The two cores are also both at 2.9 m elevation. The upper 48 cm of this core was not recovered during coring. The top sediment is a dark terrigenous mud that becomes coarser with depth (Fig. 4). At 0.75 m, the sediment is a mixed sand and silt before becoming almost completely basaltic sand by 0.87 m depth, and that sand continues to 1.15 m. From 1.15 m to 1.28 m there is a gradual change from terrigenous basaltic sand to marine carbonate sand. Between 1.28 m and the bottom of the core at 5.15 m, the core contains medium and coarse marine carbonate sand of various shades of white, yellow,

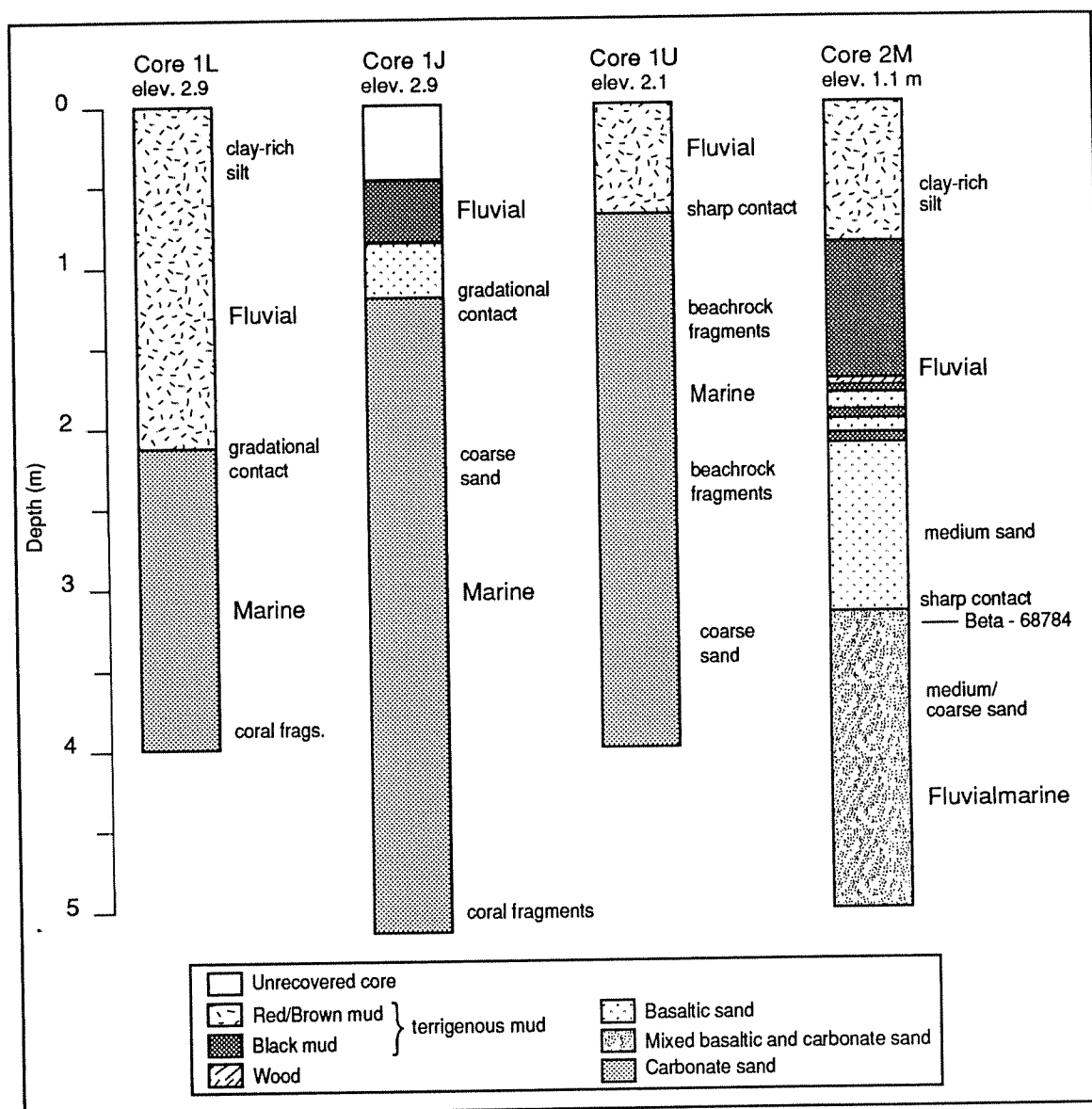


Figure 4: Four cores showing typical stratigraphy found on the Hanalei coastal plain in detail. Figure 3 shows the location of these four cores. Dated sample in core 2M (2720 - 2410 cal. yr. BP, Beta #68784) is carbonate in fluvialmarine sand. Depth is in meters below ground surface.

and brown. Coral pieces slightly less than 1 cm in length are found at 4.00 to 4.05 m, whereas coral pieces larger than 1 cm long are found between 5.09 and 5.15 m. Here again, the core top is 2.9 m above mean sea-level, placing all 1.62 m of marine sediments in the range 1.28 to 2.9 m depth above mean sea-level.

Core 1U is positioned c. 450 m northeast of core 1J, midway between the basaltic uplands and the present-day meander of the Hanalei River (Fig. 3). This core contains 0.70 m of terrigenous mud with a small amount of fine sand overlying thick marine carbonate sand (Fig. 4). A sharp contact, inferred to be a disconformity, separates the two facies. The marine facies contains several layers of coarse sand and beachrock fragments. The core top is at an elevation of 2.1 m, resulting in the 1.4 m of marine sand between 2.1 and 0.70 m depth being above modern mean sea level. This core typifies the stratigraphic column for much of the Hanalei coastal plain: relatively thin terrigenous facies of mud and sand disconformably overlying thick marine carbonate medium sand containing layers of coarse sand, mollusks, coral, and beachrock fragments.

Unlike the other three cores, core 2M does not contain carbonate sand from a strictly marine environment (Fig. 4). It is located in the extreme southwest part of the Hanalei River meander and is typical of the cores found inside the meander (Fig. 3). It contains 0.88 m of clay-rich red-brown silt overlying 0.84 m of black silt. Below this are a series of thin alternating layers consisting of wood, black mud, and medium basaltic sand. Between the depths of 2.10 and 3.17 m, medium basaltic sand is dominant. A sharp contact, an inferred disconformity, separates this strictly fluvial facies and the fluvial-marine sand underlying it. The fluvial-marine facies is medium to coarse sand in size and was radiocarbon dated. The carbonates at depth 3.22 to 3.28 were dated as being 2720 - 2410 calibrated (cal) yr. B.P. (Beta #68784; Table 1). With a ground surface

elevation of only 1.1 m, core 2M is significantly lower than the other cores described. As a result, the top of the fluvial-marine sand is 2.07 m below modern mean sea level.

Noncored Regions

Two regions of the coastal plain were not cored. The first is the east end of the coastal plain, which lies within the Hanalei National Wildlife Refuge and has been altered by the creation of wetlands for waterfowl and taro farming. Although the two rows of cores, HAN 1-HAN 6 and 2A-2E, and core HAN 7 were taken in relatively undisturbed locations, the top portion of cores were not considered reliable due to possible disturbance. The second region not cored is covered by the town of Hanalei and was not cored due to the stratigraphic disturbance associated with the construction of buildings and roads in the town.

Regressive Overlap Boundary

The upward change in facies from marine carbonate sand to fluvial sediment represents a shift in environment of deposition. The conversion of an environment from marine to nonmarine sediment deposition is termed a regression. The contact between the two sediment types is called a regressive overlap boundary (ROB). The top of the marine layer is inferred to represent the most recent preserved time the marine environment occupied a particular location. The bottom of fluvial sediments is inferred to be the earliest time of fluvial deposition. As a result, the ROB represents a period of time that passed between two environments of deposition. This is particularly true if the ROB is also a disconformity as it commonly appears to be on the Hanalei coastal plain, as discussed below. The time span between environments was at least a period of no

deposition but is more likely to be a time of erosion thereby increasing the apparent interval between depositional environments.

The three cores, 2V, 2X, and 3A, contain ^{14}C dated samples from close to or immediately above and below the ROB. Core 2V has a fluvial sample of wood from 107 cm to 110 cm dated 1410 to 1310 cal yr. B.P., and a marine carbonate sand sample from 110 cm to 130 cm depth dated 3110 to 2860 cal yr. B.P. (Table 1). The resulting ROB represents a lacuna of 1450 to 1800 years. The other two cores contain samples of modern wood directly above the ROB and give 3960 - 4100 year (core 2X) and 2760 - 3120 year (core 3A) lacunas. Three samples of carbonate sand from the beach surface and littoral zone of the modern bay give ages of 1300 - 1190 cal yr. B.P., 1200 - 1020 cal yr. B.P., and 1070 - 910 cal yr. B.P. (Table 1). If such antecedent carbonate sand was deposited in core 2V below the ROB, the ROB lacuna may be 150 to 890 years (original lacuna length 1450 - 1800 years minus extreme ages of the antecedent carbonate sand 1300 and 910 years). As a result, an ROB on a disconformity may represent a lacuna as great as 4100 years, where the underlying marine carbonates have been partially eroded, to as little as 150 - 890 years, where paleoshorelines contained volumes of antecedent marine sediments. The lacuna length depends on the amount of erosion and how soon deposition replaces it at a particular location of the coastal plain.

Rates of Sediment Deposition

Long-term (≥ 1000 yr) sediment accumulation rates on the Hanalei coastal plain were calculated using radiocarbon dates from layers of carbonate sand, woody plants or plant detritus. Short-term (≤ 150 yr) sedimentation rates were calculated separately using sediment horizons dated independently with both ^{137}Cs and ^{210}Pb .

In sections of the floodplain, the long-term sediment accumulation rate increases as the distance to the Hanalei River decreases (Fig. 5). Areas with the highest accumulation rates indicate where floodplain erosion and deposition associated with the Hanalei River has been most active. Five cores with multiple dates display stratigraphic inversion where older dates overlay more recent dates (Table 1). In three of these cases, the deeper sample was used to calculate the accumulation rate because the stratigraphic inversion of these dates suggests that the upper-most sample was reworked before final deposition. In the fourth case, core HAN 7 (1.16 ± 0.49 mm/yr), the sediment accumulation rate was calculated by averaging the rates given by the three dated samples. In the fifth case, core 1W (0.61 ± 0.02 mm/yr), the upper-most date represented the contact between the overlying fluvial sediment and the marine layer and was used to calculate the accumulation rate of the fluvial sediment. Contours were not placed on the Waipa floodplain or the Hanalei floodplain southeast of the U-meander because of insufficient data.

Three areas of the coastal plain show steep gradients in the amounts of sediment accumulation (i.e., the contour lines are close together). These areas include inside the large meander of the Hanalei River, between the Hanalei River and the basaltic uplands on the east end of the coastal plain, and directly south of the Hanalei River meander between the river and the mountains (Fig. 5). In the first two locations, the contours are parallel to the local reach of the Hanalei River. In the third case, the contours are perpendicular to the river.

Results from the ^{137}Cs and ^{210}Pb analyses on the three short, thick cores were somewhat ambiguous. Core 1 was obtained 100 m from the Hanalei River south of the meander while cores 2 and 3 were obtained 400 m and 650 m from the river, respectively. While the three cores showed increased sedimentation closer to the river, they gave very

different sedimentation rates depending on the dating technique used. Lead-210 rates varied from 2.32 ± 0.77 mm/yr in core 1 to 0.94 ± 0.12 mm/yr in core 3. From the same cores and samples, cesium-137 gave sedimentation rates almost an order of magnitude greater with 26.1 ± 2.9 mm/yr and 15.1 ± 0.5 mm/yr from cores 1 and 3 respectively (Fig. 6).

DISCUSSION

The Hanalei River follows the pattern set by many rivers by obtaining most of its sediments from specific sections of its basin as exemplified by the Huanghe (Yellow River) of northern China (Zhang *et al.*, 1990). The steep, weathered mountains in the headwaters of the Hanalei River basin are particularly susceptible to erosion, especially after devegetation (Ebisemiju, 1990). Because of a lack of roads and trails into the upper valley, any devegetation in the upper Hanalei basin appears to be from natural causes. While these natural erosional processes supply the river with sediment, the lower river section, that lying on the coastal plain, seems to be a sink for fluvial sediment.

Sediment Accumulation Rates

Long-term sediment accumulation rates (≥ 1000 yr) as determined by radiocarbon dates reflect patterns of erosion and subsequent preferential deposition in eroded areas. The area inside the meander of the Hanalei River shows sediment accumulation rates that are proportional to the distance from the river (Fig. 5). This region has also been eroded by the movement of past Hanalei River channels (Fig. 7a and 7b). The increasing sediment accumulation rates are a result of preferential infilling of the river paleochannel rather than more frequent flooding closer to the present river channel.

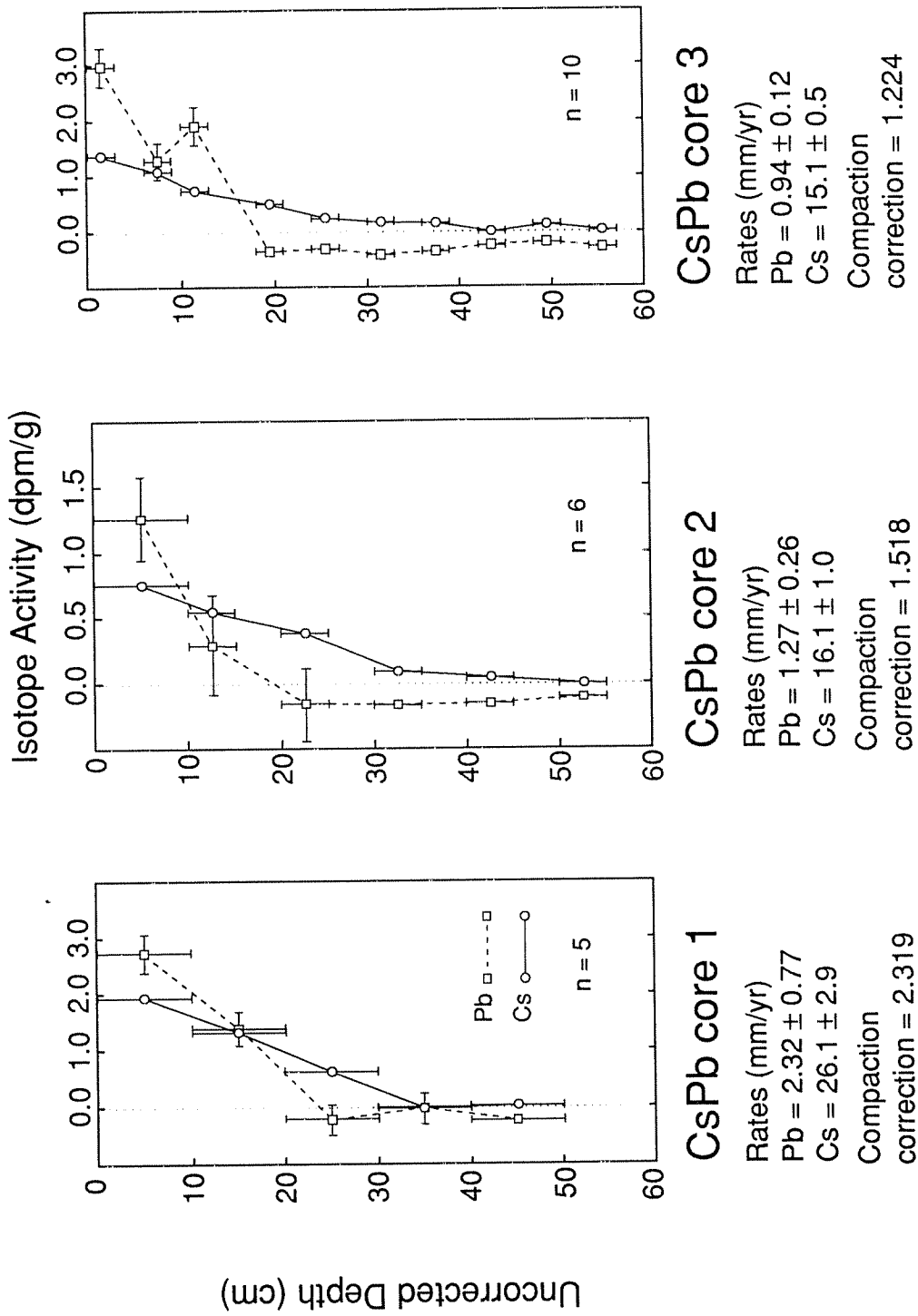


Figure 6: Profiles of three cores showing depth and cesium and lead radioactivity strength of each tested sample. The horizontal errors in many of the lead samples and all of the cesium samples are smaller than the squares or circles used to show their locations. The locations of these cores are shown in Figure 5.

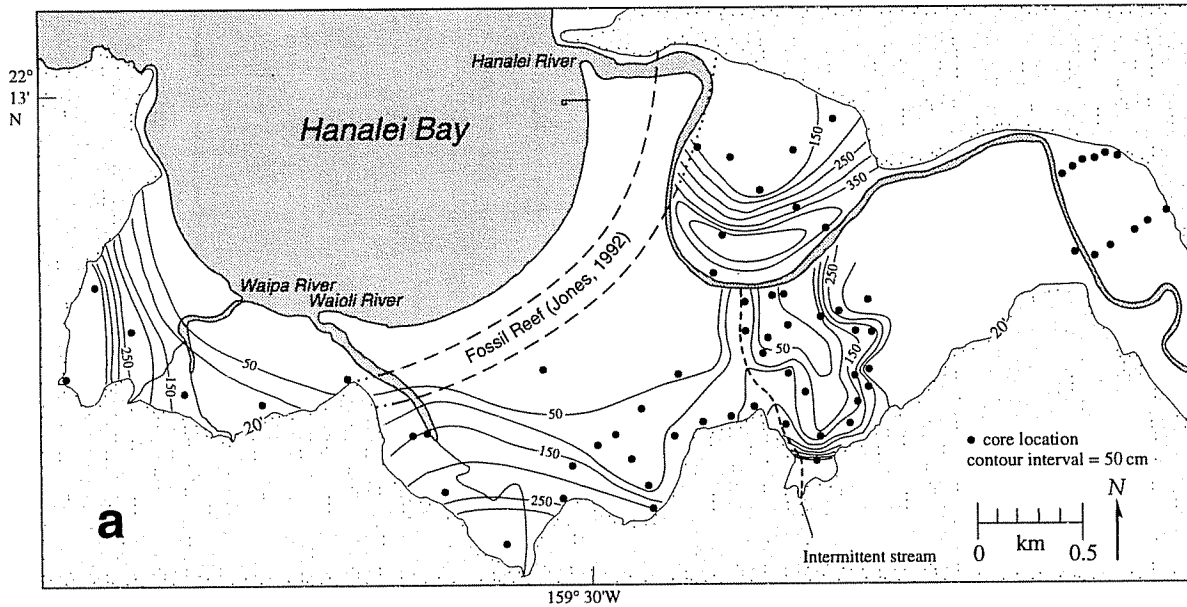


Figure 7a: Fluvial sediment thickness above the marine lithosome. The contour interval is 50 cm. Also shown is the inferred fossil reef of Jones (1992).

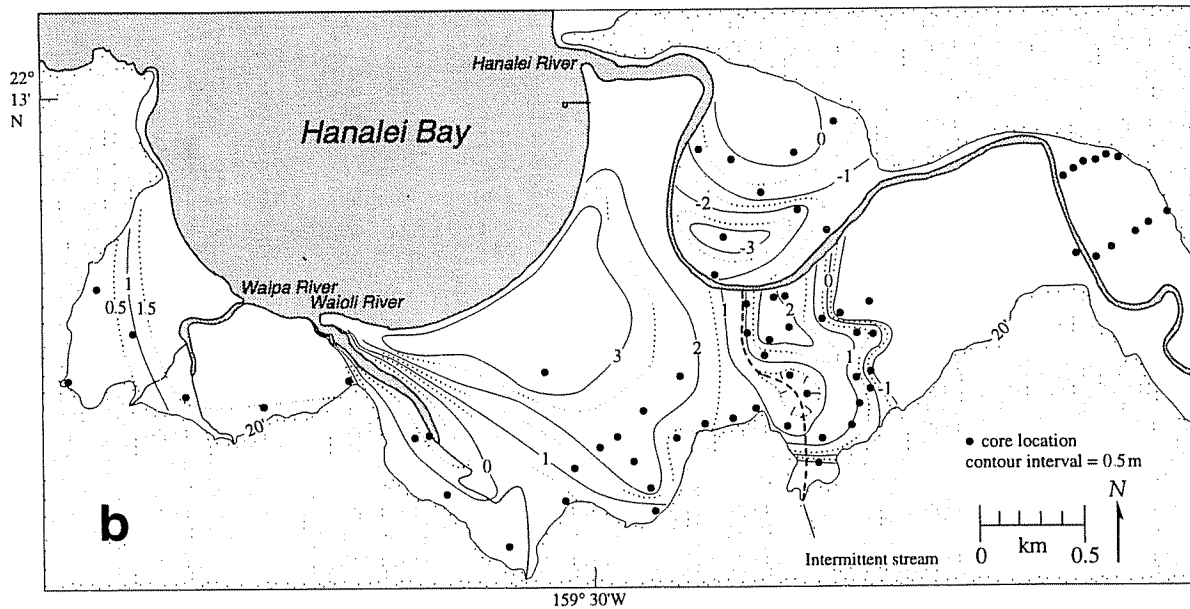


Figure 7b: Elevation of the surface of the marine and fluviomarine facies underlying fluvial flood deposits. Contour interval is 0.5 m. Modern mean sea level is the reference datum.

The east end of the coastal plain, between the Hanalei River and the basaltic uplands, has been perhaps the most fluviially active section of the coastal plain. It certainly has the highest sediment accumulation rates (approaching 3.0 mm/yr) (Fig. 5). Using only ground surface to sample depth to determine accumulation rates, there is a steep gradient in rates increasing towards the river (Table 1 and Fig. 5). Cores HAN 1, HAN 2, HAN 3, and 2B show some variation in sediment accumulation rates (Table 1) which appears to be associated with the infilling of a passing paleochannel meander of the Hanalei River. Although core HAN 1 has moderate rates from sample 1 to the ground surface (0.56 ± 0.06 mm/yr) and between sample 2 and sample 1 (0.42 ± 0.11 mm/yr), there is a significant increase in the accumulation rate between samples 3 and 2 (2.01 ± 0.65 mm/yr), which covers the time period between *c.* 6850 and 6290 cal yr. B.P. Core HAN 2 also shows a medium accumulation rate from sample 1 to the ground surface (0.53 ± 0.02 mm/yr), but a large increase between samples 2 and 1 (2.53 ± 0.68 mm/yr), which represents *c.* 4620 to 3870 cal yr. B.P. Samples 1 and 2 of core HAN 3 have overlapping dates by twenty years so this core is not the best example to base hypotheses on. Sample 2 does have a significantly higher sediment accumulation rate to the ground surface than sample 1 (1.20 ± 0.04 mm/yr versus 0.81 ± 0.03 mm/yr). Since the low rate from sample 1 to the surface is factored into the rate of sample 2 to the surface, the rate between the two samples must have been very rapid. Additionally, since the two dates overlap, there is a possibility that they were deposited during a single high discharge event. Core 2B shows relatively high sediment accumulation rates from both samples 1 and 2 (1.04 ± 0.05 mm/yr and 1.17 ± 0.04 mm/yr, resp.), but the rate jumps to 2.29 ± 1.01 mm/yr between the two samples. These samples span the period *c.* 5320 to 4840 cal yr. B.P.

The general sediment accumulation trend in this area indicates that the Hanalei River has been migrating westward. If the high sediment accumulation rates do indeed represent infill of abandoned channels, the four cores dating such channels weakly support a westward migration. Core location HAN 1 was abandoned before location HAN 2, but, as previously mentioned, HAN 3 does not follow the westward migration. Core 2B appears as though it should be younger than core HAN 2, however, it is not in line with the other cores and therefore cannot be eliminated for being older than HAN 2. A young sample (1310 - 1190 cal yr. B.P.) found at depth (361 - 364 cm) and the resulting high sediment accumulation rate (2.91 ± 0.15 mm/yr) in core 2E shows that the channel infilling continued to the west from core 2B.

Unlike the first two regions, between the Hanalei River meander and the mountains, the sediment accumulation rate contours are perpendicular to the river and rather low (max. = 1.00 ± 0.06 mm/yr; Table 1 and Fig. 5). Rather, these contours are parallel to paleoshorelines shown in Figures 8, 9, and 10. Coastal erosion at the mouth of the Hanalei River channel crossing these shorelines is probably the cause of erosion in this area. Although preferential deposition in low areas after erosion had ceased would create the high sediment accumulation rates, the erosion was significantly long enough ago that the overall rate has become rather low.

Sedimentation Rates

The short-term sedimentation rates (≤ 150 yr) derived from the ^{210}Pb profiles are more consistent with the long-term sediment accumulation rates calculated using radiocarbon than with the short-term rates derived from the ^{137}Cs profiles. Despite the fact that calculating the sedimentation rate by using the deepest appearance of ^{137}Cs as the 1954 horizon is not the best methodology (Milan *et al.*, 1995), the lack of ^{137}Cs peaks

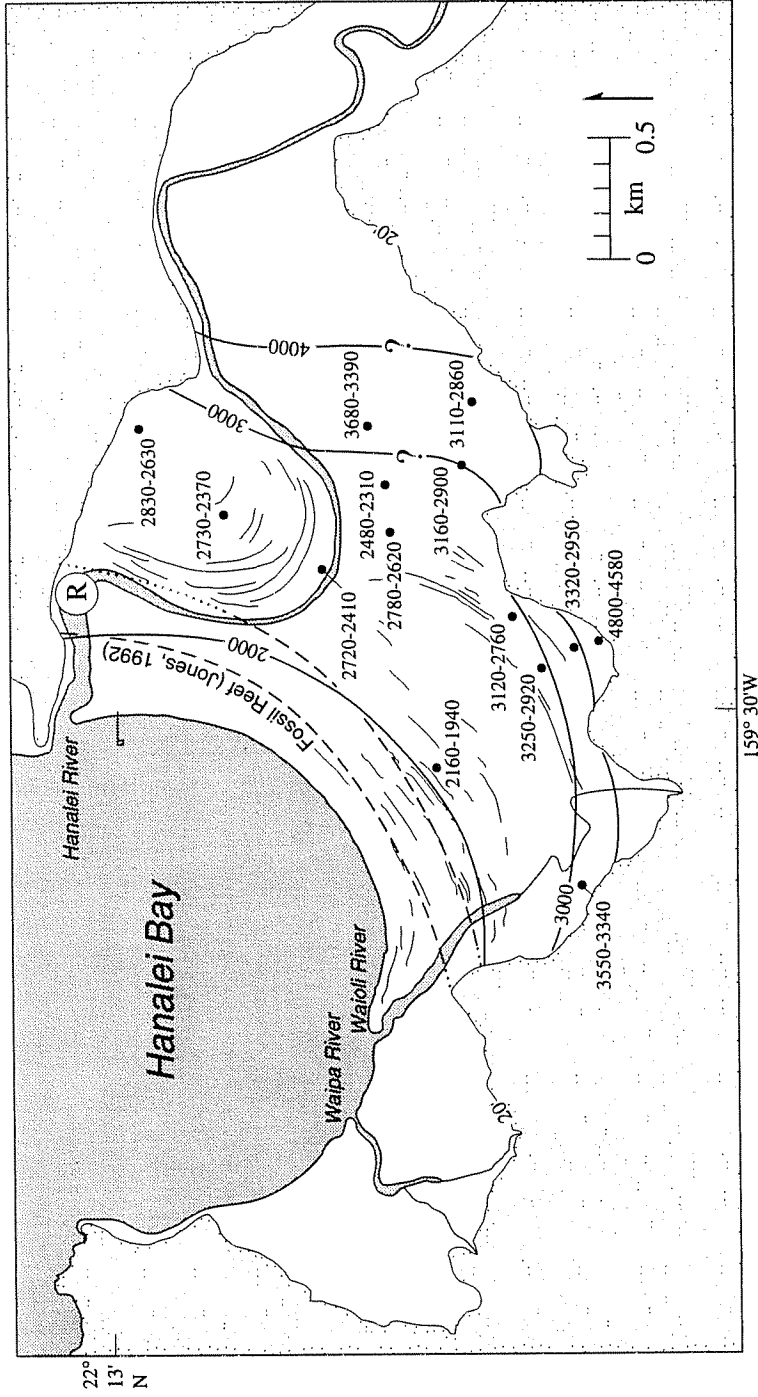


Figure 8: Isochrons of the top of the marine lithosome indicating possible paleoshorelines. All dates are in calibrated radiocarbon years before present (BP). R represents an *in situ* reef described by Jones (1992). Beach accretion ridges, as well as the sample dates and modern bay shape, help constrain the reconstructed shape of paleo-Hanalei Bay.

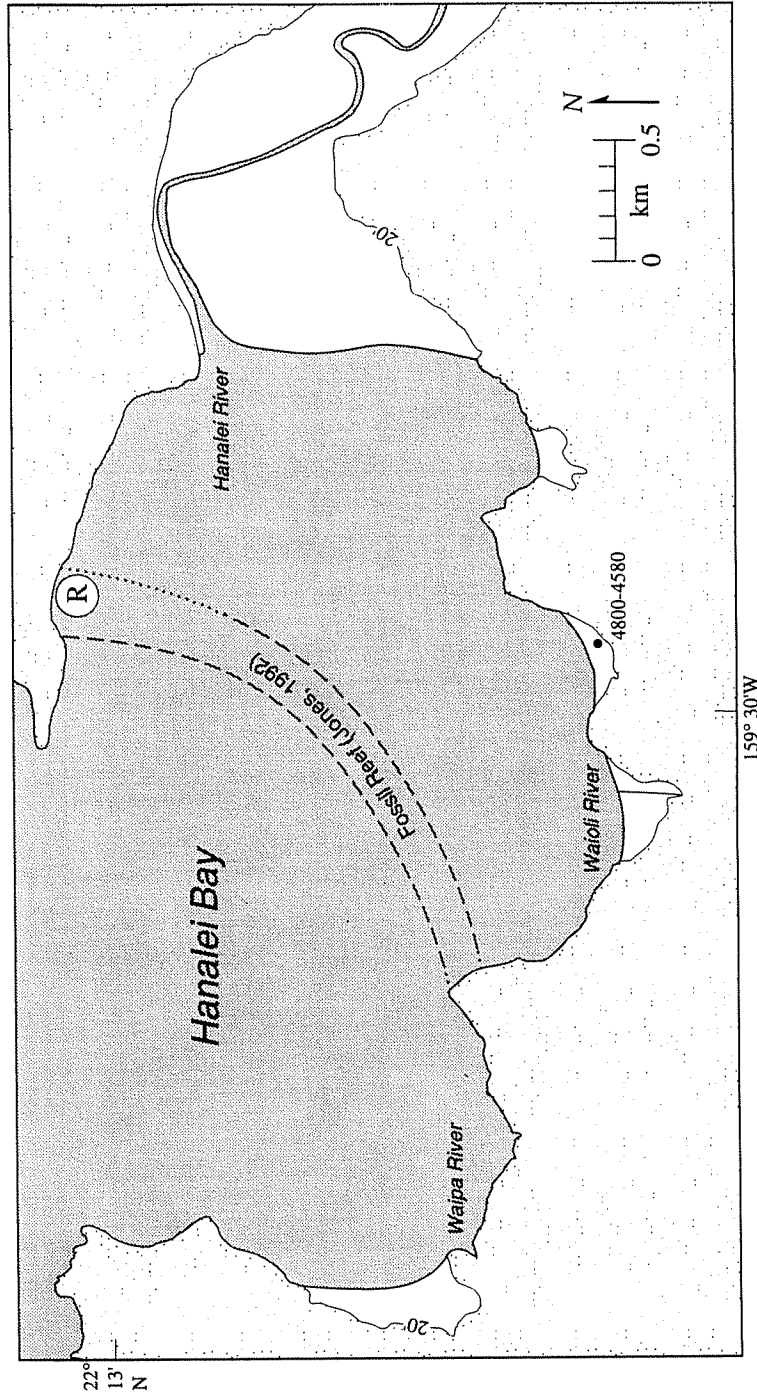


Figure 9: Dated samples from the top of the marine lithosome indicate this 4000 yr. paleoshoreline. All dates are in calibrated radiocarbon years before present (BP). R represents an *in situ* reef described by Jones (1992).

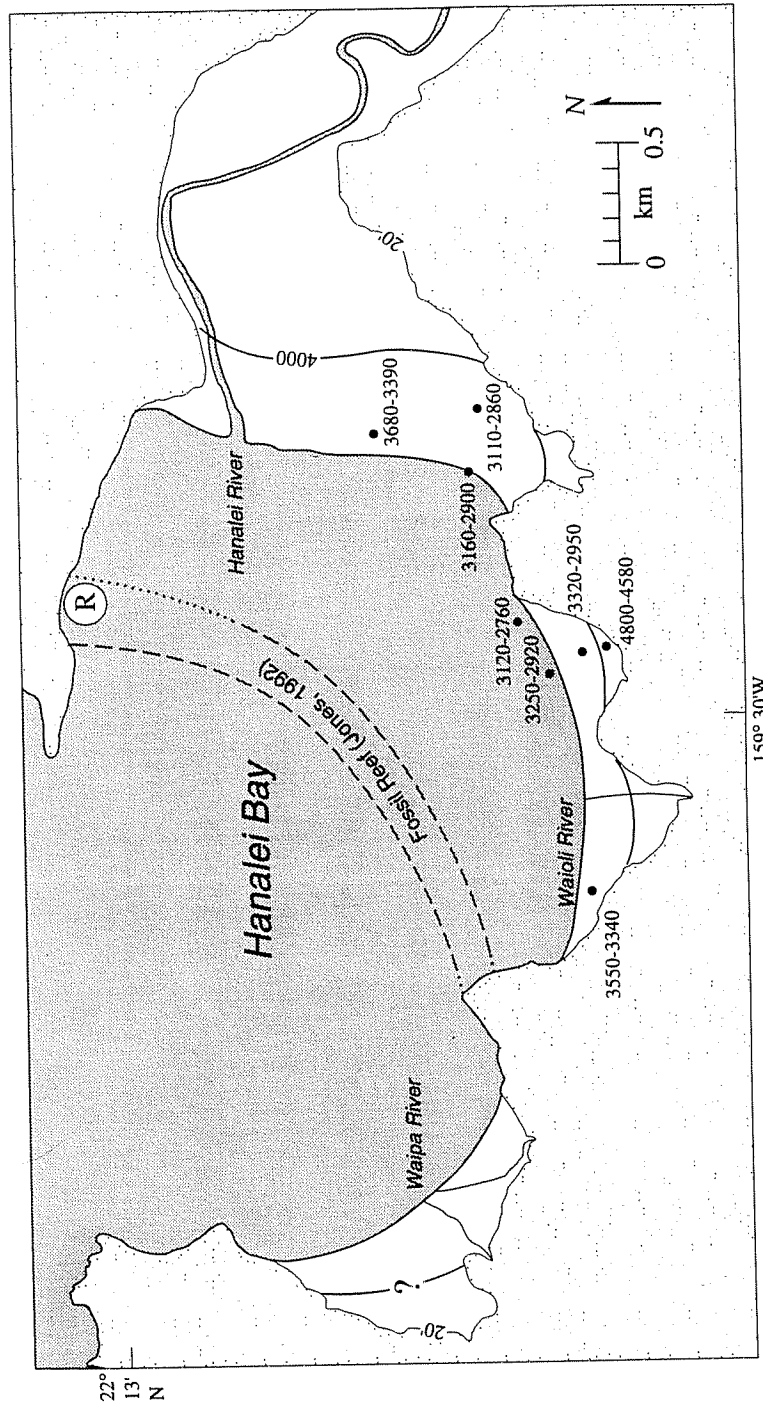


Figure 10: Dated samples from the top of the marine lithosome indicate this 3000 yr. paleoshoreline. All dates are in calibrated radiocarbon years before present (BP). R represents an *in situ* reef described by Jones (1992).

in the profiles left little choice (Fig. 6). In CsPb core 1, the deepest significant amounts of ^{137}Cs appear at 25 uncorrected cm. If 1954 ^{137}Cs deposition has decayed to below detectable levels, this could be the 1958 or even 1963-1964 horizon. If this is true, the sedimentation rate could be 16.1 or 18.7 mm/yr respectively which is even farther from the standards set by ^{14}C and ^{210}Pb . If the lead and carbon standards are correct, the first ^{137}Cs should appear at ~ 4.0 cm depth of core 1. All ^{137}Cs found below ~ 4.0 cm would have to be accounted for by downward migration.

Core 2 has the same problems as core 1. The sedimentation rate of 16.1 ± 1.0 mm/yr far outpaces the rates given by the other two radioisotopes in this core. There is a large increase in the amount of ^{137}Cs radioactivity at 22.5 uncorrected cm (Fig. 6). If this is the 1954 horizon, the sedimentation rate would be 8.54 mm/yr, and the ^{137}Cs below 25 cm migrated downward. The 22.5 cm sample could also be the 1963-1964 horizon, but that would result in a sedimentation rate of 11.0 mm/yr. Following the rate set by ^{210}Pb (1.27 ± 0.26 mm/yr), the deepest ^{137}Cs should be is 3.3 cm, well within the shallowest sample taken from this core.

Although it contains more peaks in its ^{137}Cs graph, with a calculated ^{137}Cs sedimentation rate of 15.1 ± 0.5 mm/yr, core 3 suffers from the same problems as the cores 1 and 2 (Fig. 6). Cesium-137 may extend to a sample depth of 49.5 cm. If this value is significant and is due to anything other than migration, the sedimentation rate will only increase. No ^{137}Cs was found in the 43.5 cm sample, but it was found in the 37.5 cm sample. If this quantity is significant and represents the 1954 horizon, the calculated sedimentation rate only decreases to 11.5 mm/yr, and, if it is the 1958 or 1963 horizon, the rate increases to 12.8 or 14.8 mm/yr respectively. The next significant increase in ^{137}Cs activity is in the 19.5 cm sample. However, even if this is the 1954

horizon, the sedimentation rate is still almost 6 mm/yr. Not until 3.07 cm depth would the 1954 horizon be found if ^{137}Cs were to give the same sedimentation rate as ^{210}Pb .

In all three cores, the ^{137}Cs gives much higher sedimentation rates than the ^{210}Pb . Because the ^{137}Cs rates are so (unrealistically?) high, the ^{210}Pb rates are consistent with the long-term sediment accumulation rate found with radiocarbon dates, the methodology used to determine the two sets of rates is more acceptable for ^{210}Pb than it is for ^{137}Cs , and the appearance of ^{137}Cs below ^{210}Pb in the cores, the rates calculated from the ^{210}Pb profiles are more acceptable than those found with the ^{137}Cs profiles. The possibility of downward migration by ^{137}Cs is considered likely on the Hanalei coastal plain resulting in unreliable sedimentation rates calculated with ^{137}Cs . Krishnaswami *et al.* (1971) found sedimentation rates to be 4 mm/yr using ^{137}Cs as compared with 1.2 mm/yr using ^{210}Pb , and consider post-depositional diffusion of ^{137}Cs to be a possible cause of apparent downward movement of ^{137}Cs in their lacustrine sediments. On the Hanalei coastal plain however, leaching would seem to be a more likely cause of ^{137}Cs movement. The fine grain size of the surface sediments in the coastal plain would seem to prevent the unassisted downward diffusion of ^{137}Cs . Additionally, although cesium is not highly soluble, in the very wet environment of the Hanalei coastal plain, its moderate solubility is possibly enough to allow it to be leached downward.

Paleoshorelines

The top of the marine lithosome is assumed to represent the last preserved record of marine deposition. Periodic events, tsunami and hurricane storm surge, have impacted the shoreline around Hanalei Bay during the past, but they are not considered likely to have formed the types and patterns of deposits found throughout the coastal plain. Tsunami typically do not leave extensive, thick marine deposits such as are found on the

coastal plain (Dawson, 1994). Hurricanes may leave such deposits, but historically have approached Kauai from the south or east and so have not created the maximum storm surge and waves in the north-facing bay needed to produce the expanse of marine sediments found (Fletcher *et al.*, 1995). Another possibility, onshore winds, is also considered an unlikely source. Observations of the cored marine facies do not show the well-sorted fine-grained fractionation typical of calcareous eolian transported sediment. The carbonate unit contains moderately-sorted layers of fine, medium, and coarse grained sand as well as poorly sorted layers of all three sizes. While bedding was present in the cores, cross-bedding was not observed. The position of the coastal plain in relation to the sediment source, the bay and beach, also requires a wide range of wind directions to deposit marine sediment in all parts of the coastal plain where it is found. Nor is there a modern analogous location of eolian deposition. Finally, none of the periodic events or eolian transport are likely to be the sole producer of the consistent gradient of younger sediments closer to the bay that is found (Fig. 8).

Radiocarbon dates, corrected for isotopic fractionation and adjusted for the marine reservoir ($\Delta R = 115 \pm 50$; Stuiver and Reimer, 1987), were obtained from the contact between underlying marine sand and overlying fluvial deposits. Dates from the regressive contact in fourteen cores permit the construction of former marine fronts or approximate shorelines (Figs. 8, 9, 10, and 11). No ROB dates were obtained from cores on the Waipa River floodplain. Beach accretion ridges mapped by Moberly (1968) further constrain the placement of paleoshorelines (Fig. 8). Despite this, neither the ridges nor the radiocarbon dates were inflexible guidelines in the construction of the paleoshorelines as can be seen where the 3000 yr shoreline crosses a ridge at a slight angle and passes through a series of cores with dates on either side of 3000 yr. Regardless, as observations of the modern Waioli River mouth indicate, the very dynamic

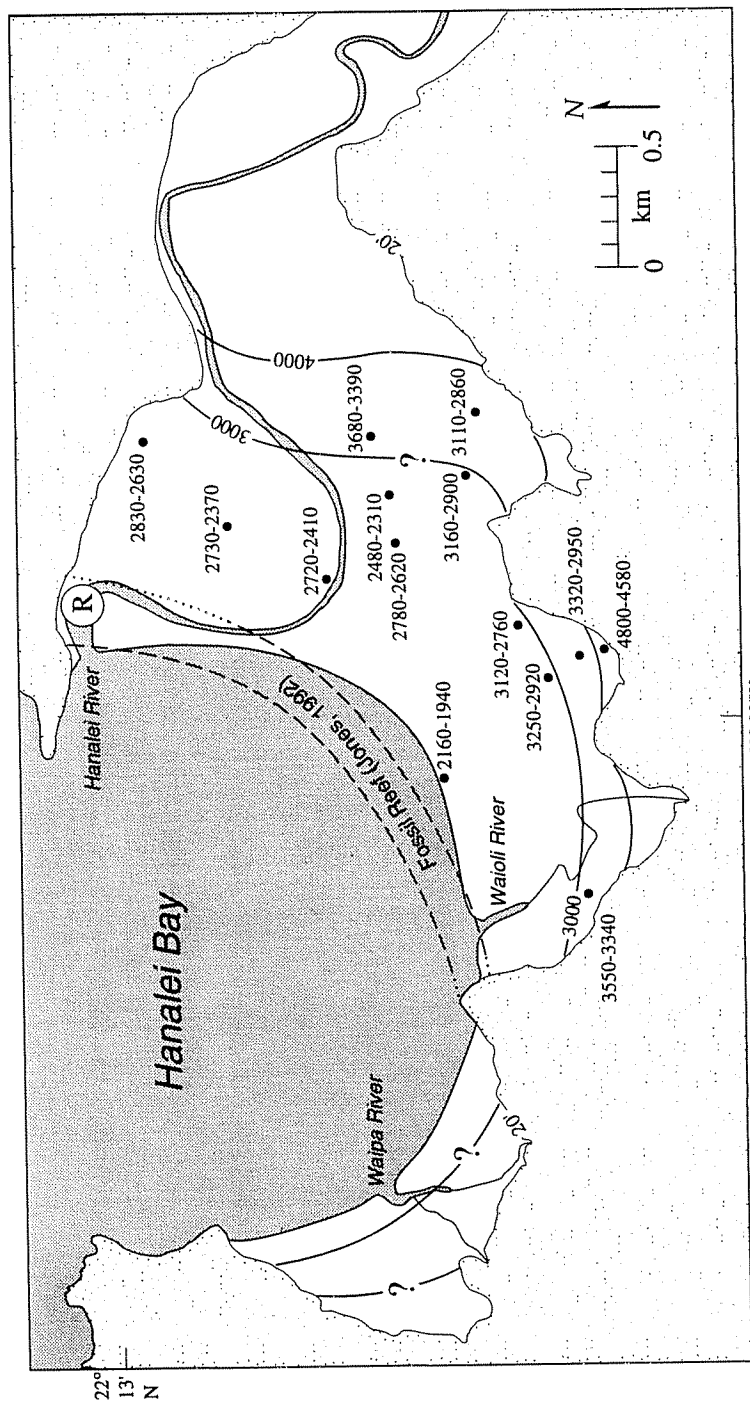


Figure 11: Dated samples from the top of the marine lithosome indicate this 2000 yr. paleoshoreline. All dates are in calibrated radiocarbon years before present (BP). R represents an *in situ* reef described by Jones (1992).

system of migrating bars and spits makes precise paleoshoreline reconstruction problematic. The paleoshorelines have been constructed to represent a mean position in a rapidly evolving location.

The shorelines in Figs. 8, 9, 10, and 11 can be explained by beach progradation owing to an abundant supply of marine sediment or to a relative sea-level fall. However, neither these ridges nor the shorelines indicate whether beach progradation was due to a relative sea-level fall or to an abundant supply of marine sediment.

4000 yr

If sea level stabilized at modern level at the post-glacial culmination, the newly formed Hanalei Bay would have extended to the base of the volcanic highlands. Marine sediment began infilling the bay, and by 4000 yr the shoreline consisted of pocket beaches at the mouths of streams separated by rocky basaltic headlands (Fig. 9). Each pocket beach would have had the concave seaward planform that typifies beaches in semi-protective embayments.

Jones (1992) interpreted a possible *in situ* reef at location R as evidence of a sea-level highstand and proposed a fringing reef stretching most of the way across paleo-Hanalei Bay. Jones (1992) measured the reef at 1.8 ± 0.3 m above present mean sea-level. Samples from this reef date 4200 ± 70 to 3230 ± 80 cal yr. B.P. (Beta #41951, 2, 3, and 4; Jones, 1992). The paleoshorelines portrayed at 3000 yr. B.P. and 4000 yr. B.P. in Figs. 9 and 10 would have permitted reef growth at this location. Jones also hypothesized the existence of a buried reef extending under the town of Hanalei. Reconstructions in Figs. 9 and 10 indicate that Jones' buried reef would have created a barrier reef and lagoon system in paleo-Hanalei Bay. If this were the case, the ROB under the modern coastal plain may reflect lagoonal infilling rather than strictly beach progradation, and

marine sediment accumulation rates would reflect lagoonal infilling rates not beach accretion rates.

3000 yr

By 3000 yr, beach progradation or lagoonal infilling had joined several of the small pocket beaches into three larger beaches separated by the two main basaltic ridges that terminate on the modern coastal plain (Fig. 10). The three beaches were centered around the three river mouths and undoubtedly had dynamic river mouth bar and spit systems that fluctuated with wave energy and fluvial discharge. The mouth of the Hanalei River dominated the largest section of beach and may have meandered across much of its shoreline. Reef growth as a barrier reef, proposed by Jones (1992), was still possible at this time.

2000 yr

By 2000 yr (Fig. 11), the Waioli and Hanalei River sections of beach had prograded enough to join together to form one large beach, while the smaller Waipa River beach continued to prograde until the two beach sections were separated by just the tip of the major basaltic ridge that terminates on the modern coastal plain. The proposed barrier reef would have been partially buried by this time with the exposed section more of a fringe reef than a barrier reef. The presence of elevated marine carbonate sand between the Hanalei and Waioli Rivers indicates that the two rivers never joined (Fig. 7b). If the barrier reef were located as proposed, then it would have also prevented the Hanalei River from meandering too far west and thereby connecting with the Waioli River.

Terrigenous and Marine Lithosomes

Variation in the thickness of terrigenous sediment (Fig. 7a) and the elevation of the surface of the marine and fluvial-marine facies (Fig. 7b) around the coastal plain indicates the locations of past deposition and erosion. On the Waipa coastal plain and the center of the Hanalei coastal plain, the fluvial facies thicken inland and the ROB elevation decreases; but, there are some important deviations from this pattern.

Near the Hanalei and Waioli Rivers and part of the Waipa River, either deep burial by fluvial sediment, or erosion, has caused marine deposits to be absent from the cores (Fig. 3). Deltaic deposition by the river may have prevented marine sediment deposition from reaching these areas. Alternatively, marine sands may have been initially present, and subsequently eroded to a depth exceeding that cored.

Inside the large meander of the Hanalei River, fluvial facies thickness increases towards the south and the elevation of the fluvial-marine facies decreases (Fig. 7a and 7b). The fluvial-marine sediments in the southern part of this area are commonly 250 cm or more deeper than in the northeast, indicating greater deposition, and the ROB elevation is more than 3 m below not only sea level but also the ROB in the northeastern part of the meander, indicating greater erosion. This pattern indicates erosion of the fluvial-marine facies by a paleoriver channel followed by abandonment of the channel and subsequent preferential deposition within the former channel. This is consistent with the meander scars described by Moberly (1968) and a history of channel meandering.

South of the meander, an intermittent stream flows out of the mountains (Fig. 7a and 7b). A localized low area in the surface of the marine unit there coincides with a thickening of the fluvial sediments as well as a disconformity between the two facies. Apparently, following the regression, this stream eroded the marine lithosome before

entering the Hanalei River or the bay, causing the low region which was then filled with fluvial flood deposits.

The eastern end of the marine lithosome plateau is extremely steep where it faces into the Hanalei River valley (Fig. 7b). It is likely that the Hanalei River eroded into the marine sediments here when the paleoshoreline was in this area 3000 to 4000 yr. B.P. (Figs. 9 and 10).

The V-shape in the marine lithosome elevation contours near the Waioli River also indicates erosion of the marine layer (Fig. 7b). The river may have locally eroded as much as 2.5 m of the marine facies.

Barrier Reef Complex

The presence or absence of a barrier reef complex, proposed by Jones (1992), is a central issue in the reconstruction of the middle- to late-Holocene history of the Hanalei coastal plain. The source of the sediment which allowed the shoreline to prograde is a critical piece of the puzzle. The isolation of the bay by rocky headlands severely limits the amount of longshore sediment the bay receives. Although the marine sand in Hanalei Bay does contain basaltic grains and other terrigenous sediments, most of the marine sand in the bay (~75%), on the beach (~80%), and under the coastal plain is derived from marine organisms and not from fluvial discharge (Moberly and Chamberlain, 1964). The only mechanisms left to cause beach progradation are abundant marine production and a relative fall in sea level. A barrier reef would make it much easier for marine production to be the cause of progradation by creating a low energy lagoon shoreward of the reef. Of course, the proposed reef is elevated (Jones, 1992) so a relative fall in sea-level would have to be incorporated into the process. A relative fall in sea-level could account for the progradation with or without the presence of a barrier reef. Regardless of the vertical

movement of sea level, the low energy lagoon behind the reef should be an area of higher deposition for terrigenous sediment than the fore reef. Qualitative observations of marine sediments on both sides of the proposed reef did not appear to fulfill such a requirement. Additionally, the presence of a barrier reef would require a mechanism whereby the reef buries itself in its own sediment.

Hanalei River Meander

The stratigraphy inside the U-shaped meander appears to be typical of areas underlain by fluvial-marine sediment (Fig. 12). The contact between the fluvial and fluvial-marine sediments lies at depths ranging between 100 cm and 480 cm and dates from 2730 - 2370 cal yr. B.P. (Beta #68783) to 2830 - 2630 cal yr. B.P. (Beta #68786). Fluvial deltaic deposition, represented by the underlying fluvial-marine sediment, occurred at the former mouth of the Hanalei River until ~2600 yr. B.P. Overlying the fluvial-marine sediment is fluvial sand marking former river channels and levee deposits. As the river meandered to the southwest, abandoned channels filled with organic-rich sediment creating anoxic conditions that produced the black silt that is a frequent component of the stratigraphy. The upper-most layer in these cores is red-brown mud from recent river flood deposition.

Core 2M contains a layer of coarse black sand with coarse marine fragments similar to modern local river beds under the influence of the tidal marine front. Although, radiocarbon dates of these fluvial-marine sediments place the maximum age of the channel at 2720 - 2410 cal yr. B.P. (Beta #68784), the river may have eroded to this level more recently before continuing its meander to the southwest. The coastal plain southeast of the U-meander contains no marine material, thus suggesting that large volumes of fluvial sediment deposition prevented marine intrusion.

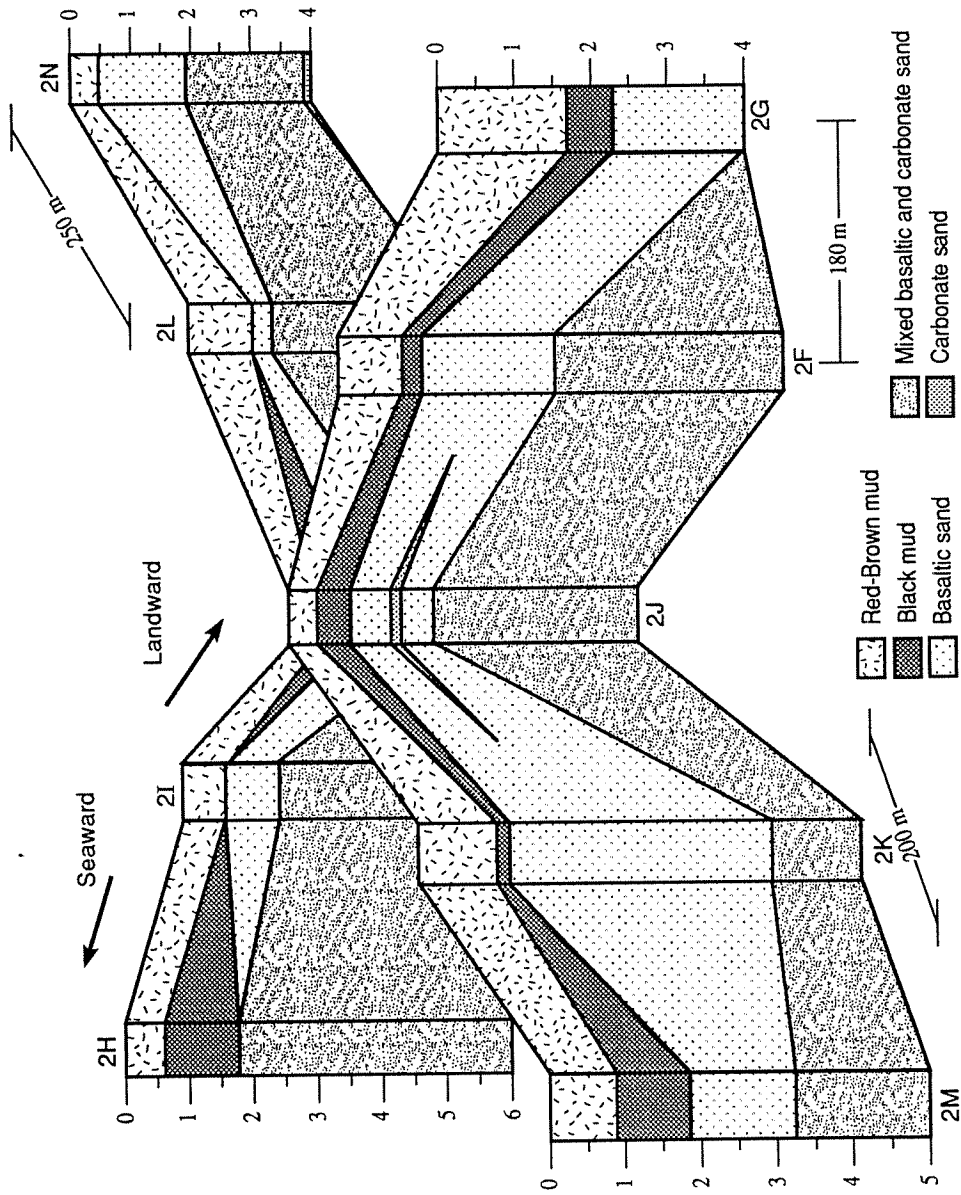


Figure 12: Fence diagram of the stratigraphy inside the large meander of the Hanalei River. Note the possible event deposit in core 2J. Figure 3 shows the location of each core in this figure on the coastal plain. Core depths are in meters.

Age Anomalies

An interesting anomaly appears in core 2J. A layer of marine sand 20 cm thick lies between layers of fluvial sand (Fig. 12). This marine sand was radiocarbon dated at 4810 - 4620 cal yr. B.P. (Beta #68782), and a sample of wood from the fluvial deposits immediately below it was dated 2730 - 2370 cal yr. B.P. (Beta #68783). The marine sand grades from fine to medium sand between 143 and 159 cm, and reverse grades back to fine sand between 159 and 163 cm. This deposit, both chronologically and stratigraphically anomalous, may represent marine flooding, such as may occur during a hurricane or tsunami, which struck the area shortly after 2730 - 2370 yr. B.P. Without more evidence, it is impossible to do more than speculate as to the layer's origin.

Core 2X (Fig. 3) also contains an age anomaly where an age of 4100 - 3960 cal yr. B.P. (Beta #75915) at the top of the marine layer places an older age distal to the mountains than the surrounding cores would indicate (Table 1 and Fig. 8). The top of the marine layer in core 2X is at 195 cm, which is significantly deeper (>50 cm) than the dated ROB in other cores proximal to the mountains (Fig. 7a). This core may indicate another location where the marine layer has recently been eroded by streams. This is supported by the superposition of modern wood (Beta #75914) intermixed with fluvial-marine sediments between 188 and 195 cm.

The top of the carbonate sand is nearly 1 m deeper in core 3A than it is in adjacent cores 2Y and 2Z (Figs. 3 and 7a). However, with a dated age of 3120 - 2760 cal yr. B.P. (Beta #75919), the top marine sediment of core 3A is contemporaneous or younger than the top marine sediments of either cores 2Y (3250 - 2920 cal yr. B.P.; Beta #75916) or 2Z (3320 - 2950 cal yr. B.P.; Beta #75917). Despite this, the low elevation and juxtaposition

of modern sediment (Beta #75918) would indicate that this is an erosional surface similar to the one found in core 2X.

Region Dominated by the Hanalei River

Sedimentary processes of the Hanalei River have dominated the region where it emerges onto the east end of the coastal plain for at least 7000 years (Fig. 3). Because dates obtained from fluvial sediments there are evenly spread between 3500 and 7000 cal yr. B.P. (Table 1), the marine environment is not likely to have inundated this area. Core 2B has an age of 5580 - 5320 cal yr. B.P. (Beta #68774) at 630-640 cm while core HAN 1 reaches 7180 - 6850 cal yr. B.P. (Beta #55539) at 458 cm. No evidence of a marine environment was found in either one of these cores nor in any of the other ten cores taken from this area. This region, therefore, is useful in defining the area not affected by marine deposition.

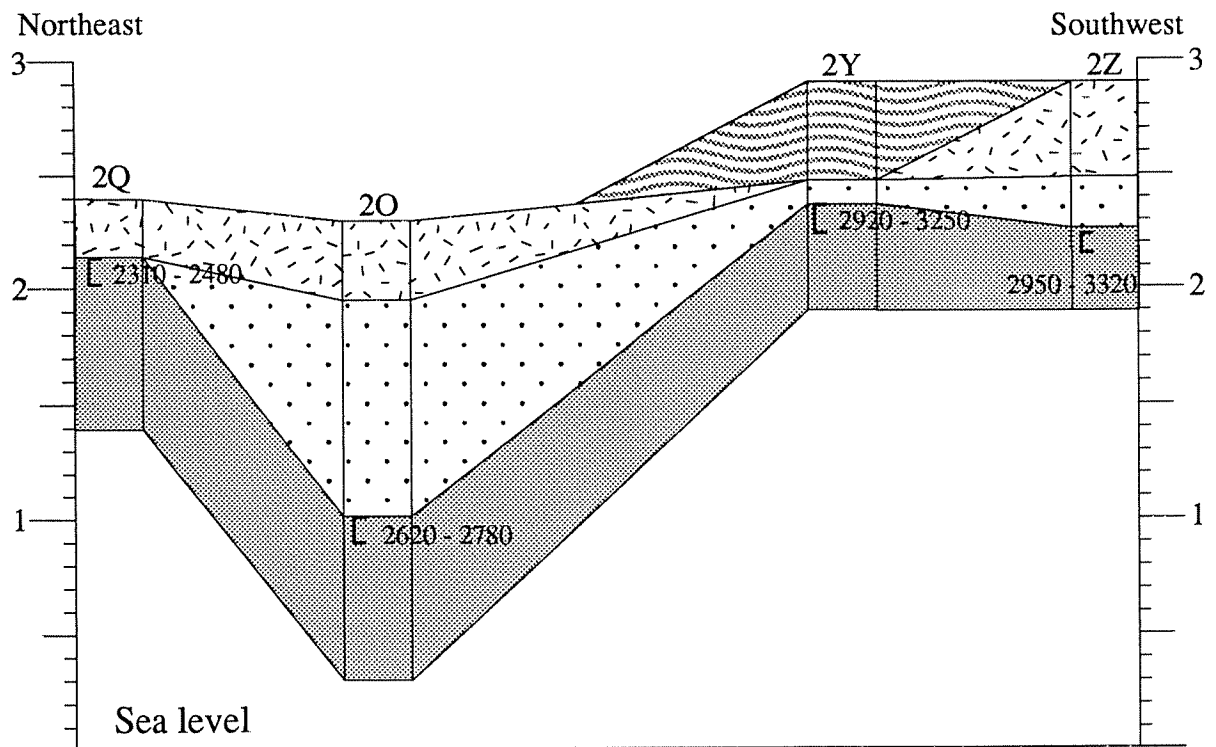
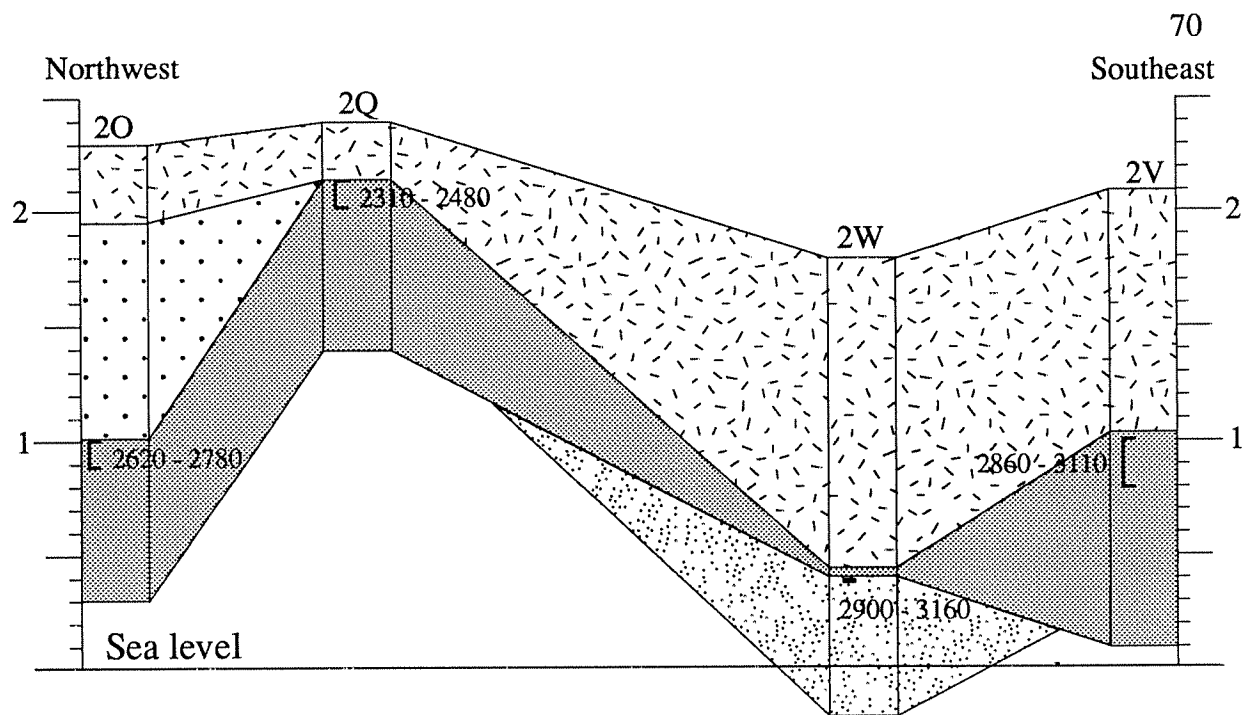
Sea-level Highstand

When combined with the reef in growth position (Jones, 1992), the fourteen dates from the ROB strongly suggest a relative sea-level highstand ending around 4000 yr. B.P. on Kauai. Jones (1992) placed the highstand at 4200 to 3230 cal yr. B.P., with which the new ROB dates generally agree. Stearns (1977, 1978) suggested a relative sea-level highstand (3000-4000 yr. B.P.) and an ensuing marine regression on neighboring Oahu based on observations from Kapapa Island and samples from Hanauma Bay. The dates of the ROB on the Hanalei coastal plain show a marine regression occurring from 4000 yr. B.P. to the near present (Figs. 8, 9, 10, and 11). Marine regressions on Oahu and Kauai (Matsumoto *et al.*, 1988; Jones, 1992) may be the result of hydroisostatic emergence (Nakada, 1986; Lambeck, 1990) or geoidal fluctuations related to deglaciation (Mitrovica

and Peltier, 1991; Tushingham and Peltier, 1991). Because the two islands may have independent relative sea-level histories, their highstands are not necessarily simultaneous, and their regression rates do not need to be identical.

Three cores, 2Q, 2Y, and 2Z, were dated directly at the ROB contact and do not contain inverted ages or evidence of erosion. Three more cores (2O, 2V, 2W) meet the first two criteria but show some evidence of erosion (Fig. 13). The ROB from cores 2O and 2W is situated within the shallow paleochannel of the intermittent stream indicating some erosion of the surface of the marine lithosome (Figs. 7b and 13). The ROB in core 2V sits on the eroded eastern edge of the marine lithosome plateau at *c.* 1 m elevation. The small plateau 0.5 km NW of core 2V (the site of core 2Q) suggests the original elevation of the marine lithosome was ≥ 2 m (Fig. 7b). Therefore, contours indicate that the ROB in cores 2O and 2V have experienced *c.* 1 m of erosion and ROB erosion at core 2W has been *c.* 1.5 m.

Using two carbonate samples from core 2V (Beta #75911 and 75912), the carbonate sediment accumulation rate was calculated to be between 0.56 mm/yr and 57.0 mm/yr. With these accumulation rates, an additional meter of carbonate sediment would make a restored ROB 20 years to 1790 years younger than the dated samples. These six cores reflect marine deposition over the interval *c.* 2480 - 2310 cal yr. B.P. to 3320 - 2950 cal yr. B.P. and at elevations from 0.4 m to 2.4 m above modern mean sea level (Fig. 14). Restored dates and elevations make the six samples range in age from *c.* 990 - 830 (restored) cal yr. B.P. to 3320 - 2950 (unrestored) cal yr. B.P. and elevations from 1.4 m (restored) to 2.4 m (unrestored) above modern mean sea level. These dates and elevations are consistent with Jones' (1992) interpretation and the predictions of Nakada and Lambeck (1989), Mitrovica and Peltier (1991), and Tushingham and Peltier (1992) that a middle- to late-Holocene relative highstand of sea level occurred in Hawaii (Fig. 14).







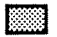
- | | | | |
|---|----------------|---|------------------------------------|
|  | Red/Brown mud |  | Mat of modern vegetation and water |
|  | Basaltic sand |  | Mixed basaltic and carbonate sand |
|  | Carbonate sand | | |

Figure 13: Subfacies profiles using cores 2O, 2Q, 2W, and 2V and 2Q, 2O, 2Y, and 2Z. Brackets within the cores are range from which the dated samples were taken. The scales are in meters above modern mean sea level.

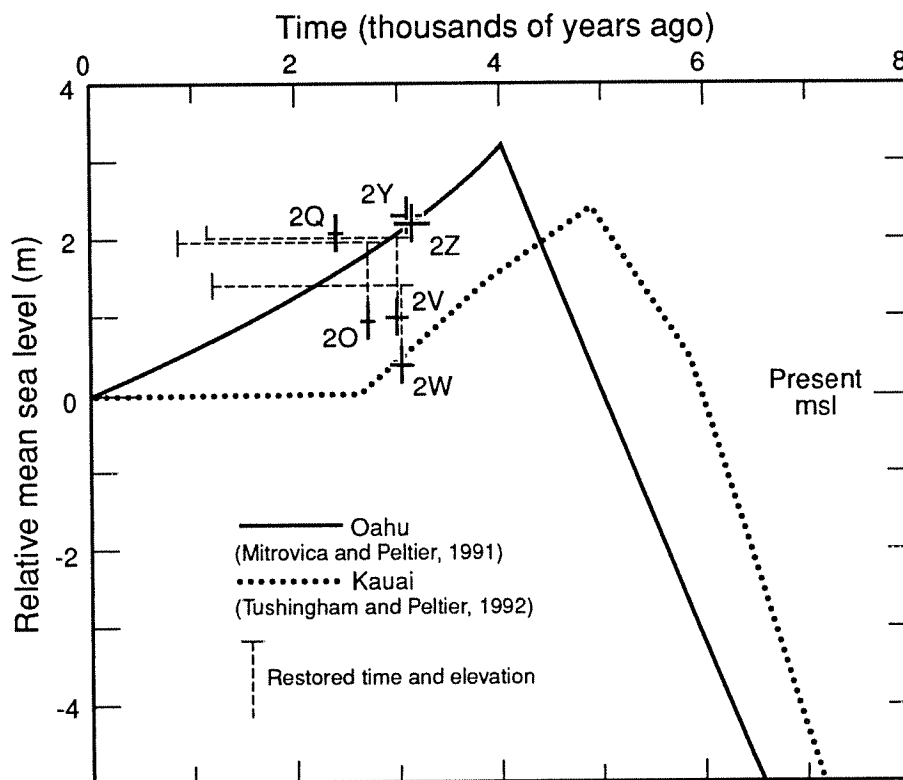


Figure 14: Plot of the age and elevation of three regression boundaries not influenced by erosion (2Y, 2Q, 2Z), and three restored to probable original paleoelevations and ages (2V, 2O, 2W). Restored elevations were calculated by adding 1 m to the measured elevation of the ROB. Restored ages were calculated using the range of sediment accumulation rates (0.056 to 5.7 cm/yr) derived from the dated carbonate sand in core 2V (Beta-75911 and Beta-75912). Also shown are the predicted sea-level histories of Mitrovica and Peltier (1991) and Tushingham and Peltier (1992). The prediction of Mitrovica and Peltier best accommodates the regression history of the coastal plain at Hanalei.

The islands of Hawaii are not alone in showing evidence of a middle to late-Holocene regression: many islands throughout the Pacific and Indian Oceans display features interpreted to be the result of a marine regression. In the Pacific, the Marshall Islands (Buddmeier *et al.*, 1975), French Polynesia (Pirzzoli and Montaggioni, 1988), the Cook Islands (Scoffin *et al.*, 1985; Ellison, 1994), Western Samoa (Rodda, 1988; Sugimura *et al.*, 1988), Tonga (Dickenson *et al.*, 1994), Fiji (Miyata *et al.*, 1988; Rodda, 1988; Nunn, 1990), the Mariana Islands (Kayanne *et al.*, 1993), and Queensland, Australia (Beaman *et al.*, 1994) all show evidence of a small (0.5-2.0 m), recent (1000-6000 yr. B.P.) relative sea-level highstand. In the Indian Ocean, features on the Cocos Keeling Islands (Woodroffe *et al.*, 1990) and the west coast of the Thai peninsula (Tudhope and Scoffin, 1994) support a relative sea-level highstand of the same age and magnitude as that seen in the Pacific.

Sediment Production

In regions where coastal sediments are predominantly produced by marine organisms, the origin of a strandplain (barring cheniers or smaller storm berms) may be ambiguous. The differences between a beach prograding because of a fall in sea level and one prograding because of abundant local marine production may be subtle. While it is possible to supply a beach with enough sediment to prograde without a drop in sea level (Carter, 1988), most researchers credit high local fluvial sediment discharge or abundant longshore transport as the predominant means of sediment supply for such progradations (McCormick, 1973; Bowman and Harvey, 1986; Stapor *et al.*, 1991; Chrzastowski and Thompson, 1992; Otvos, 1992). In the absence of such local mechanisms, but also occasionally even in conjunction with them, a relative falling sea level is usually credited (Dominguez *et al.*, 1987; Nunn, 1990; Stapor *et al.*, 1991; van de

Plassche, 1991; Chrzastowski and Thompson, 1992; Donoghue and Tanner, 1992).

While most of these studies were performed in regions where marine organisms do not produce the majority of beach sediments, research completed by Nunn (1990) and Stapor *et al.* (1991) occurred in Fiji and southwest Florida (respectively) where marine production is the major source of sediment. Regardless of this, neither researcher considered the abundant local marine production as sufficient to account for the progradations recorded.

Under optimum growth conditions, carbonate production by organisms appears to be approximately 0.5 to 1.5 mm/yr of carbonate sediment deposition (Tucker and Wright, 1990). Taking an average of 1 mm/yr, the 2.5 km² modern Hanalei Bay is large enough to have produced approximately 1.2×10^7 m³ of carbonates in the last 4800 - 4580 years (Beta #68764), enough to cover the 4.25 km² of coastal plain under an average of 2.8 m of carbonate. However, based on foraminifera production rates, Hallock (1981) found no carbonate production rates higher than equal to 0.17 mm/yr of carbonate sediment deposition on the Hawaiian Island of Oahu. This leads to a production of only approximately 2.0×10^6 m³ of carbonates in 4800-4580 years in Hanalei Bay. Even in the unlikely event that all the carbonate became sand and was all deposited on the beach, this would cover the coastal plain in only 0.47 m of carbonate sediment. Even if the area inside the Hanalei River meander was not included as part of the coastal plain (few carbonates there are above modern sea level), the 3.5 km² of the coastal plain would still be covered with only 0.57 m of carbonate sediment. The age 4800 - 4580 years (Beta sample #68764) is used in this calculation because it is the oldest carbonate sample found above modern sea level. As a result, while the presence of a prograded beach shoreline is not absolute proof of a relative fall in sea level, in the case of the coastal plain adjacent to

Hanalei Bay, a relative sea-level fall appears to be the best mechanism to produce the observed progradation.

CONCLUSION

Between 4500 and 3500 yr. B.P., the present Hanalei coastal plain was largely covered by a shallow marine bay (Figs. 9 and 10). Marine sand several meters thick (>3.5 m) was deposited over much of the area. As the shoreline prograded, beach accretion ridges were abandoned and fluvial deposits buried the marine sand (Figs. 8 and 11). River channel scouring eroded the marine unit in places and partially removed evidence of the marine environment. Simultaneously, fluvial sedimentation produced river mouth bars, spits, and river channels where terrestrial sediment mixed with marine sand. Where fluvial deposition mixes with marine influence, the stratigraphy of the Hanalei coastal plain records a marine regression beginning around 4000 yr. B.P., and a subsequent increase in deposition of fluvial sediments.

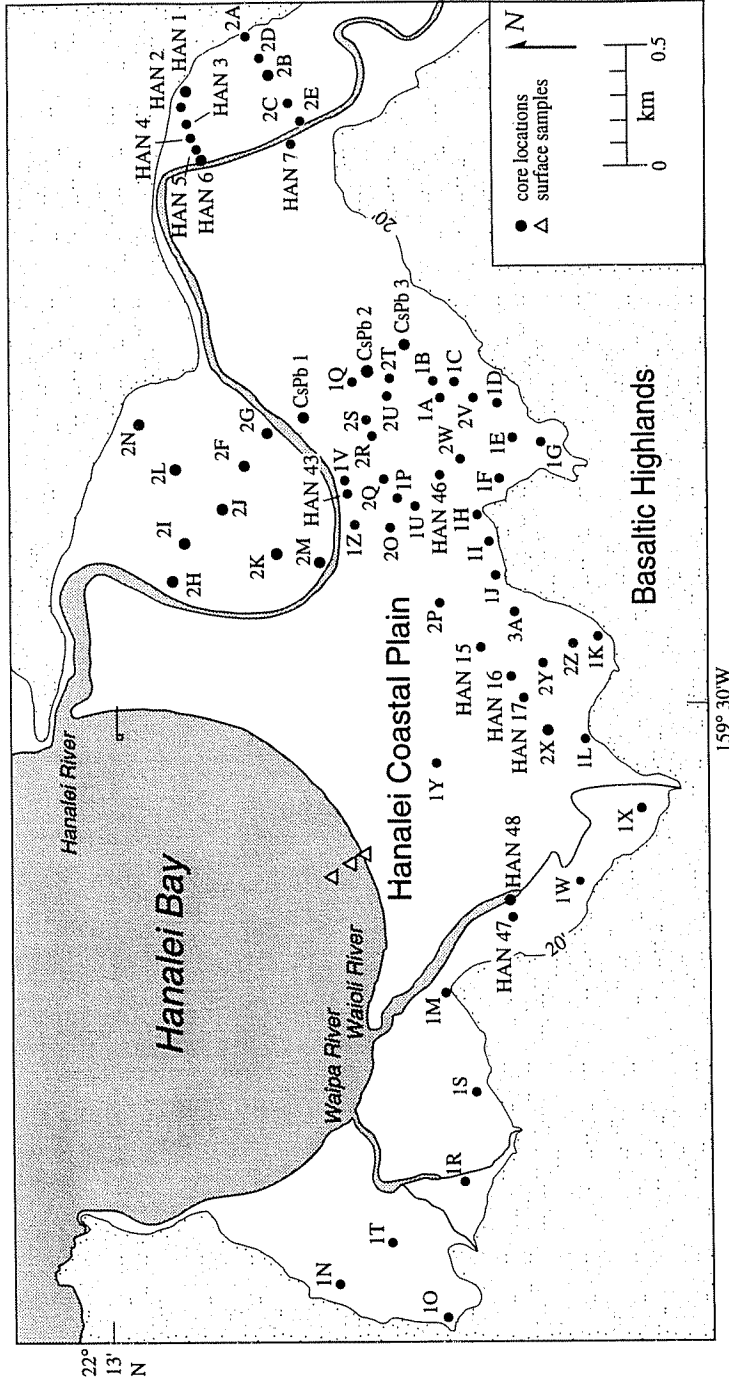
The evidence of a relative sea-level highstand in Hanalei Bay is at least partially dependent on the reef reported by Jones (1992) as being elevated and in growth position. This remains to be adequately demonstrated. The top of the marine sand layer underlying the Hanalei coastal plain lies above modern sea level, as does the modern beach, and thus it may indicate a beach deposit from a sea-level regime identical to modern. While this prograding beach may be partially the result of abundant marine deposition following the culmination of the post-glacial transgression, a fall in relative sea level, partially constrained in time and space by geophysical models (Mitrovica and Peltier, 1991; Tushingham and Peltier, 1991), provides a more complete explanation.

Based on the pattern of distribution and depth of the marine sand, the rivers have failed to meander across the entire coastal plain. Shallow marine sands located near both

sides of the Waipa and Waioli Rivers indicate they have not extensively eroded their floodplains (Fig. 7a). Likewise, although the Hanalei River has meandered across the eastern portion of the coastal plain eliminating many marine deposits located there, it has not eroded the broad marine sand deposit to its west (Figs. 7a and 7b).

The present configuration of the Hanalei coastal plain is a product of a late Holocene regression and extensive and continuous fluvial deposition. The postglacial transgression flooded the river valley before prograding beaches moved the shoreline to its modern location. Fluvial processes have since dominated the plain punctuated by periodic marine depositional events. During the regression, fluvial sedimentation patterns produced localized bars, overbank and floodplain deposits, and fluvial-marine channel deposits. The meanders of the three rivers have built and abandoned channels and bars. Recurring floods periodically cover the plain and leave deposits of sediment eroded from the upper river valleys. The sediments and their rates of deposition on the Hanalei coastal plain reflect the variations of past influences, and many cored facies are reminiscent of modern depositional environments of the region.

APPENDIX A: Map of Hanalei coastal plain showing location and name of each core.



APPENDIX B: Bearings and reference points used to locate cores on the Hanalei coastal plain.

All bearings were taken with a hand-held digital Datascope compass with a reported accuracy of $\pm 0.5^\circ$. All bearings are based on magnetic north (11.5° east of true north; approximate mean declination, 1983, U.S.G.S. Hanalei Quadrangle). All reference points can be found on the U.S.G.S. 7.5 minute Hanalei Quadrangle. Cores HAN 1 - HAN 48 were taken by Troy Rosenbush in August and September, 1992. Cores 1A - 2P were taken by Scott Calhoun, Alex Ress, and Doug Neil in June, July, and August, 1993. Cores 2Q - 3A were taken by Scott Calhoun and Eric Grossman in July, 1994. Cores CsPb 1, CsPb 2, and CsPb 3 were taken by Scott Calhoun and Eric Grossman on February 5, 1994.

Core 1A:

Large powerline tower: 273.7°
Hanalei River bridge: 28.2°

Core 1B:

Mamalahoa: 205.3°
Large powerline tower: 267.1°

Core 1C:

Mamalahoa: 206.1°
Powerline tower on ridge to west (labeled Makaihuwaa): 253.4°

Core 1D:

Water tank: 235.6°
Large powerline tower: 339.0°

Core 1E:

Water tank: 234.1°
Large powerline tower: 11.6°

Core 1F:

Sharpest curve on road down to bridge: 7.0°
Large powerline tower: 30.7°
Mamalahoa: 204.3°

Core 1G:

Mamalahoa: 205.9°
Large powerline tower: 12.4°
Hihimanu: 166.7
Water tank: $250.4^\circ ?$

Core 1H:

Mamalahoa: 202.5°

Powerline tower on ridge to the west: 251.9°
 Large powerline tower: 59.6°

Core 1I:

Powerline tower on ridge to the west: 253.6°
 Point of land on water tank ridge: 128.1°
 Puu Ka Manu: 278.8°

Core 1J:

Mamalahoa: 200.1°
 Powerline tower on ridge to the west: 255.7°
 Puu Ka Manu: 281.1°

Core 1K:

Mamalahoa: 200.4°
 Powerline tower on ridge to the west: 270.5°
 Puu Ka Manu: 289.3°

Core 1L:

Mamalahoa: 194.5°
 Powerline tower on ridge to the west: 268.0°

Core 1M:

Just west of Waioli River
 20 m mauka of highway
 5 m west of ridge coming down from Makaihuwaa

Core 1N:

Located on Waipa Stream floodplain
 Powerline tower on ridge to the east: 115.2°

Core 1O:

Located on Waipa Stream floodplain
 Mamalahoa: 158.2°
 Powerline tower on ridge to the west: 238.5°
 Powerline tower on ridge in middle of valley: 186.0°

Core 1P:

Water tank: 181.1°
 Powerline tower on west ridge: 243.7°

Core 1Q:

Water tank: 205.4°
 Powerline tower on ridge to the west: 242.1°
 Hanalei River Bridge: 40.0°

Core 1R:

Located on the Waipa Stream floodplain
Powerline tower on the ridge to the east: 99.6°
Next powerline tower to the west: 160.0°

Core 1S:

Located on the Waipa Stream floodplain
Powerline tower on ridge to the west: 254.5°
Powerline tower in valley (second tower east of above
reference point): 227.7°
Puu Ka Manu: 305.9°

Core 1T:

Located on the Waipa Stream floodplain
Powerline tower on the ridge to the west: 233.4°
Powerline tower in middle of the valley: 205.0°
Puu Ka Manu: 315.4°

Core 1U:

Water tank: 180.0°
Powerline tower on ridge to the west: 245.6°

Core 1V:

Water tank: 180.9°
Powerline tower on ridge to the west: 240.3°
18.0 meters from road (measured)

Core 1W:

Powerline tower on ridge to the west: 276.0°
Hihimanu: 132.9°

Core 1X:

Mamalaho: 191.3°
Powerline tower on ridge to the west: 285.1°

Core 1Y:

Mamalaho: 189.2°
Powerline tower on ridge to the west: 238.0°

Core 1Z:

Powerline tower on ridge east of water tank: 100.5°
Water tank: 170.2°
Powerline tower on ridge to the west: 170.2°

Core 2A:

Hanalei River bridge (west side): 285.6°
Water tank: 224.2°

Core 2B:
 Hanalei River bridge (west side): 303.2°
 Water tank: 226.1°

Core 2C:
 Hanalei River bridge (west side): 315.0°
 Water tank: 226.7°

Core 2D:
 Hanalei River bridge (west side): 297.0°
 Water tank: 227.8°

Core 2E:
 Hanalei River bridge (west side): 322.9°
 Water tank: 226.7°

Cores 2A - 2E were taken in a straight line. Core 2A is 58.5 strides east of core 2D. Core 2D is 46 strides east of core 2B. Core 2B is 59 strides east of core 2C. Core 2C is 47 strides east of core 2E. Core 2E is next to the banks of the Hanalei River. One stride is counted every time my right foot touches the ground at a walking pace and equals ~1.6 m.

Core 2F:
 Water tank: 187.3°
 Powerline tower on ridge to the west: 237.7°
 Puu Ka Manu: 267.0°

Core 2G:
 Water tank: 188.8°
 Powerline tower on ridge to the west: 242.6°
 Puu Ka Manu: 272.8

Core 2H:
 Water tank: 160.9°
 Powerline tower on ridge to the west: 218.7°

Core 2I:
 Water tank: 167.4°
 Powerline tower on ridge to the west: 223.2°
 Puu Ka Manu: 260.0°

Core 2J:
 Water tank: 174.2°
 Powerline tower on ridge to the west: 227.2°
 Puu Ka Manu: 261.2°

Core 2K:

Water tank: 166.4°
 Powerline tower on ridge to the west: 229.5°

Core 2L:
 Water tank: 184.2°
 Powerline tower on ridge to the west: 232.1°

Core 2M:
 Water tank: 162.2°
 Powerline tower on ridge to the west: 233.6°

Core 2N:
 Water tank: 182.2°
 Powerline tower on ridge to the west: 224.2°

Cores 2F - 2N were taken on the Hanalei Garden Farm on the inside of the large meander of the Hanalei River.

Core 2O:
 Water tank: 169.5°
 Powerline tower on ridge to the west: 242.4°

Core 2P:
 Hihimanu: 154.9°
 Powerline tower on ridge to the west: 245.5°

Core 2Q:
 Water tank: 186.0°
 Powerline tower on ridge to the west: 243.2°

Core 2R:
 Water tank: 196.4°
 Powerline tower on ridge to the west: 242.7

Core 2S:
 Water tank: 199.4°
 Powerline tower on ridge to the west: 242.7°

Core 2T:
 Water tank: 211.3°
 Powerline tower on ridge east of water tank: 107.5°
 (this tower was lying on its side when the bearing was taken)

Core 2U:
 Water tank: 209.2°
 Powerline tower on ridge east of water tank: 106.1°
 (this tower was lying on its side when the bearing was taken)

Core 2V:

Water tank: 227.6°

Powerline tower on ridge east of water tank: 83.7°

(this tower was lying on its side when the bearing was taken)

Core 2W:

Water tank: 206.5°

Powerline tower on ridge east of water tank: 84.0°

(this tower was lying on its side when the bearing was taken)

Core 2X:

Powerline tower on ridge to the west: 261.1°

Hihimanu (not the summit, where the 2040 foot contour crosses the ridge north of the summit): 137.2°

Core 2Y:

Powerline tower on ridge to the west: 260.4°

Hihimanu (summit): 147.5°

Core 2Z:

Powerline tower on ridge to the west: 264.7°

Hihimanu (summit): 150.5

Core 3A:

Powerline tower on ridge to the west: 257.3°

Hihimanu (summit): 152.0°

Core HAN 1:

Floodplain east of Hanalei River upriver of bridge, close to the bluff along east side of valley, in California grass across from furthest irrigation ditch.

Kaukaopua (not good bearing): 209.2°

Hanalei River bridge (west side): 297.4°

Ridge saddle behind work area?: 218.5°

Core HAN 2:

Slightly southwest of HAN 1

Hanalei River bridge: 303.5°

Core HAN 3:

30 m farther west

Bearing back to site of HAN 2: 63.0°

Core HAN 4:

An irrigation dike intersection

Bearing back to site of HAN 3: 68.1°

Distance between HAN 3 and HAN 4: ~65 m

- Core HAN 5:
West of HAN 4
Near shed on dirt road
- Core HAN 6:
West of HAN 4
Distance to Hanalei River: 10 m
- Core HAN 7:
Located on west bank of Hanalei River, ~.25 mile (.4 km) upstream of bridge, in
pasture near "planter pickup truck"
Hanalei River bridge (west side): 350.6°
Ridge notch: 219.4°
- Core HAN 15:
Powerline tower on ridge to the west: 272.5°
Mamalahoa: 218.8°
- Core HAN 16:
Roughly 10 - 20 m from house
Mamalahoa: 218.7°
Powerline tower on ridge: 279.7°
House: 56.2°
Shopping center in Hanalei: 2.9°
- Core HAN 17:
Farther along same bearing from house, large treeline thins slightly.
Shopping center in Hanalei: 13.9°
- Core HAN 43:
Approximately 20 m south of highway, just west of water tank road.
- Core HAN 46:
Notched peak (Hihimanu?): 186.5°
Near intersection of water tower road and power lines.
- Core HAN 47:
Directly under power lines, 60 m west of Waioli River
- Core HAN 48:
Directly under power lines, adjacent to Waioli River on west side.

In addition to compass bearings, cores CsPb 1 - CsPb 3 were also located with a Magellan 5000 GPS hand-held unit. The unit has a accuracy of ± 30 m. Core CsPb 1 was 100 m from the Hanalei River, core CsPb 2 was 400 m from the Hanalei River, and core CsPb 3 was 650 m from the Hanalei River.

Core CsPb 1:

Water tank: 194.7°

Powerline tower on ridge to the west: 238.0°

GPS location: 22° 12.620' N

159° 29.281' W

Core CsPb 2:

Hanalei River bridge: 35.0°

Powerline tower on ridge east of water tank: 115.4°

GPS location: 22° 12.387' N

159° 29.183' W

Core CsPb 3:

Hanalei River bridge: 24.5°

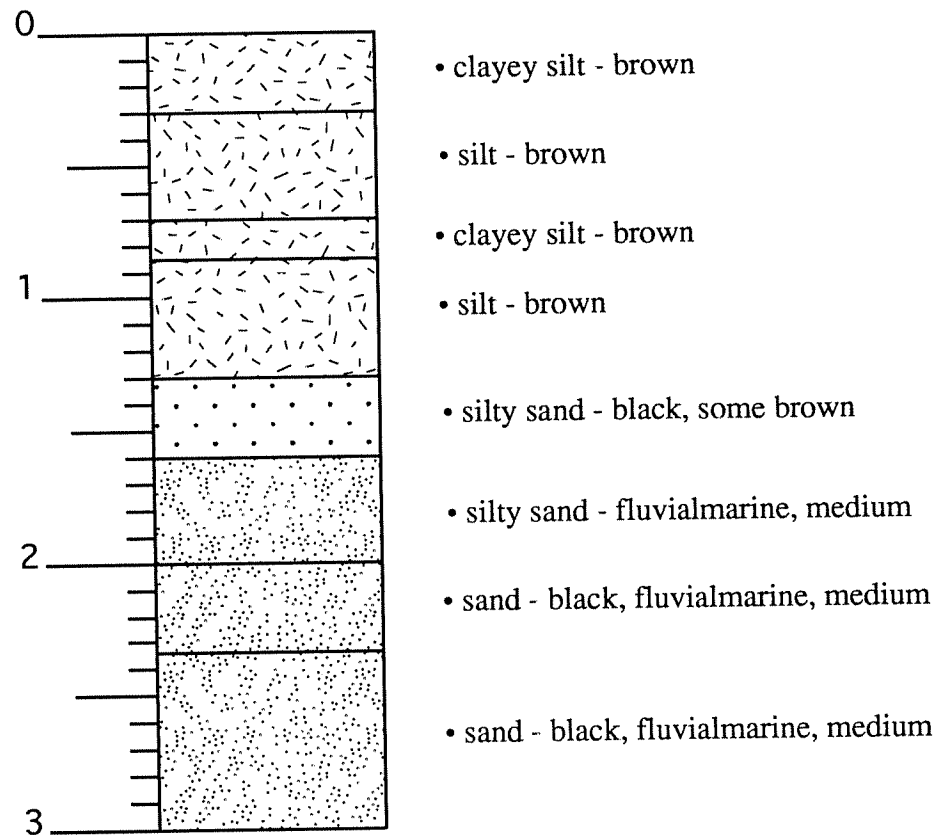
Powerline tower on ridge east of water tank: 108.5°

GPS location: 22° 12.273' N

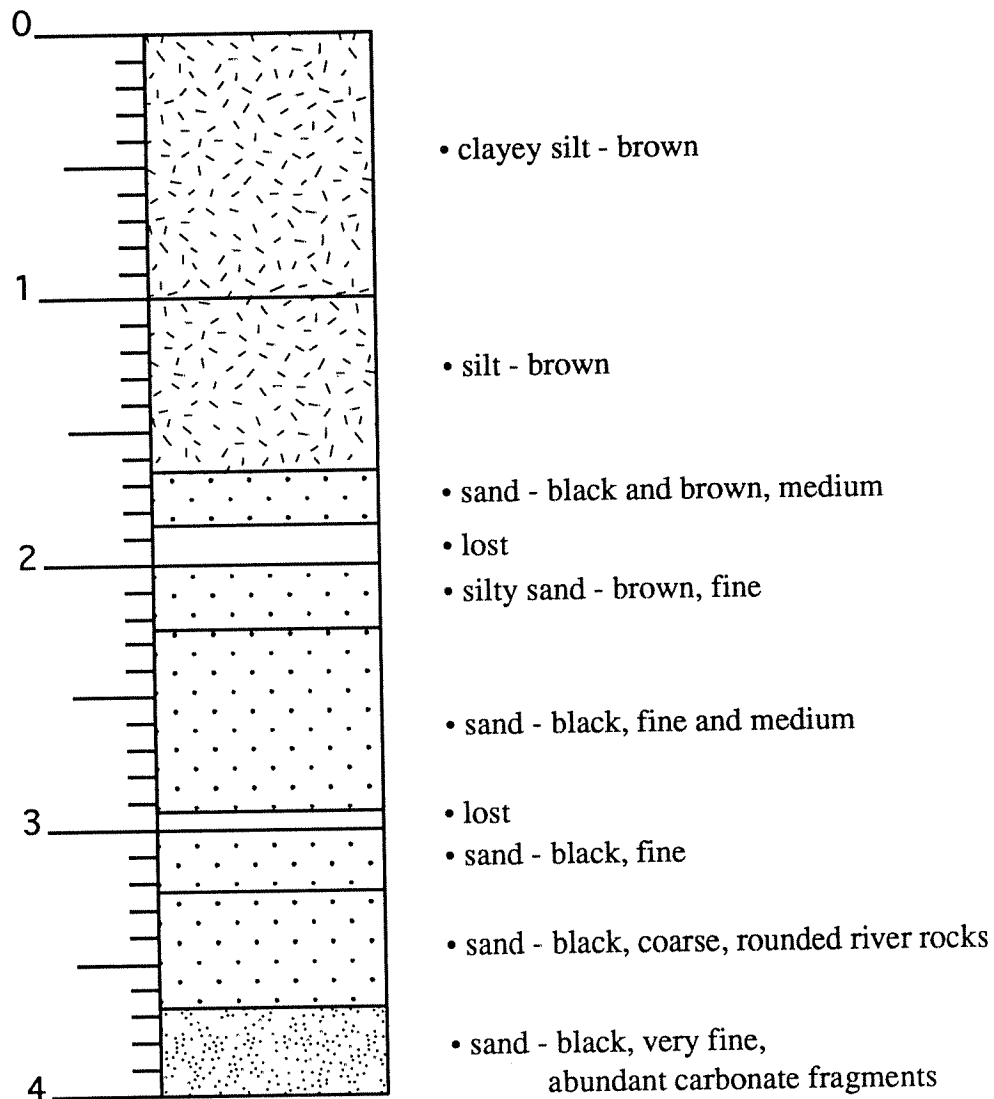
159° 29.130' W

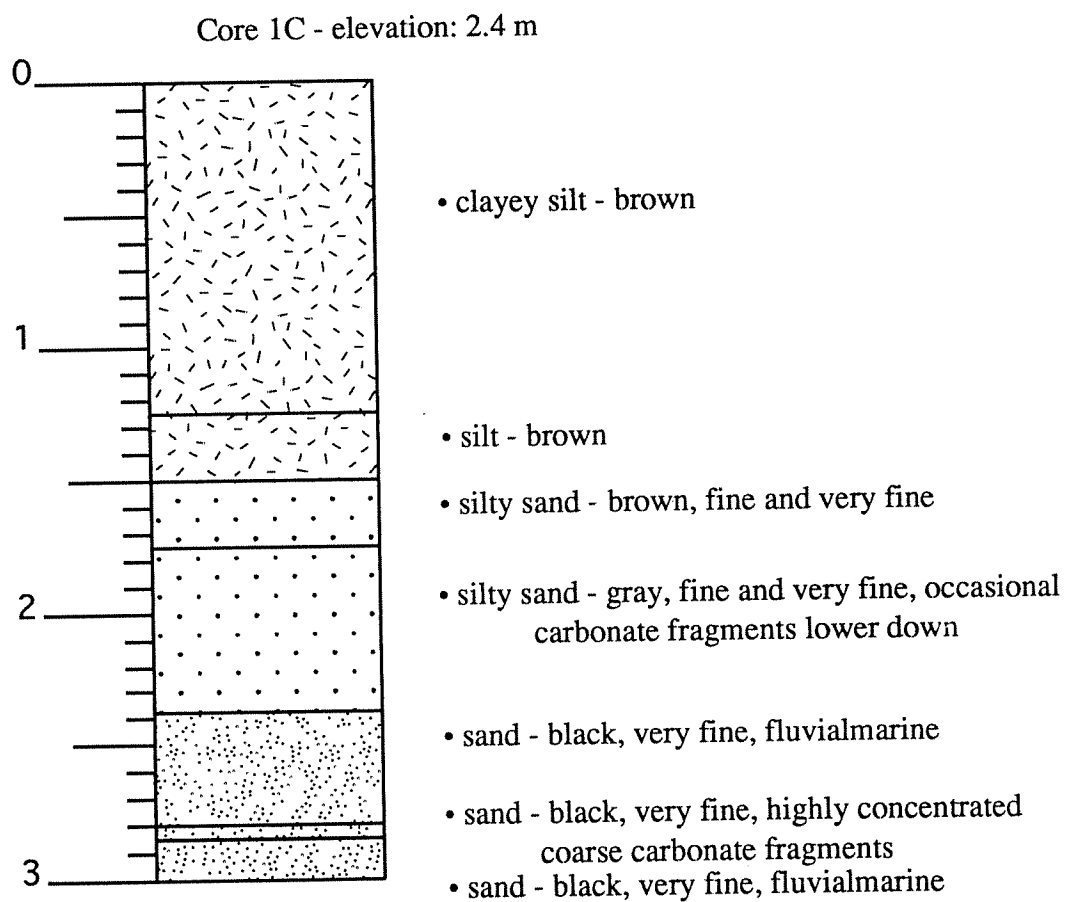
APPENDIX C: Stratigraphic columns of cores taken from the Hanalei coastal plain. Core depths are shown in meters except where noted in cores HAN 1 through HAN 7 and cores CsPb 1, CsPb 2, and CsPb 3. Depths in these cores are measured in cm.

Core 1A - elevation 2.4 m

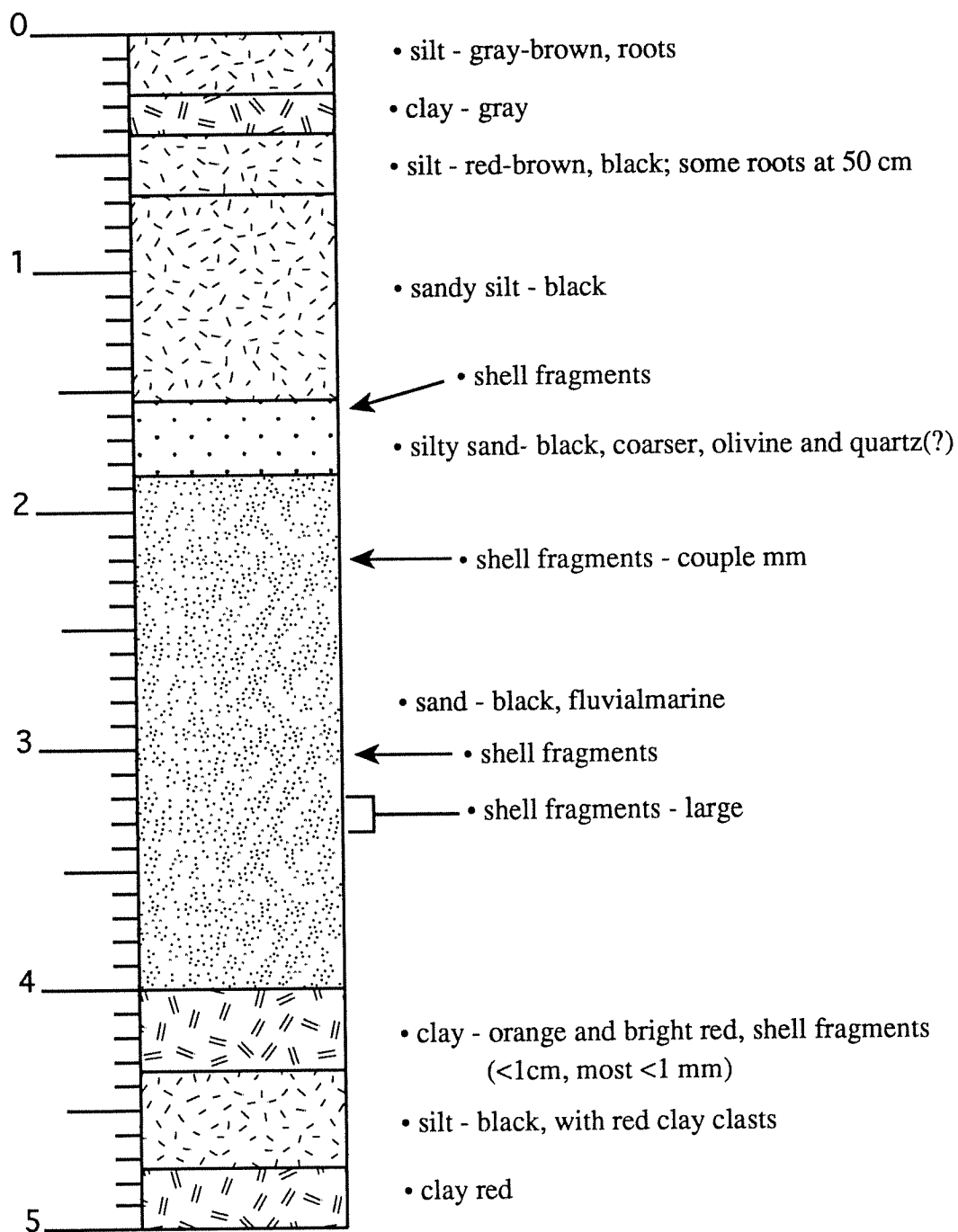


Core 1B - elevation: 2.7 m

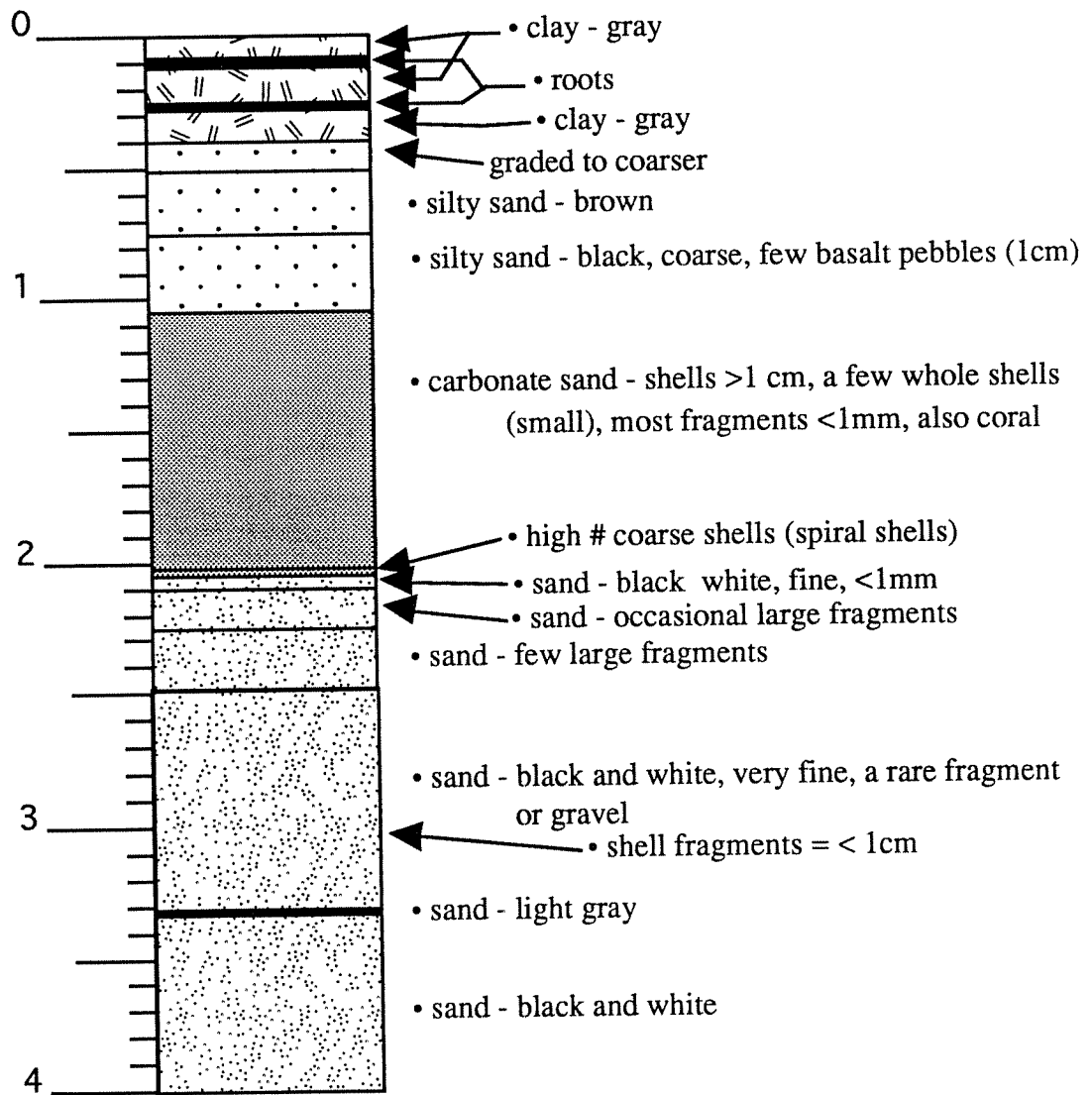




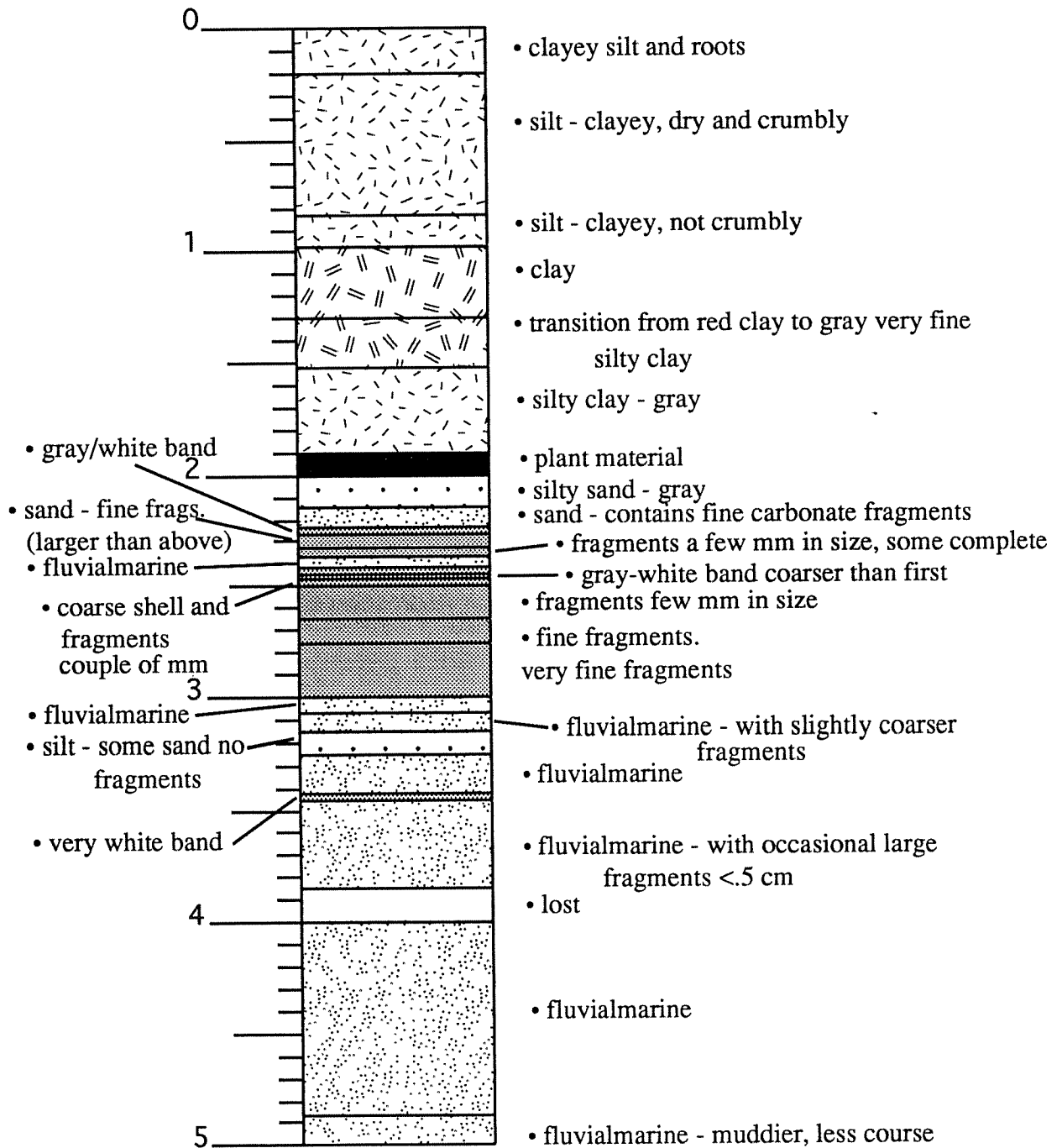
Core 1D - elevation: 2.3 m



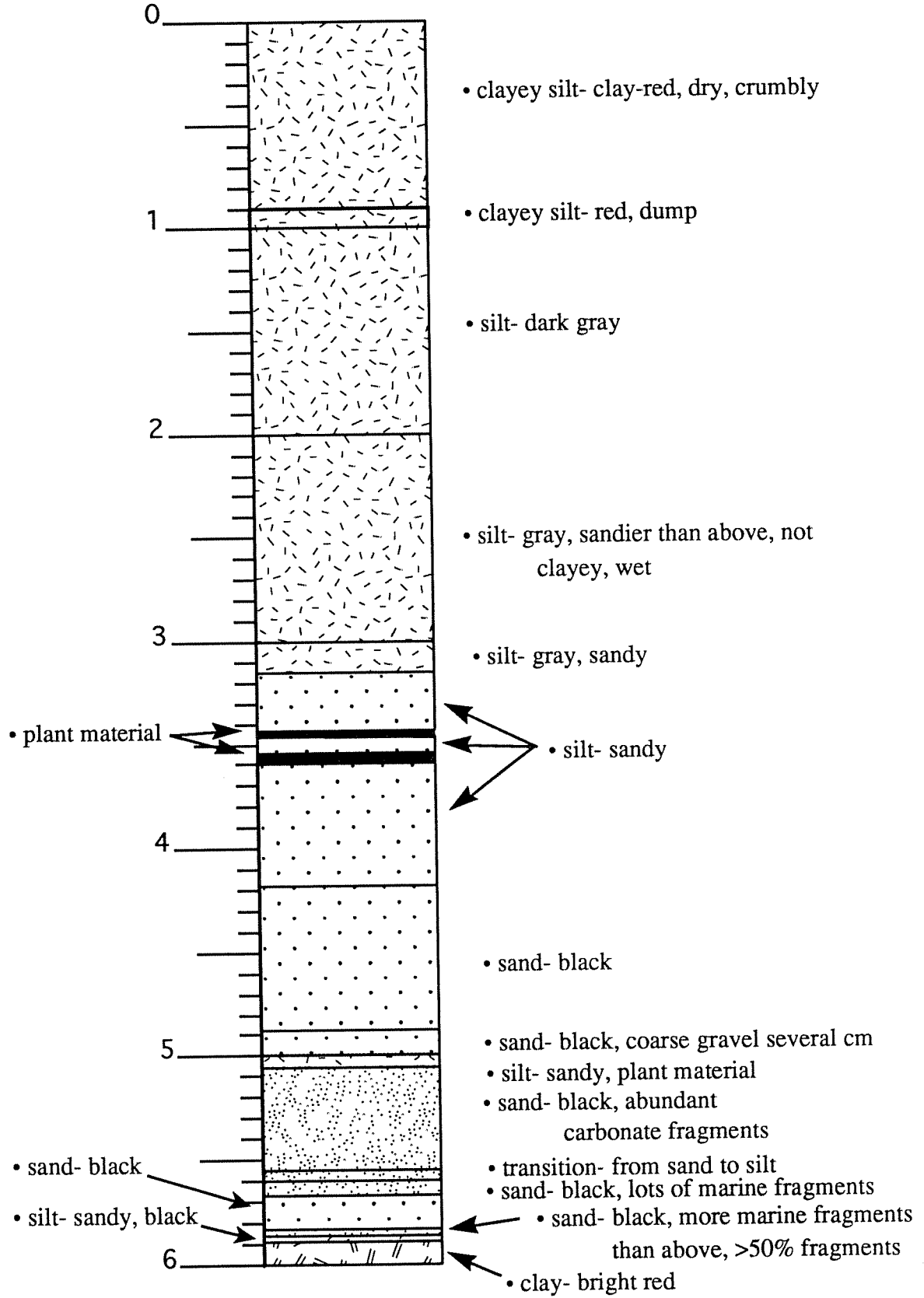
Core 1E - elevation: 2.4 m



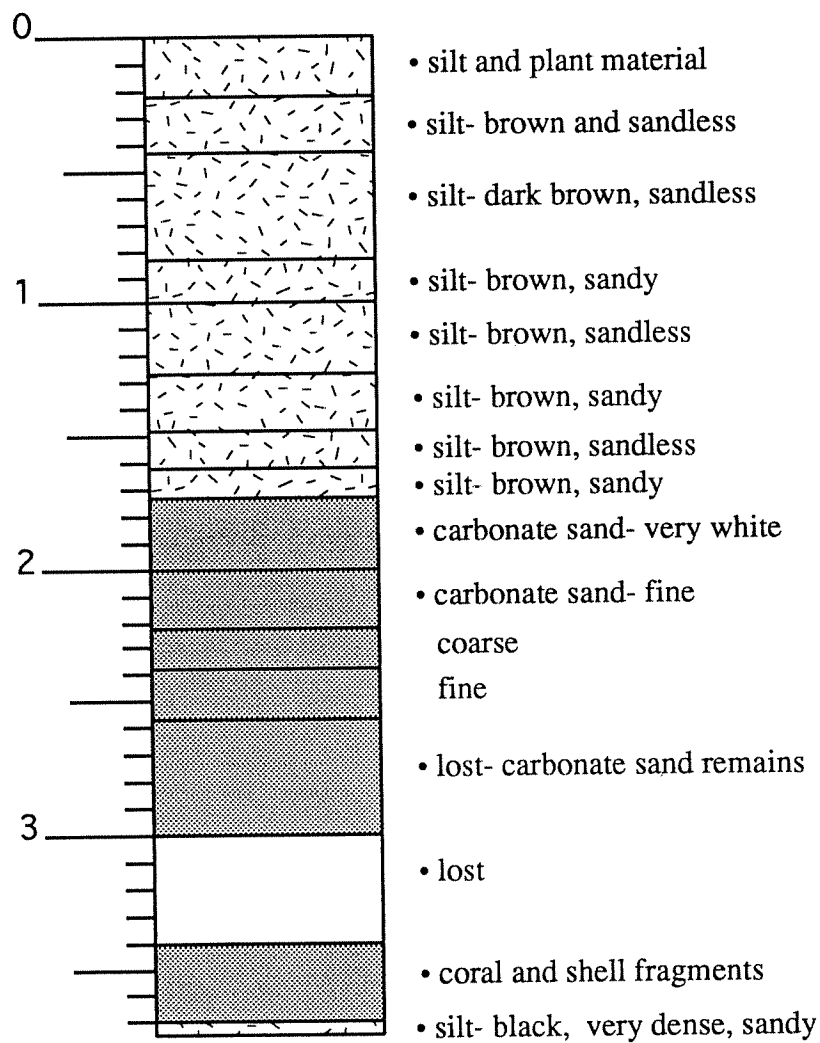
Core 1F - elevation: 2.7 m



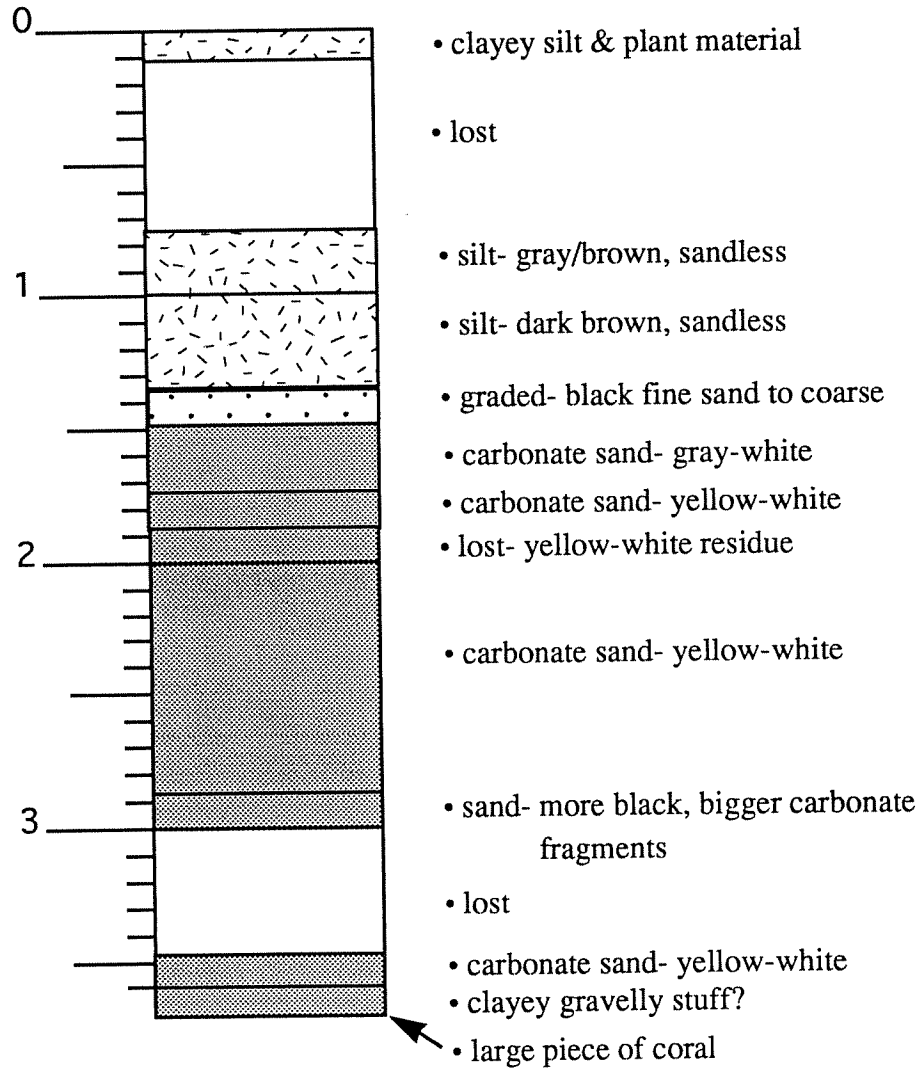
Core 1G - elevation: 4.0 m



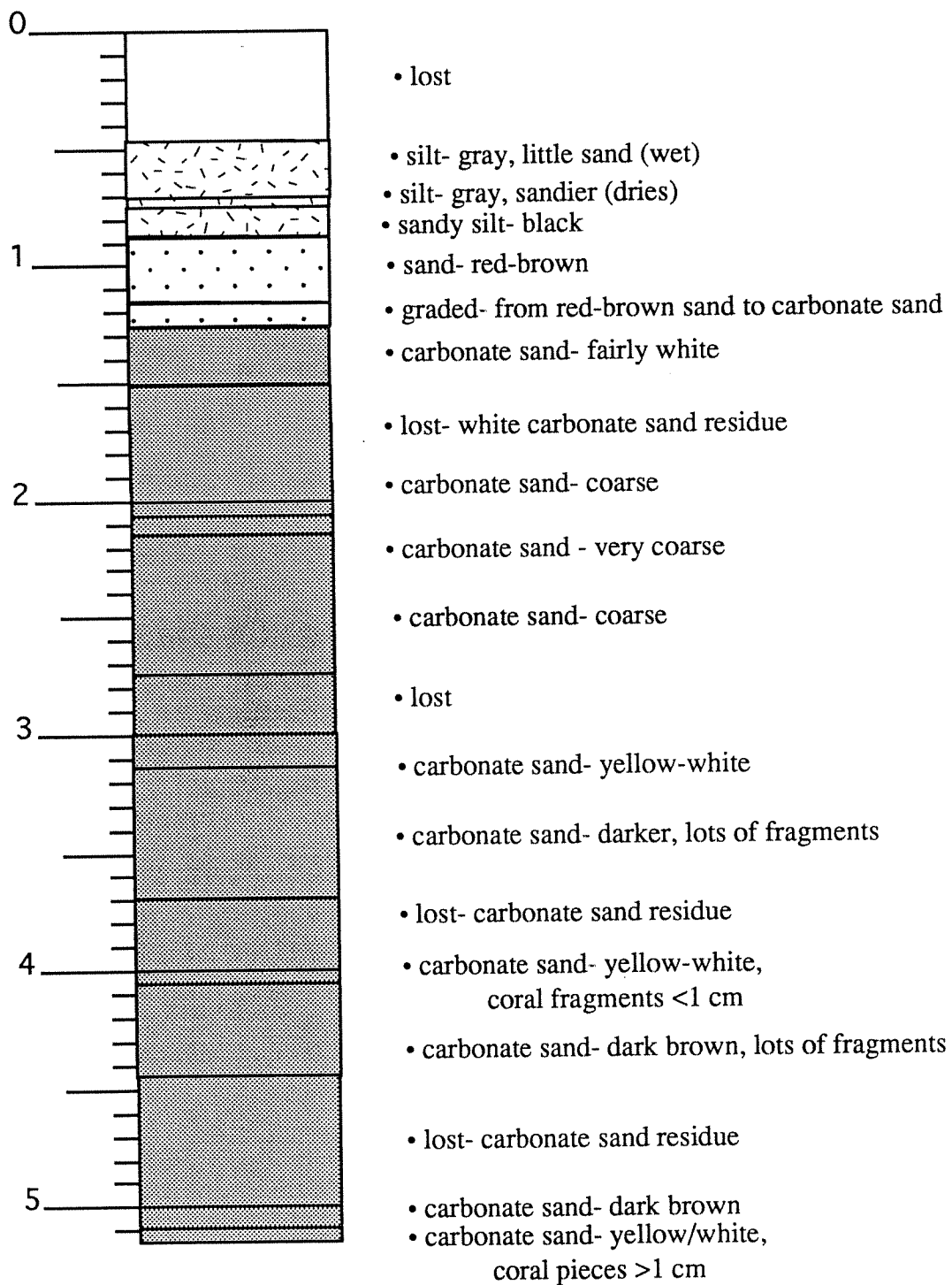
Core 1H - elevation: 2.9 m



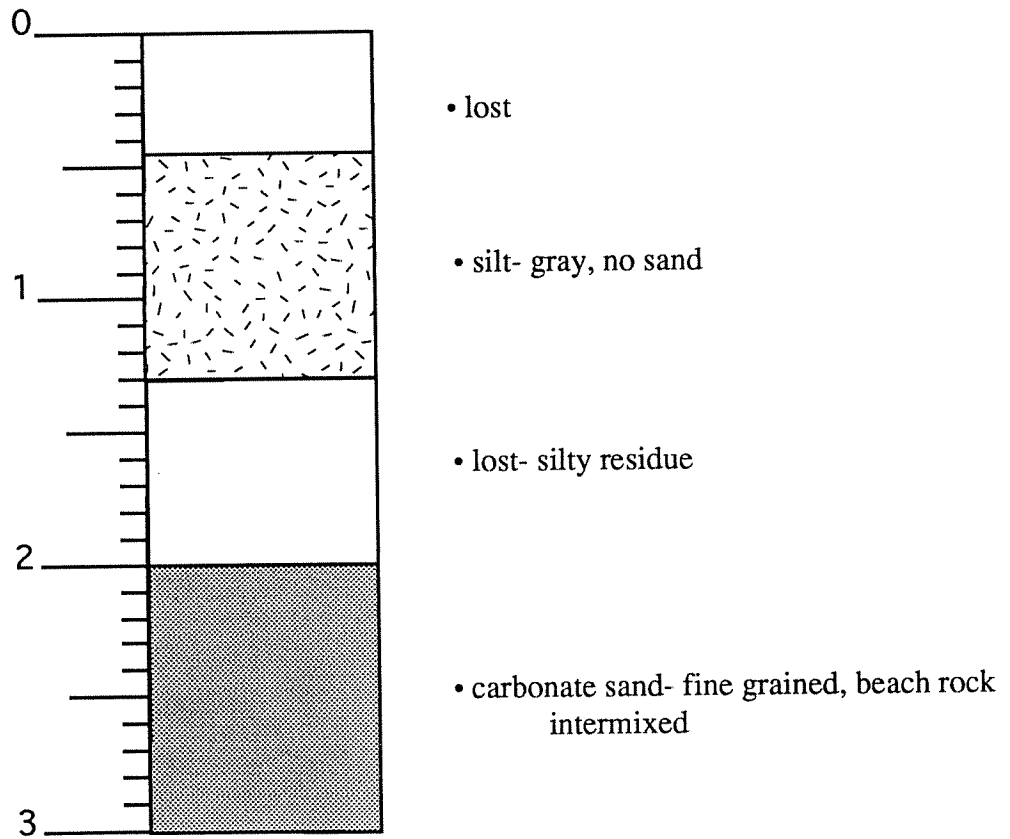
Core II - elevation: 2.9 m



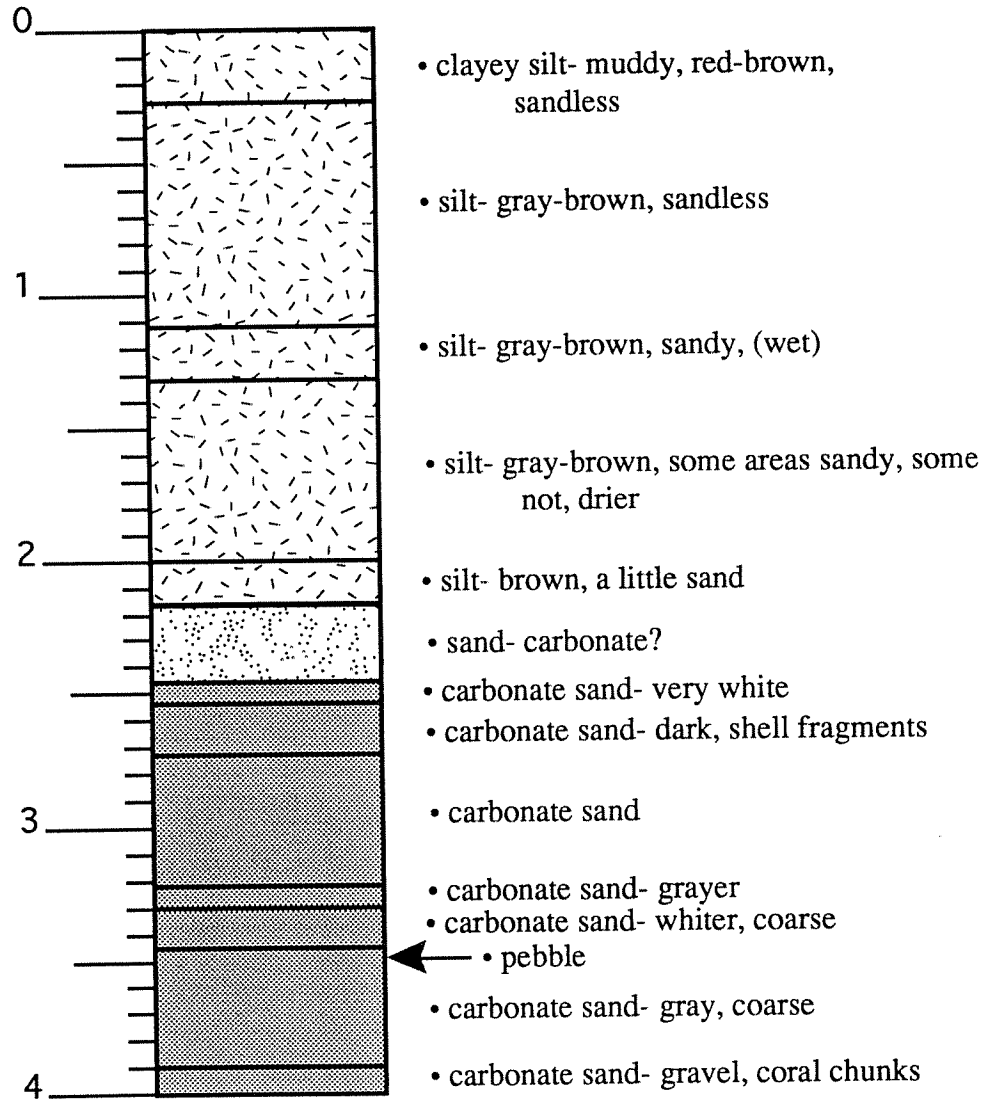
Core 1J - elevation: 2.9 m



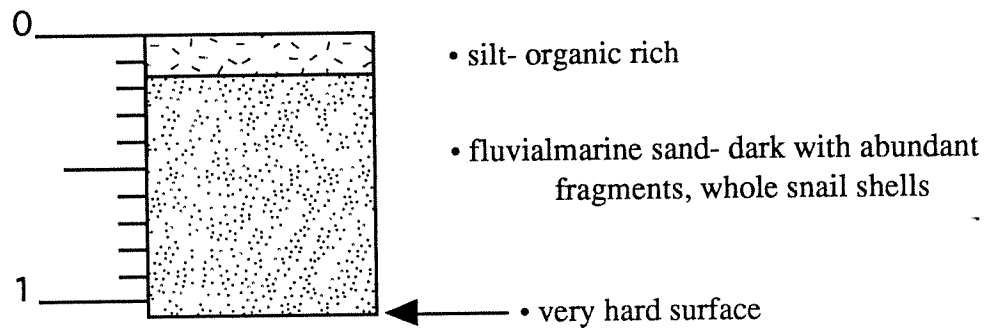
Core 1K - elevation: 2.9 m



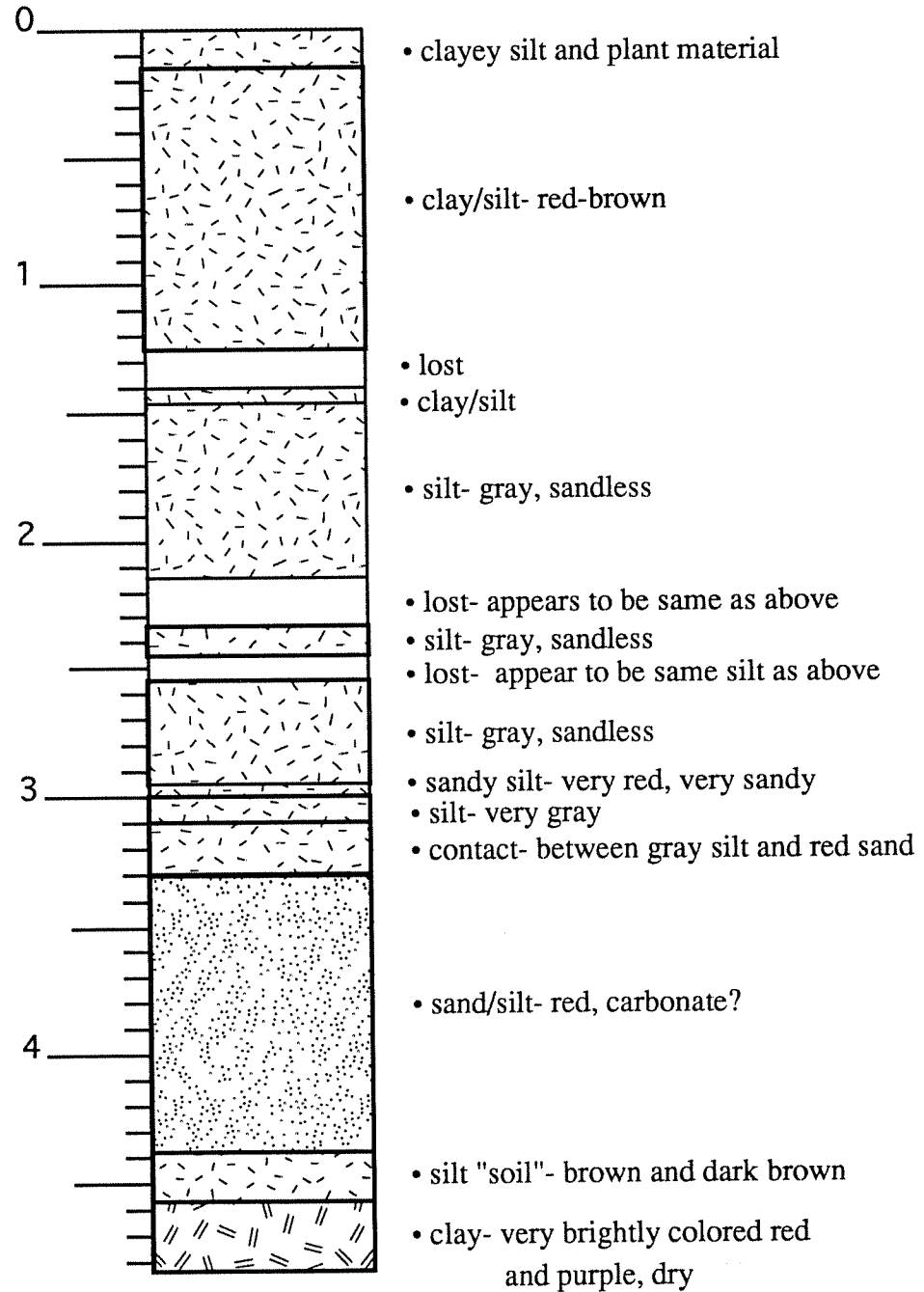
Core 1L - elevation: 2.9 m

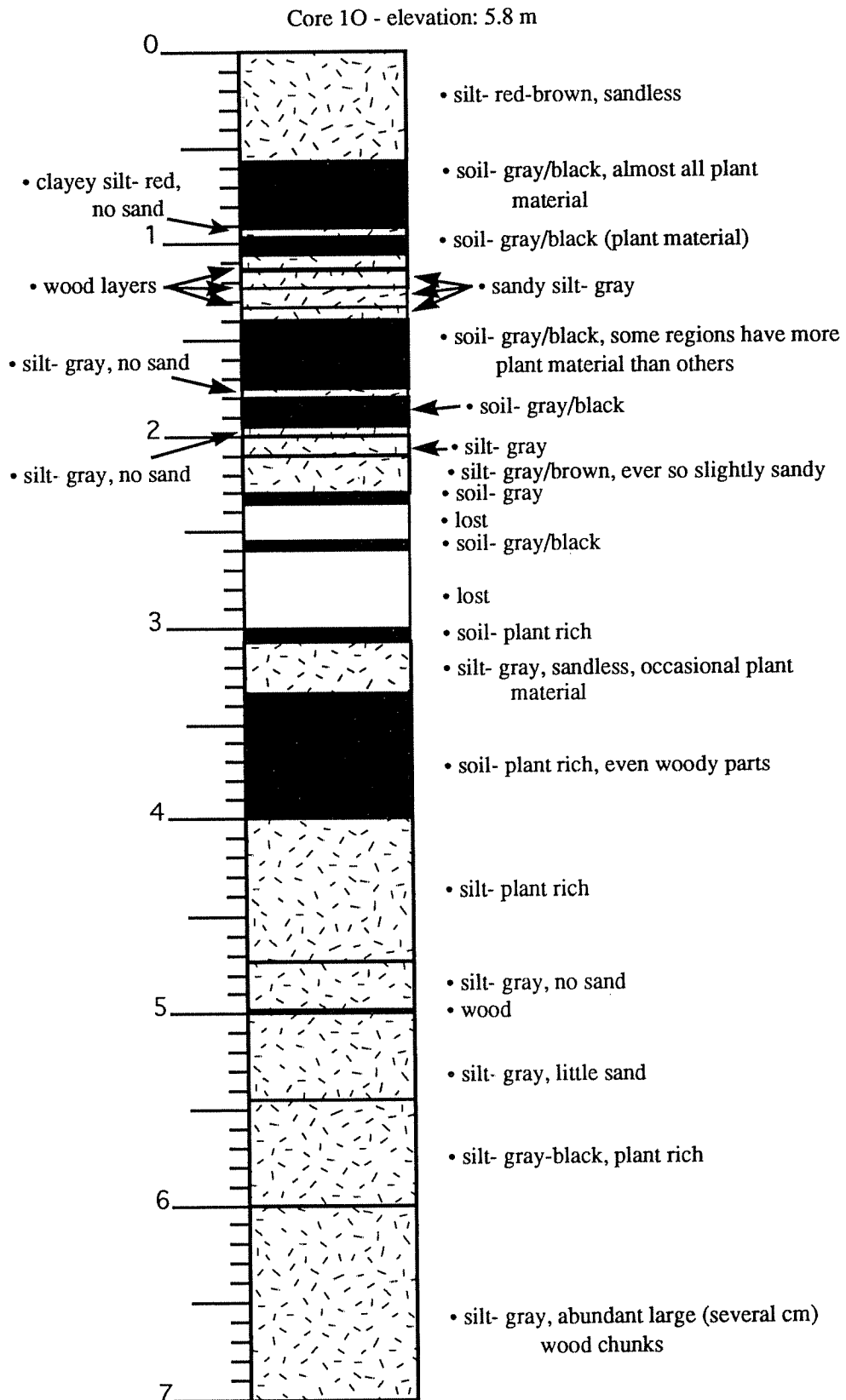


Core 1M - elevation: 1.8 m

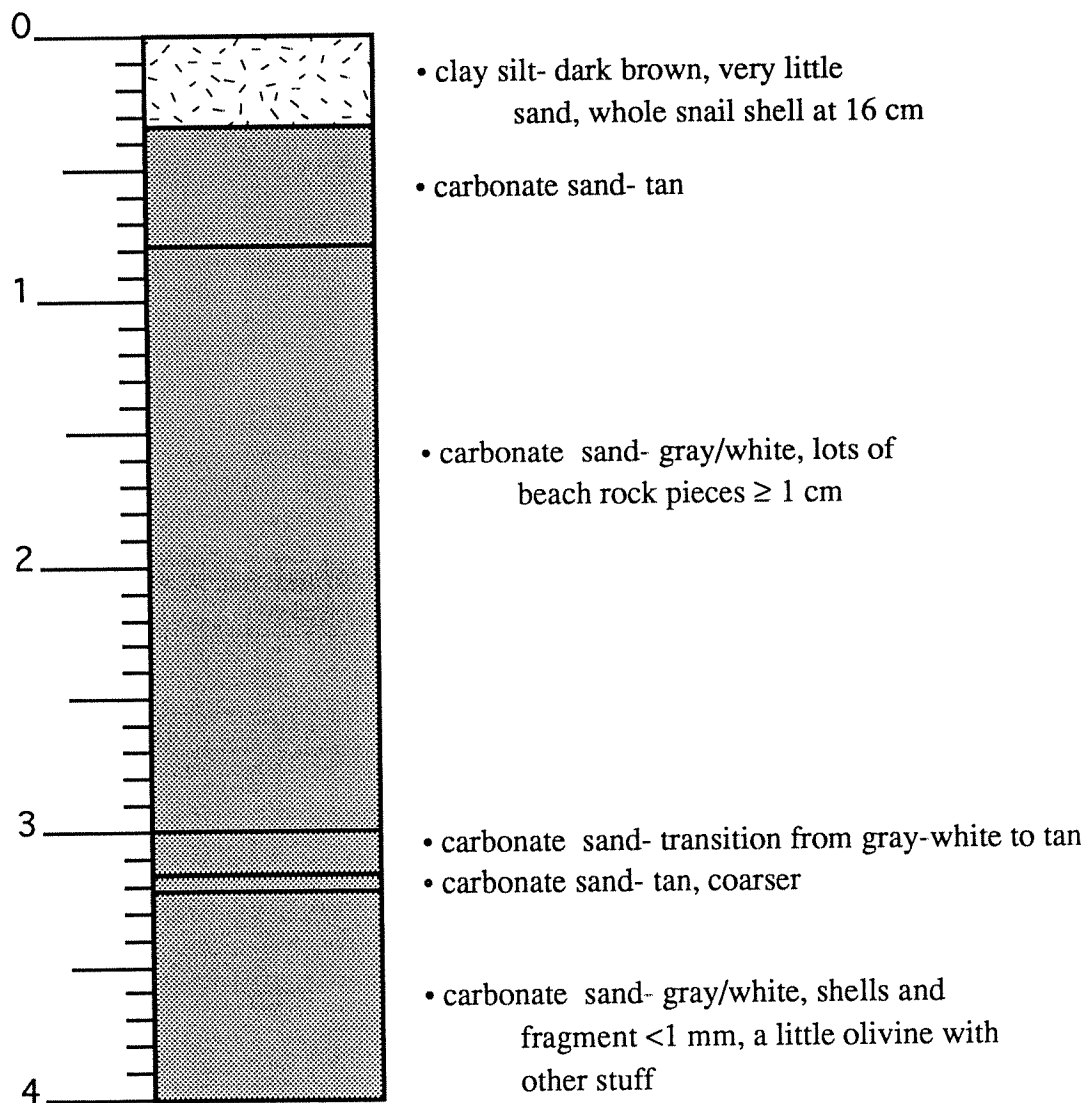


Core 1N - elevation: 1.7 m

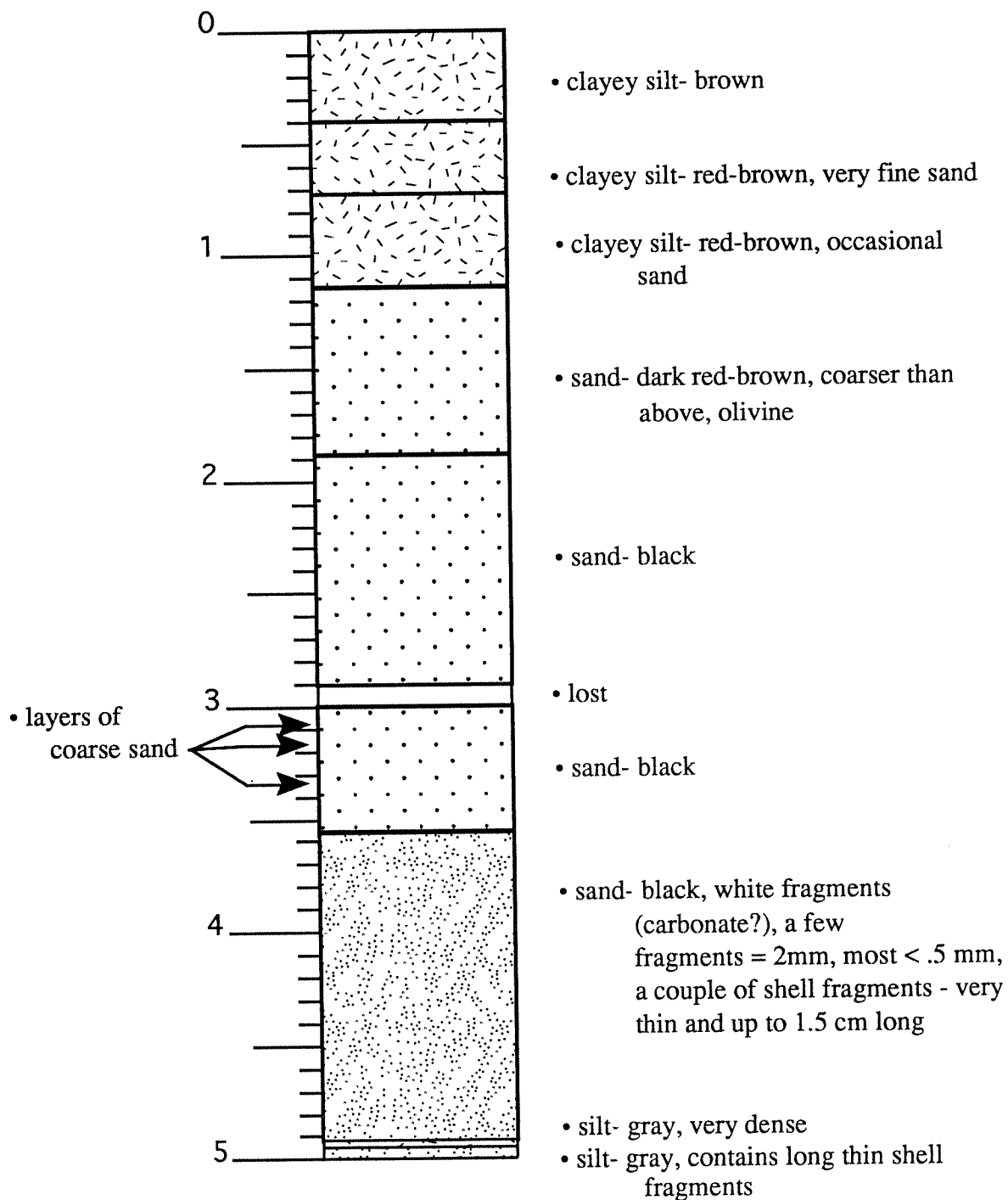




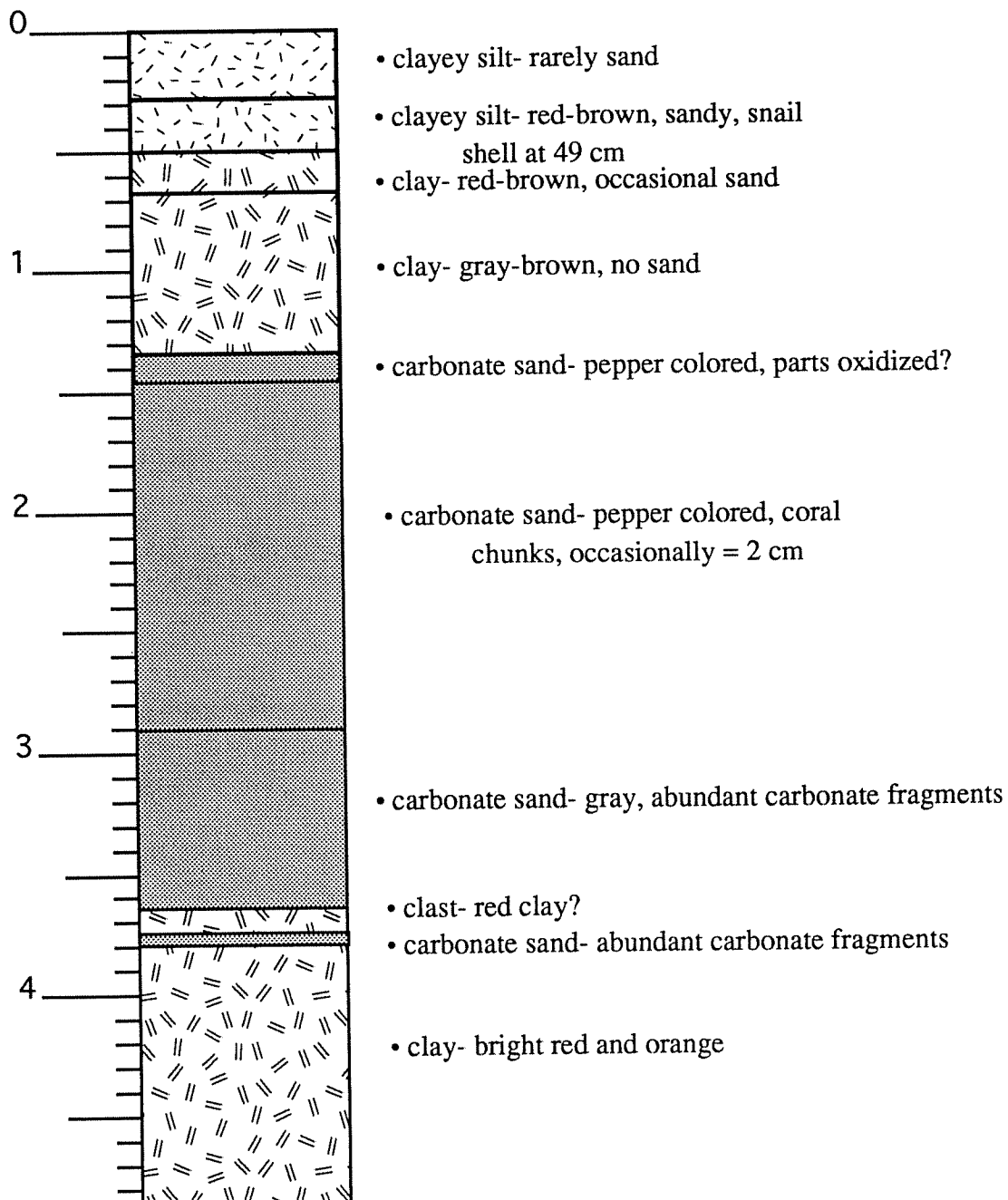
Core 1P - elevation: 2.4 m



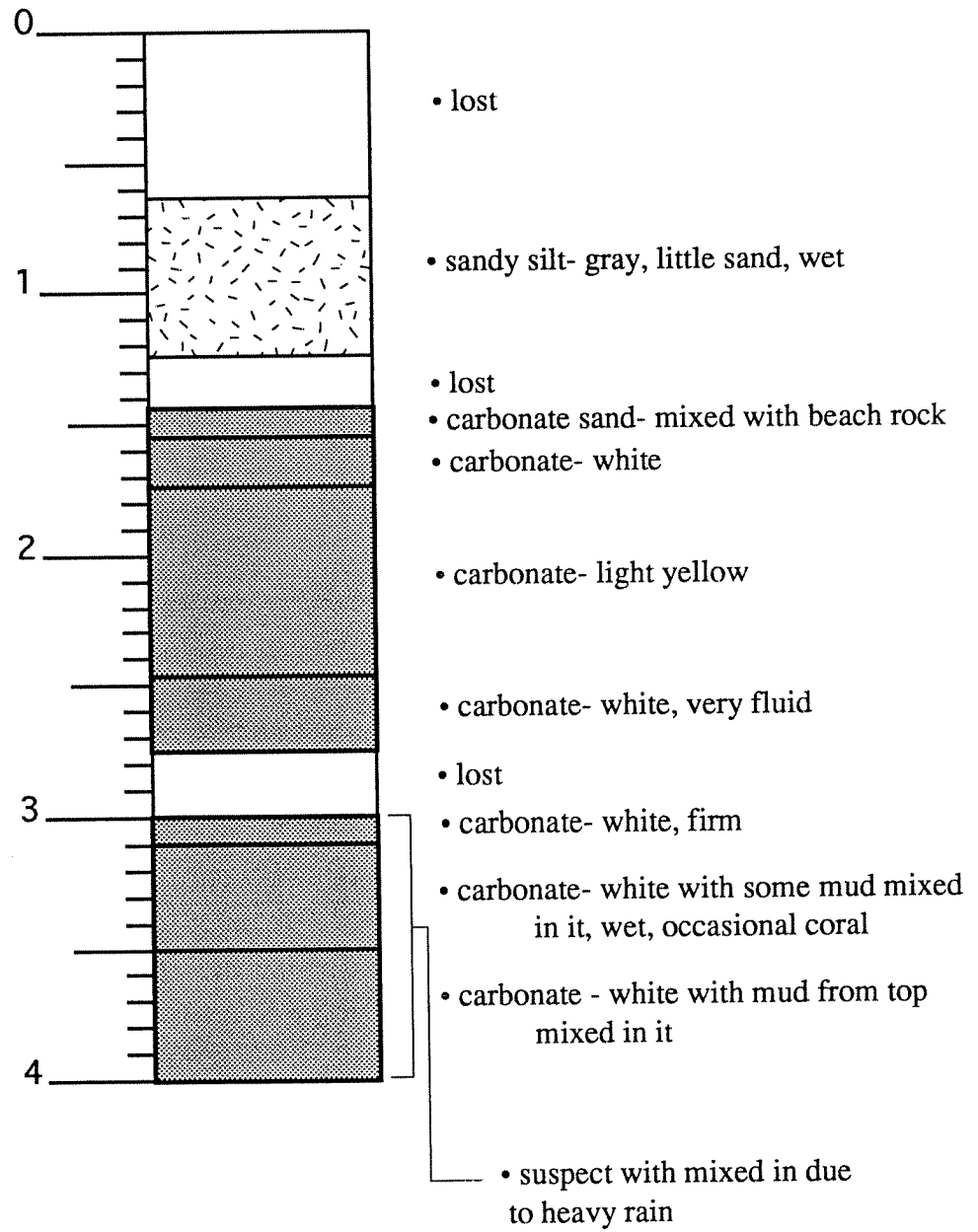
Core 1Q - elevation: 2.4 m



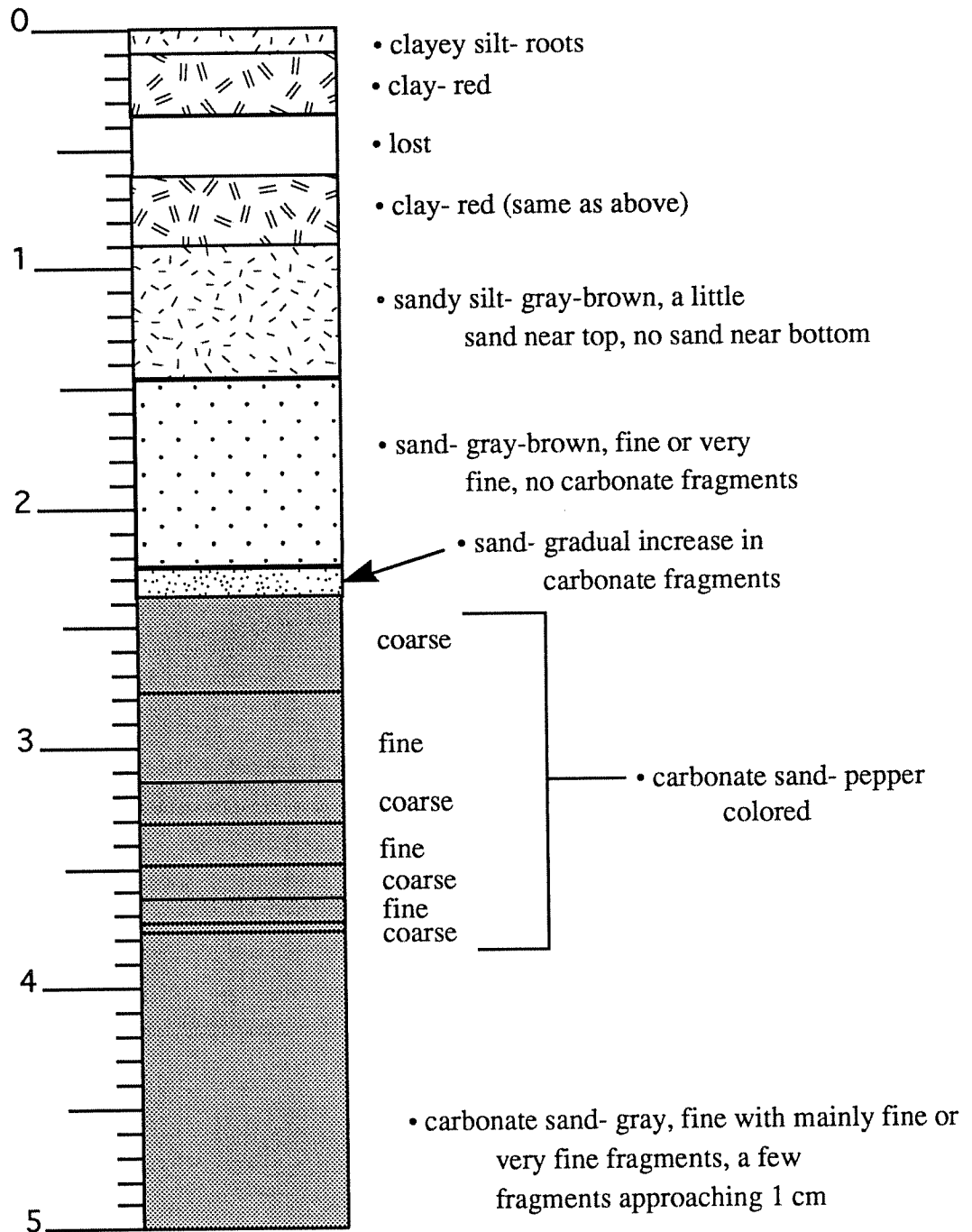
Core 1R - elevation: 2.9 m

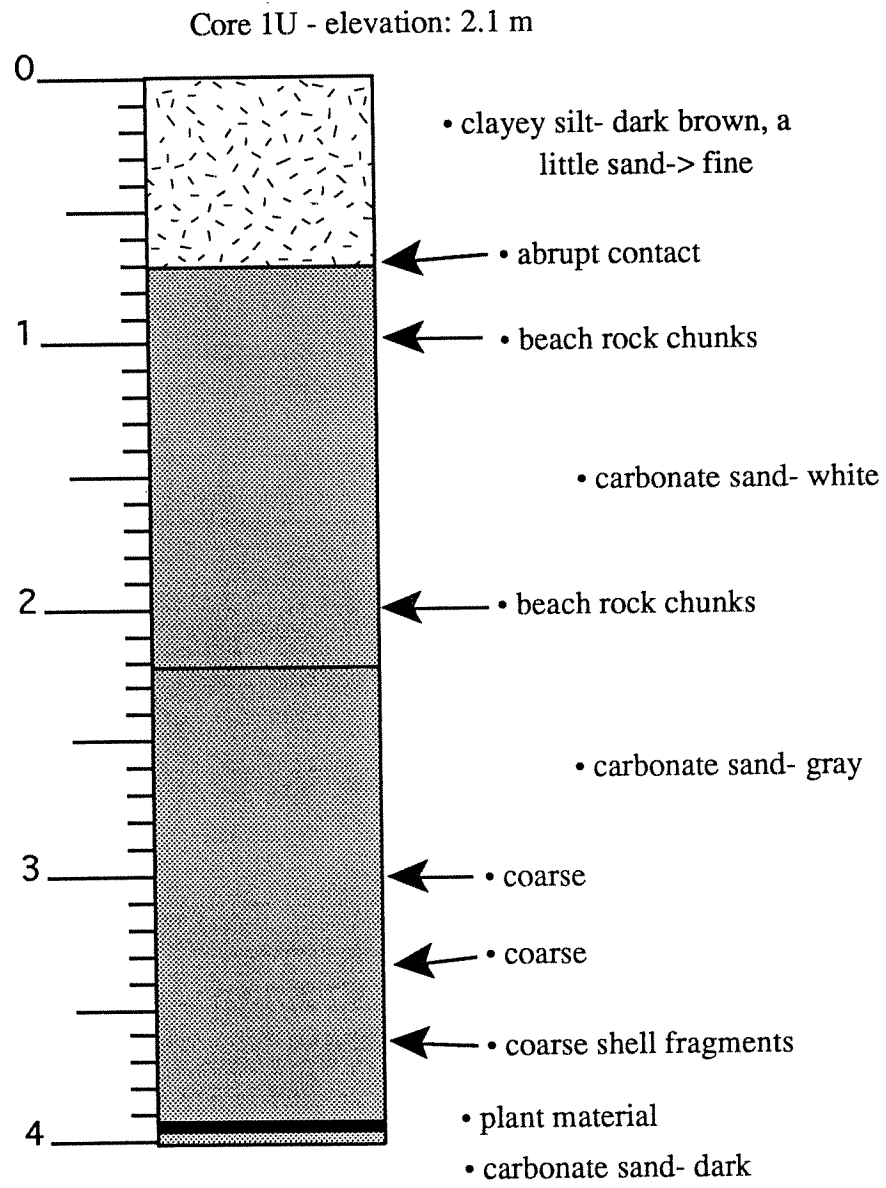


Core 1S - elevation: 2.9 m

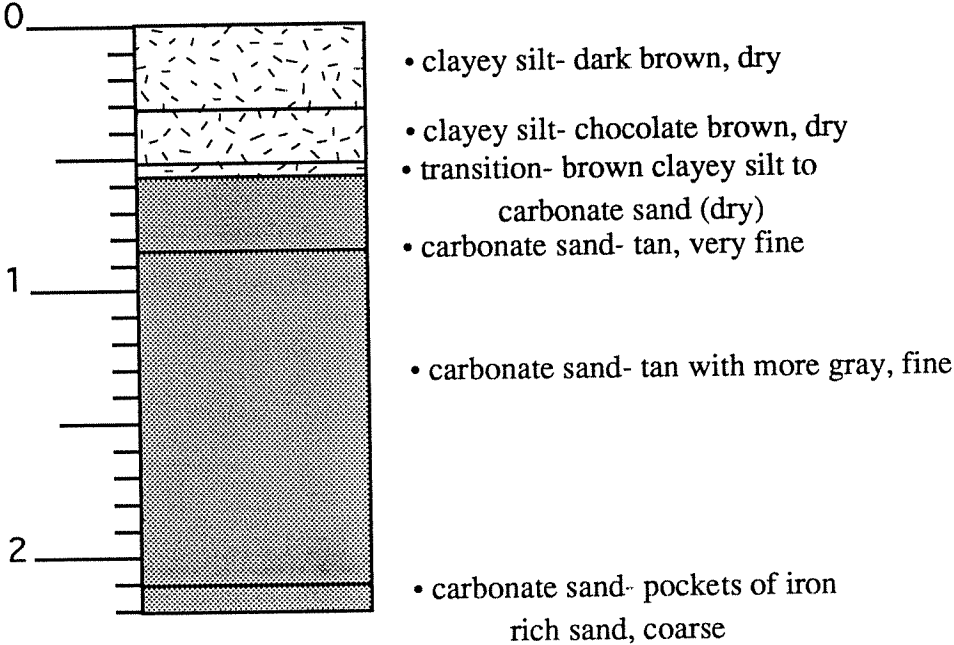


Core 1T - elevation: 3.0 m

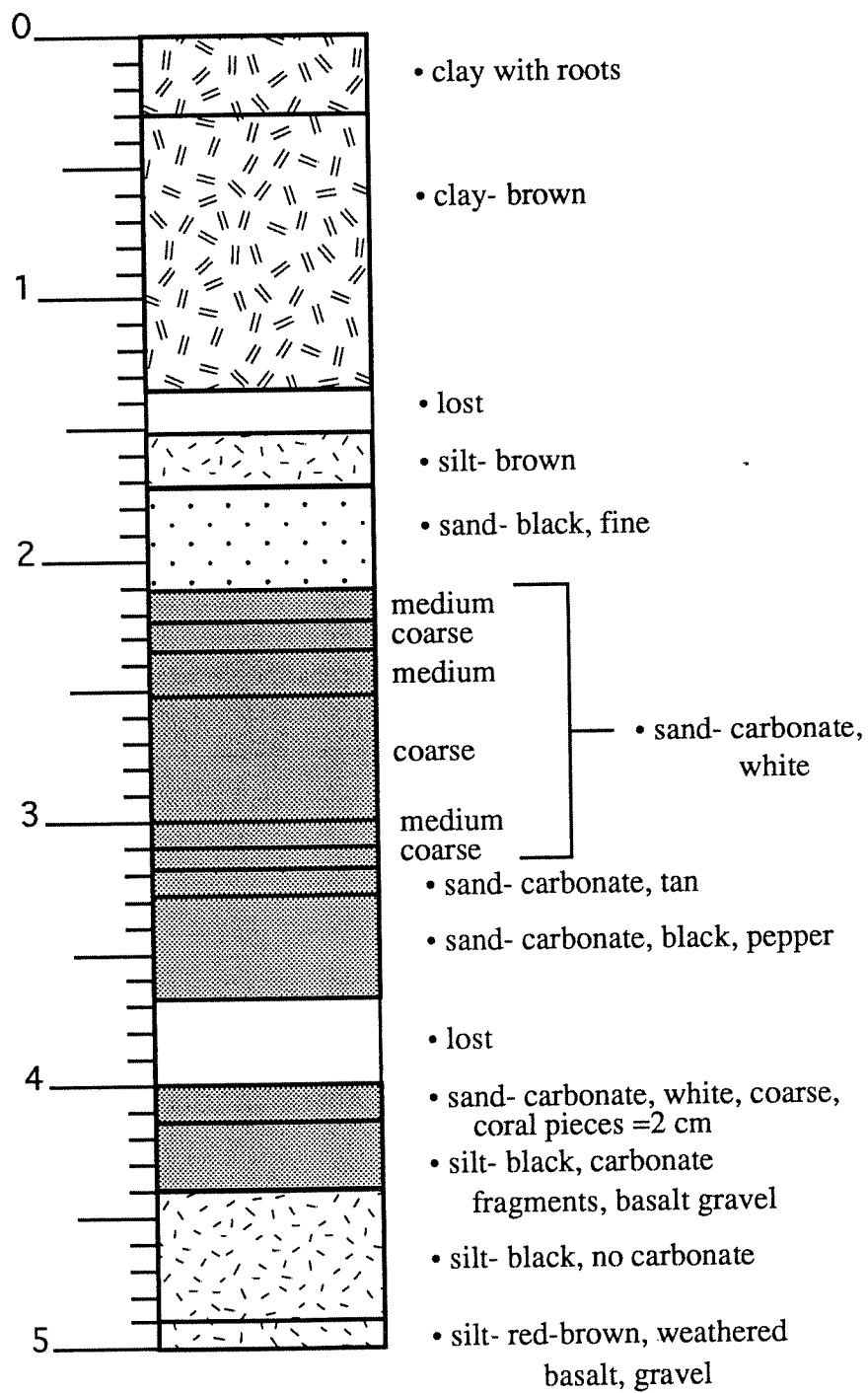




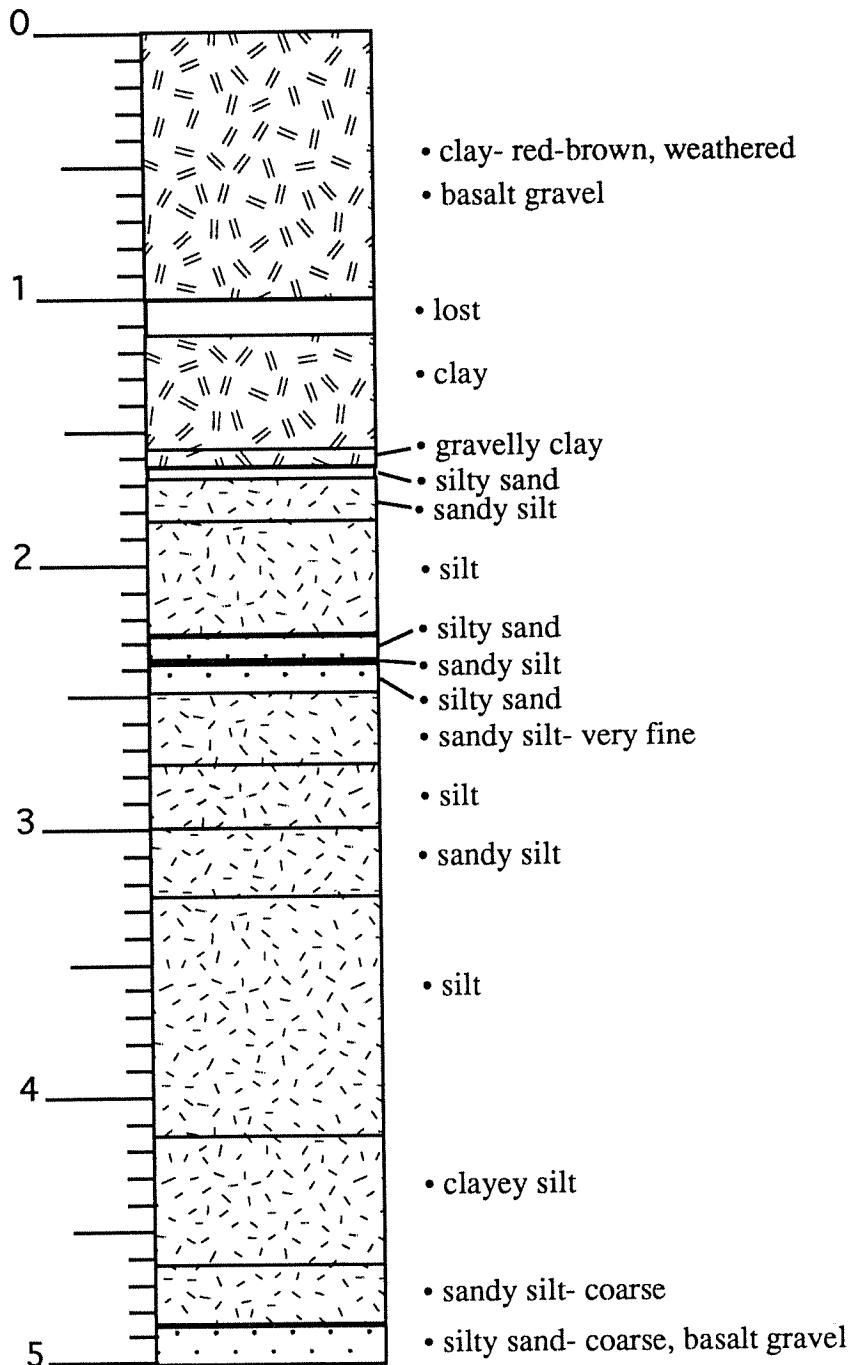
Core 1V - elevation: 2.4 m



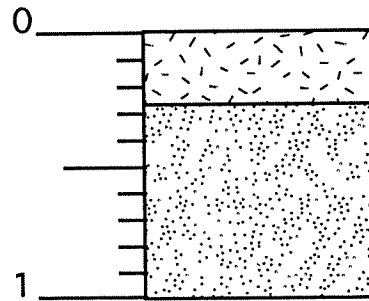
Core 1W - elevation: 2.3 m



Core 1X - elevation: 2.9 m

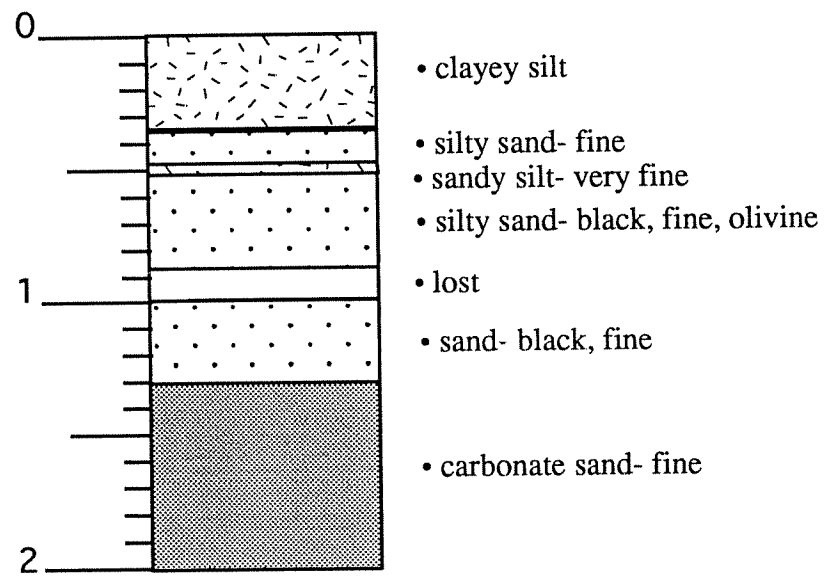


Core 1Y - elevation: 4.1 m

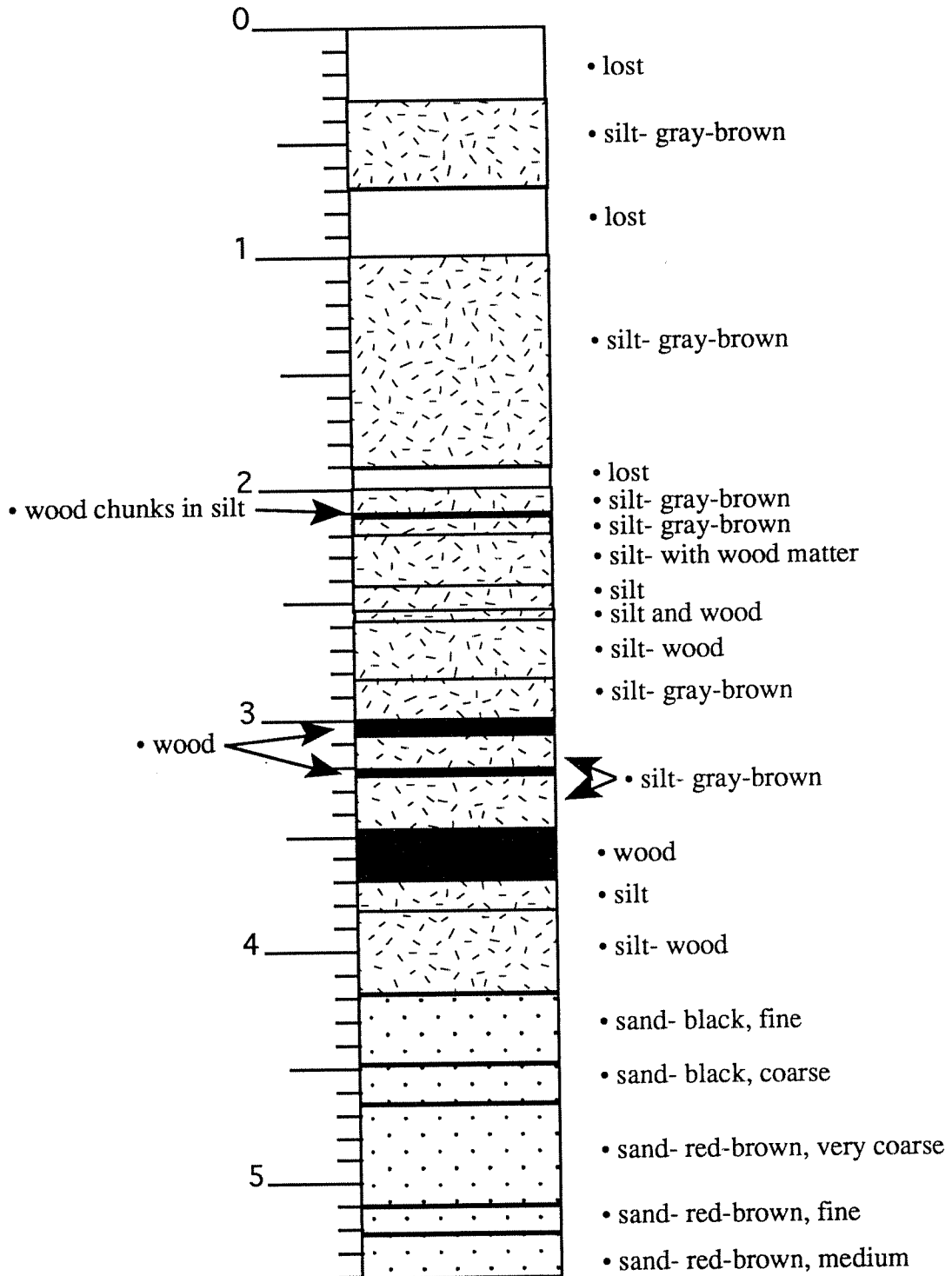


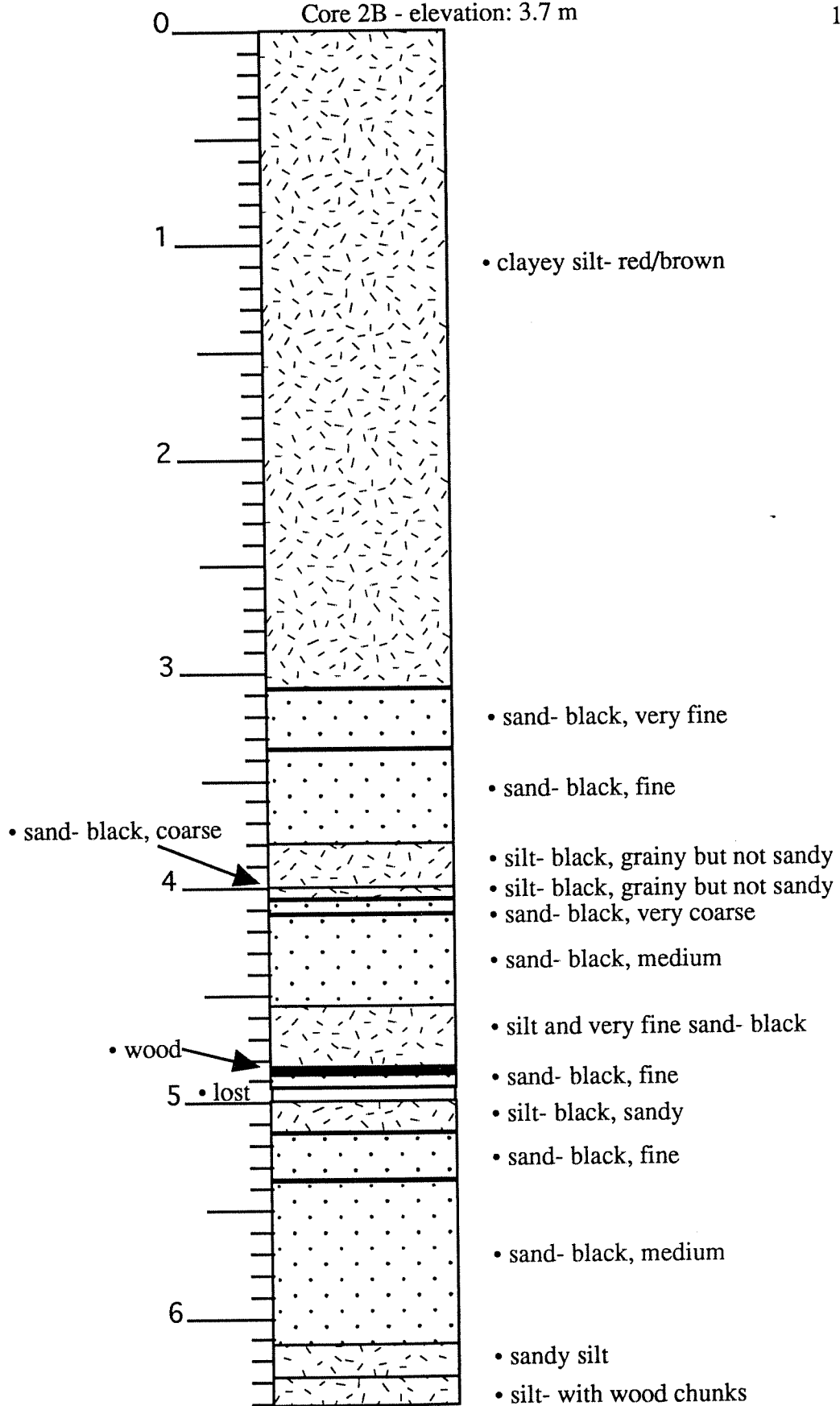
- silt- with organics and small carbonate fragments
- fluvialmarine sand- tan, medium but coarser towards bottom, more terrigenous towards bottom
- last 2 cm are more gray

Core 1Z - elevation: 2.3 m

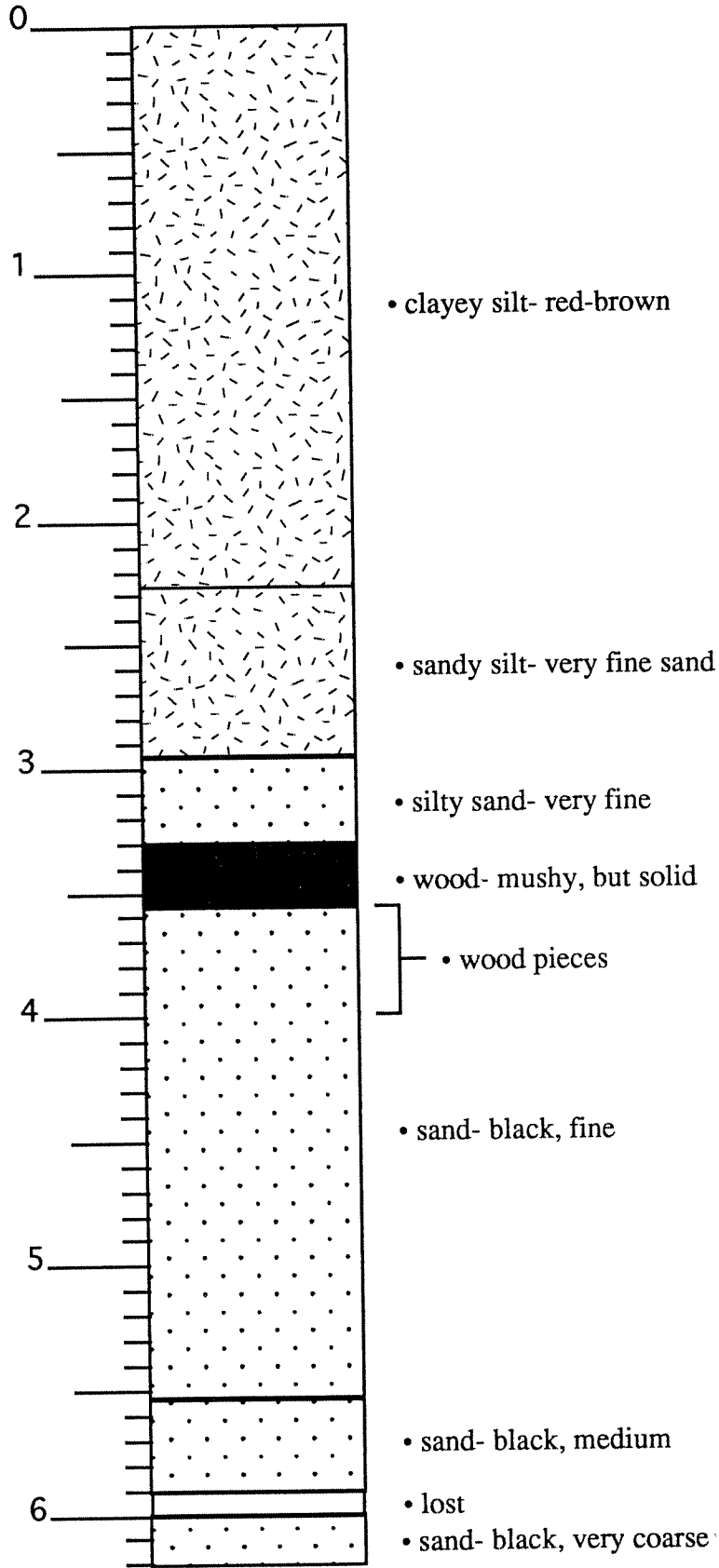


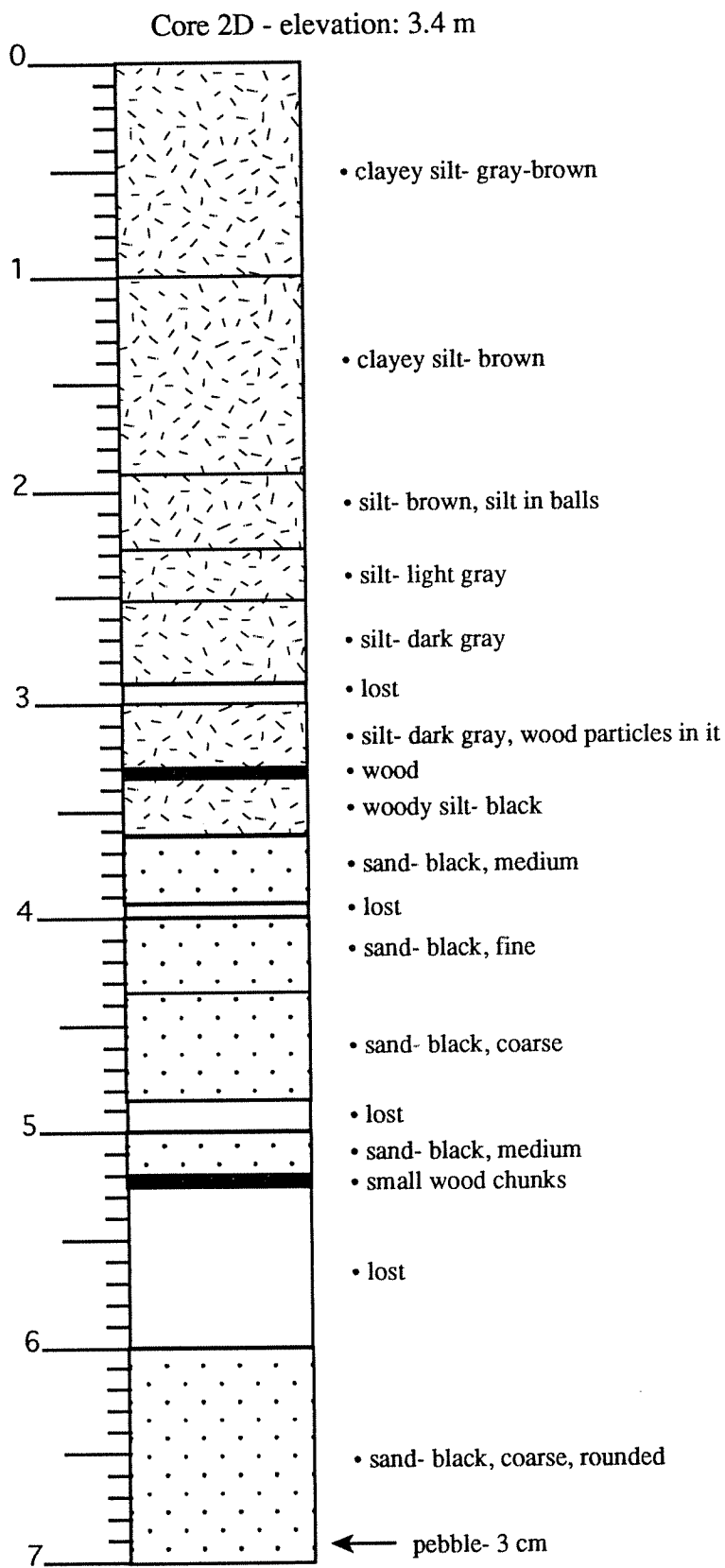
Core 2A - elevation: 2.9 m



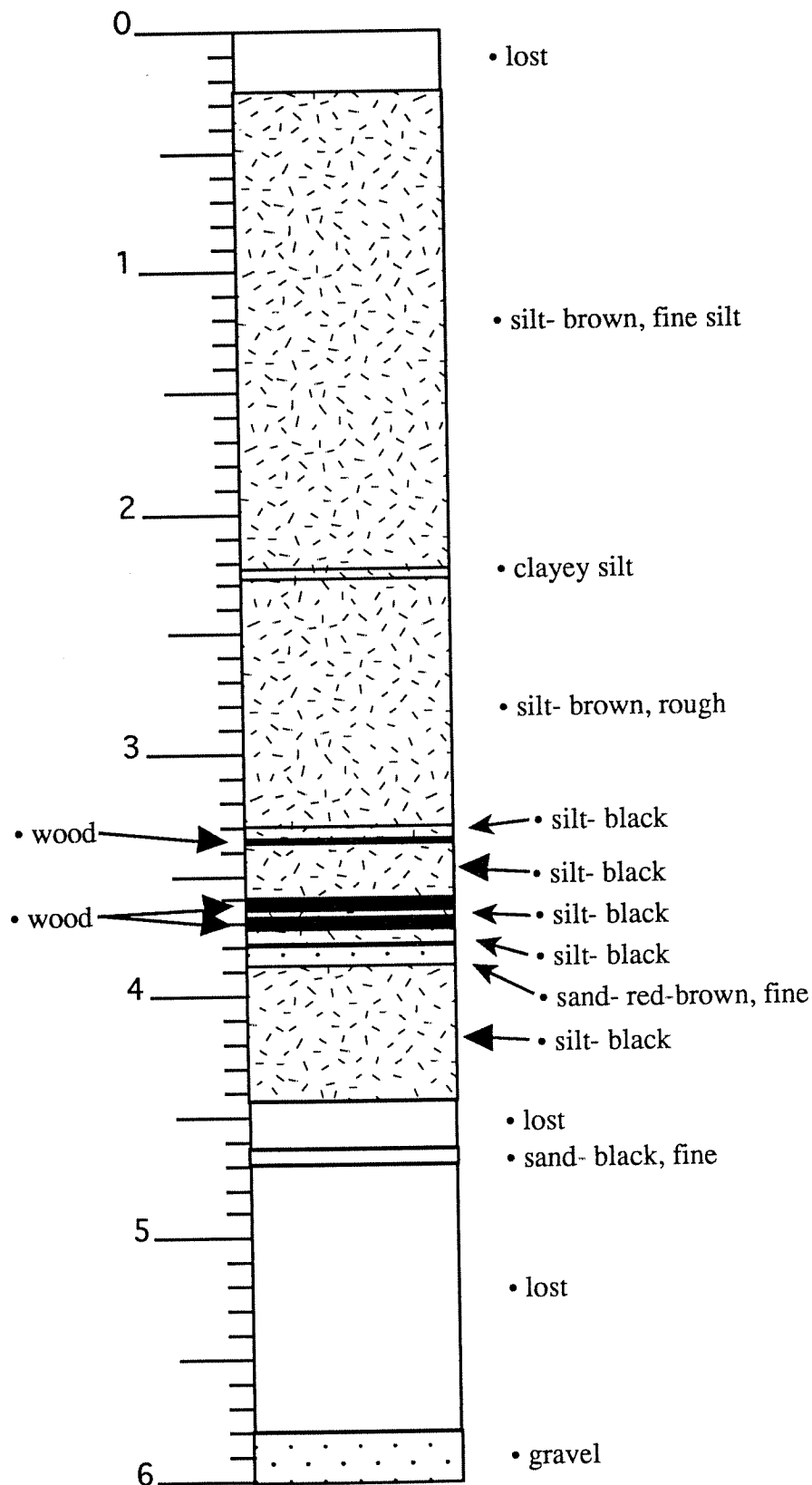


Core 2C - elevation: 4.1 m

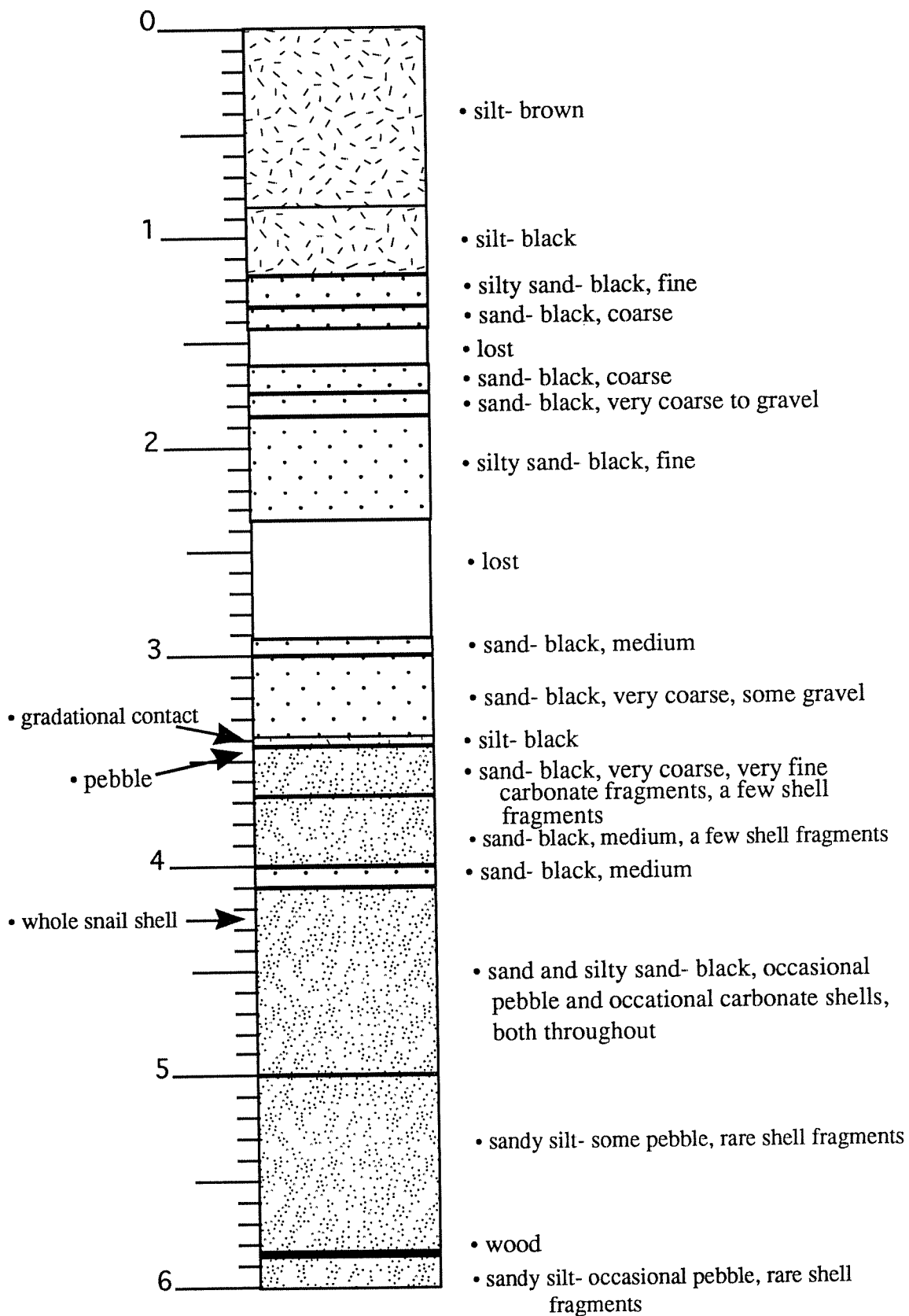




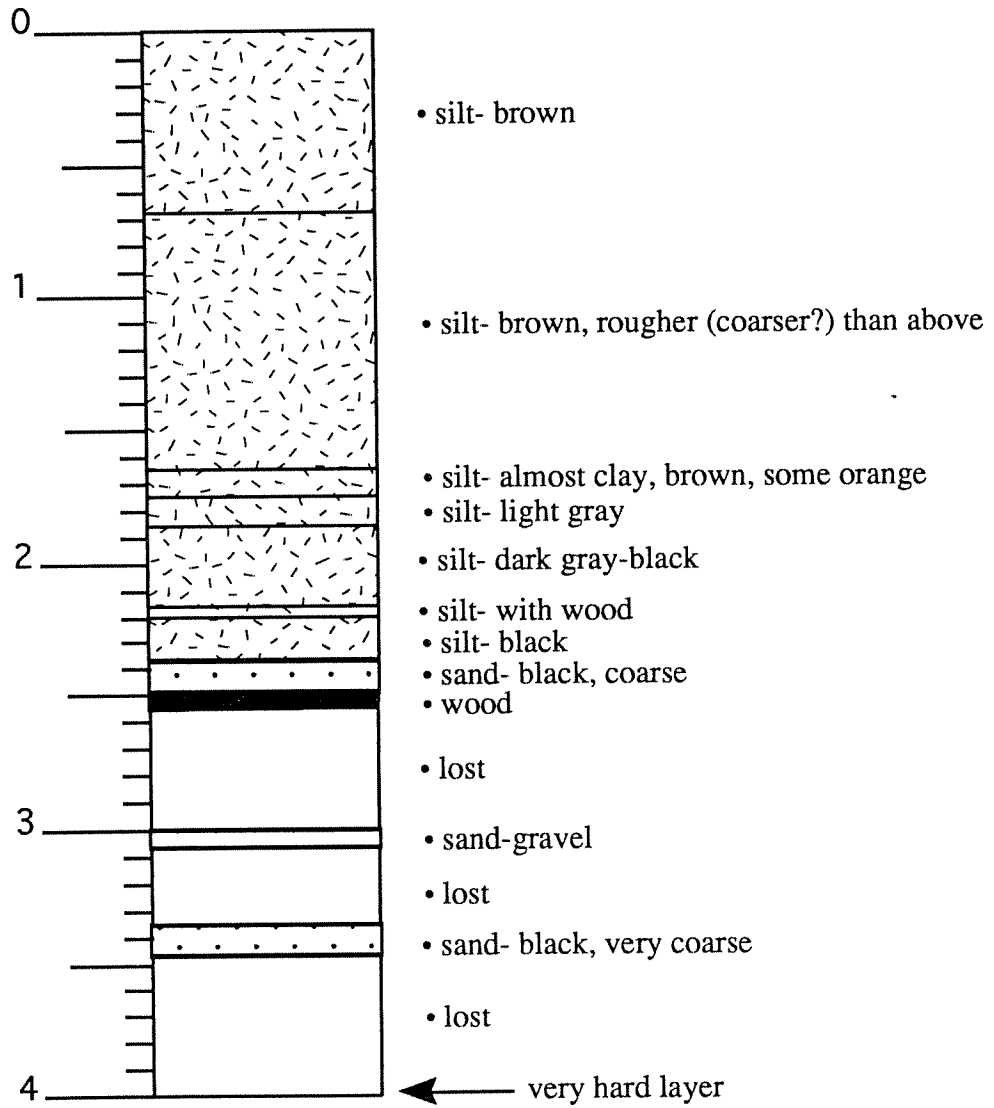
Core 2E - elevation: 4.3 m



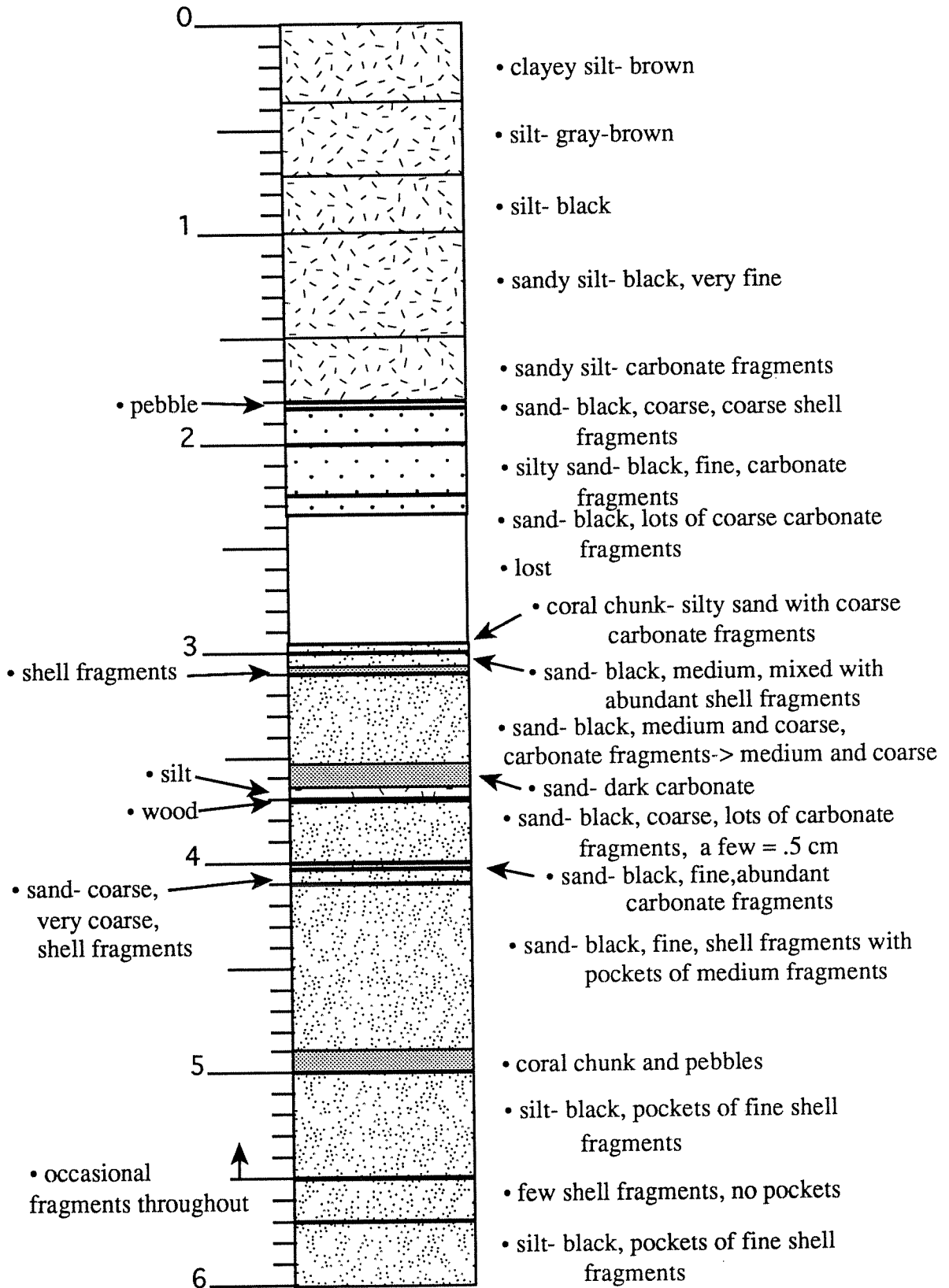
Core 2F - elevation: 1.4 m



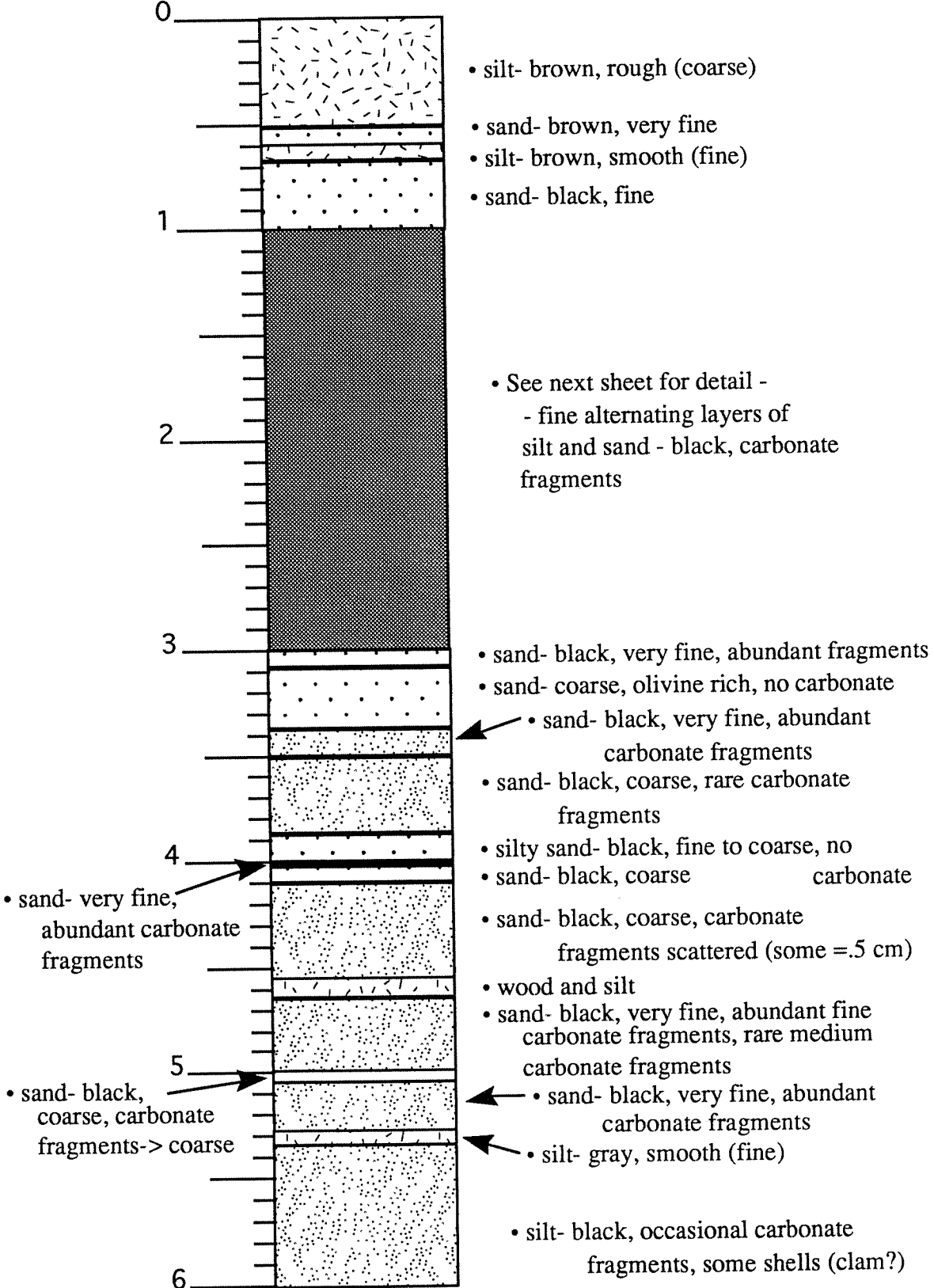
Core 2G - elevation: 2.6 m



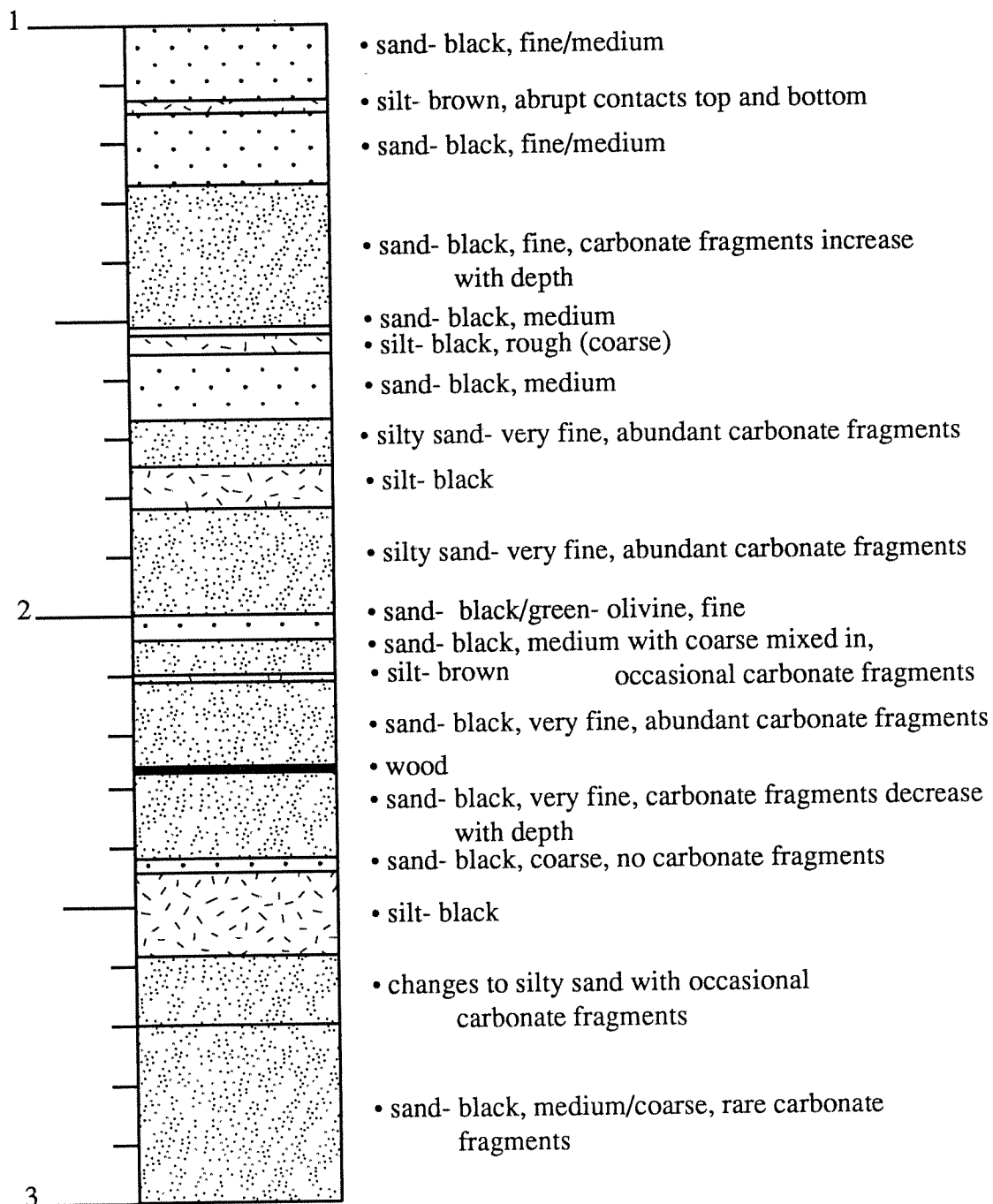
Core 2H - elevation: 0.6 m



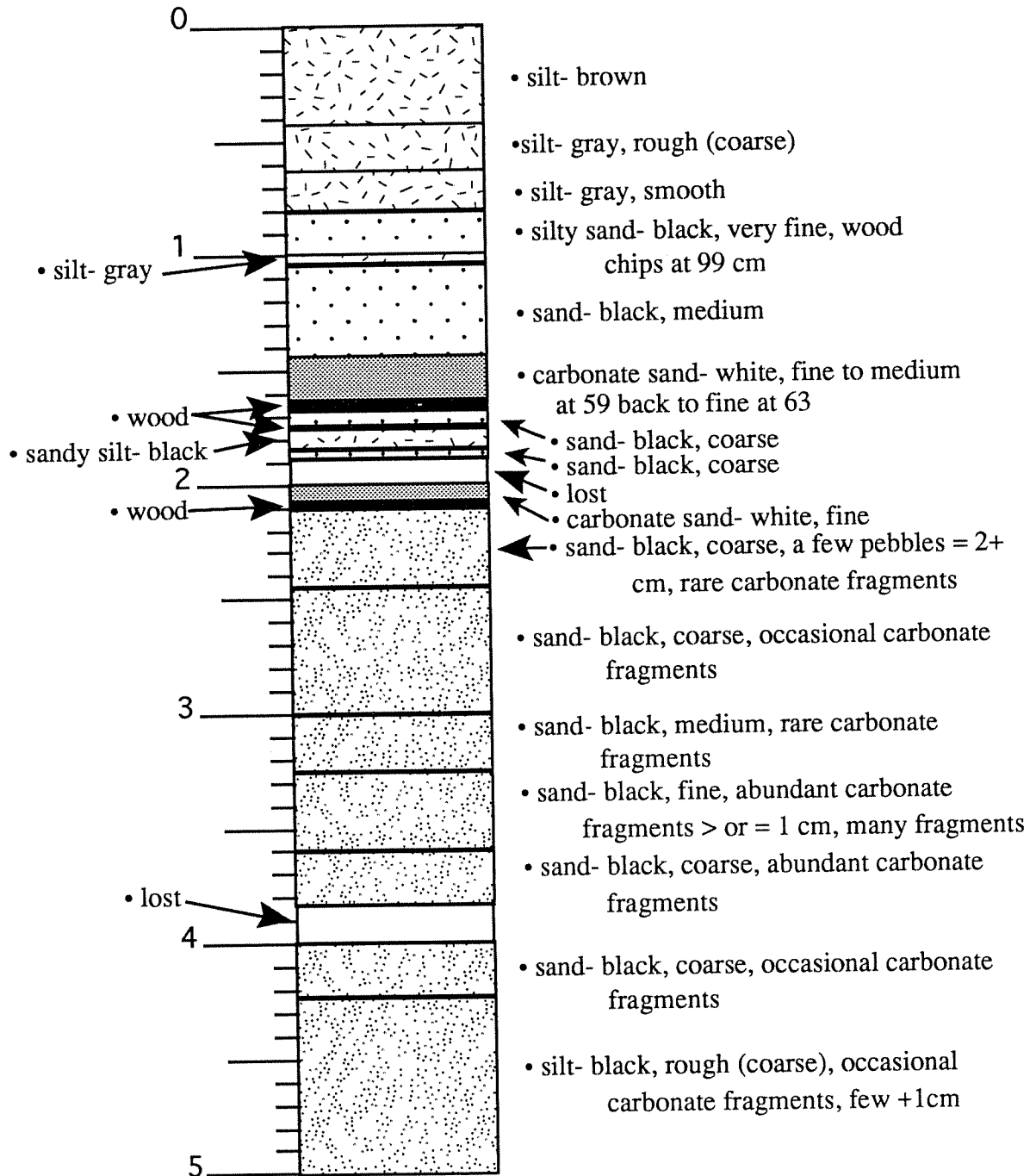
Core 2I - elevation: 1.2 m



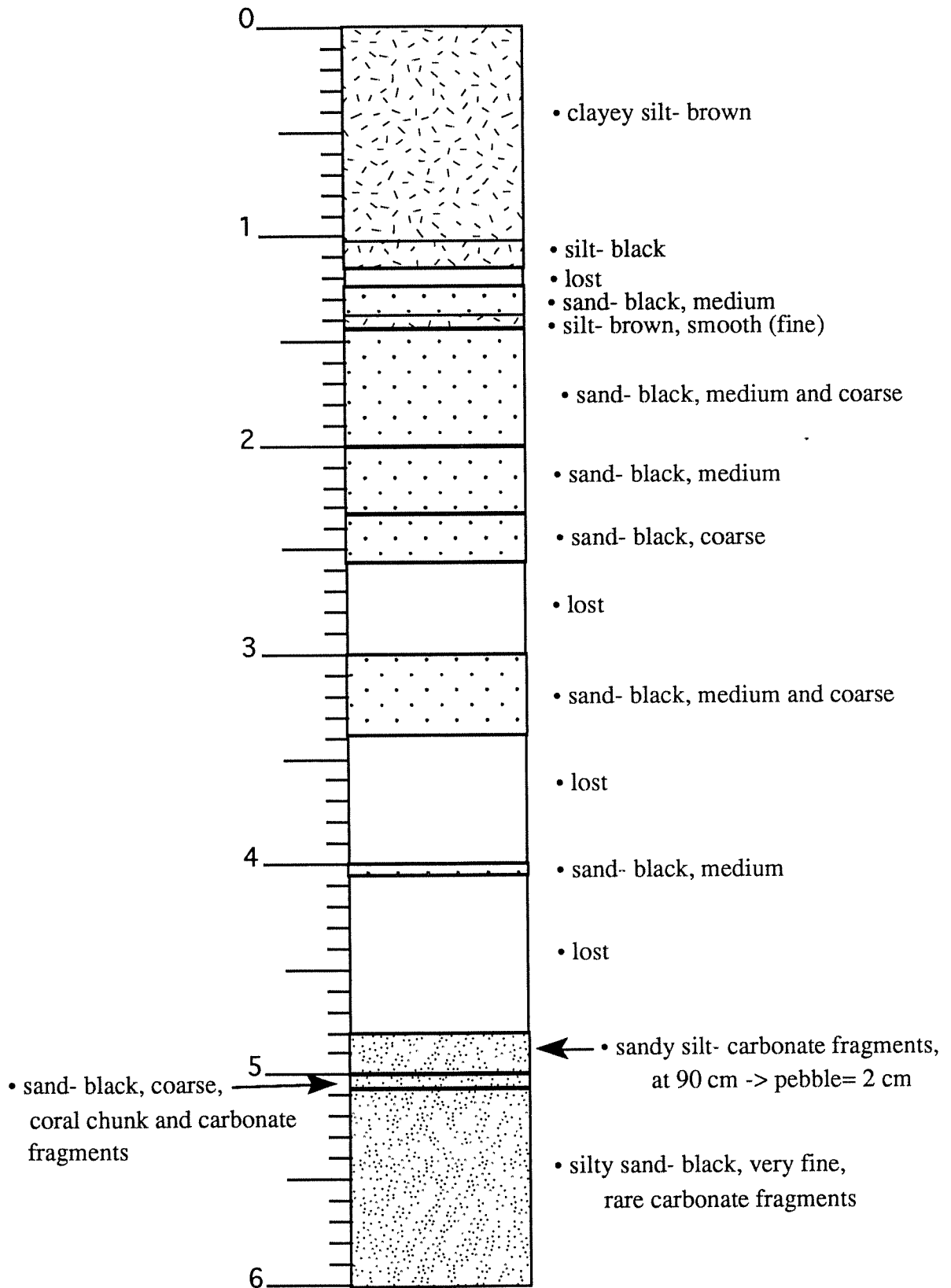
Core 2I - detail



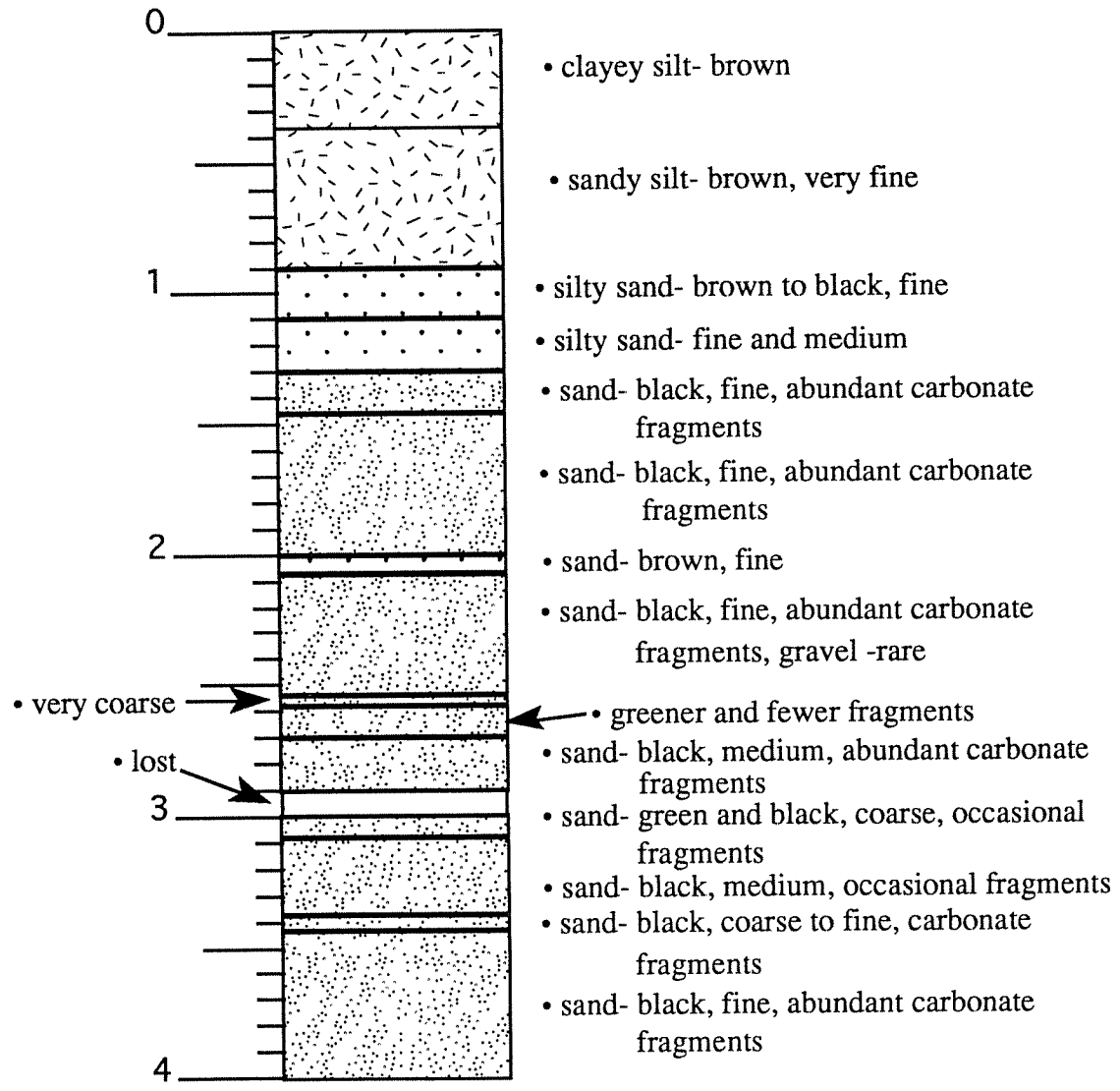
Core 2J - elevation: 1.4 m



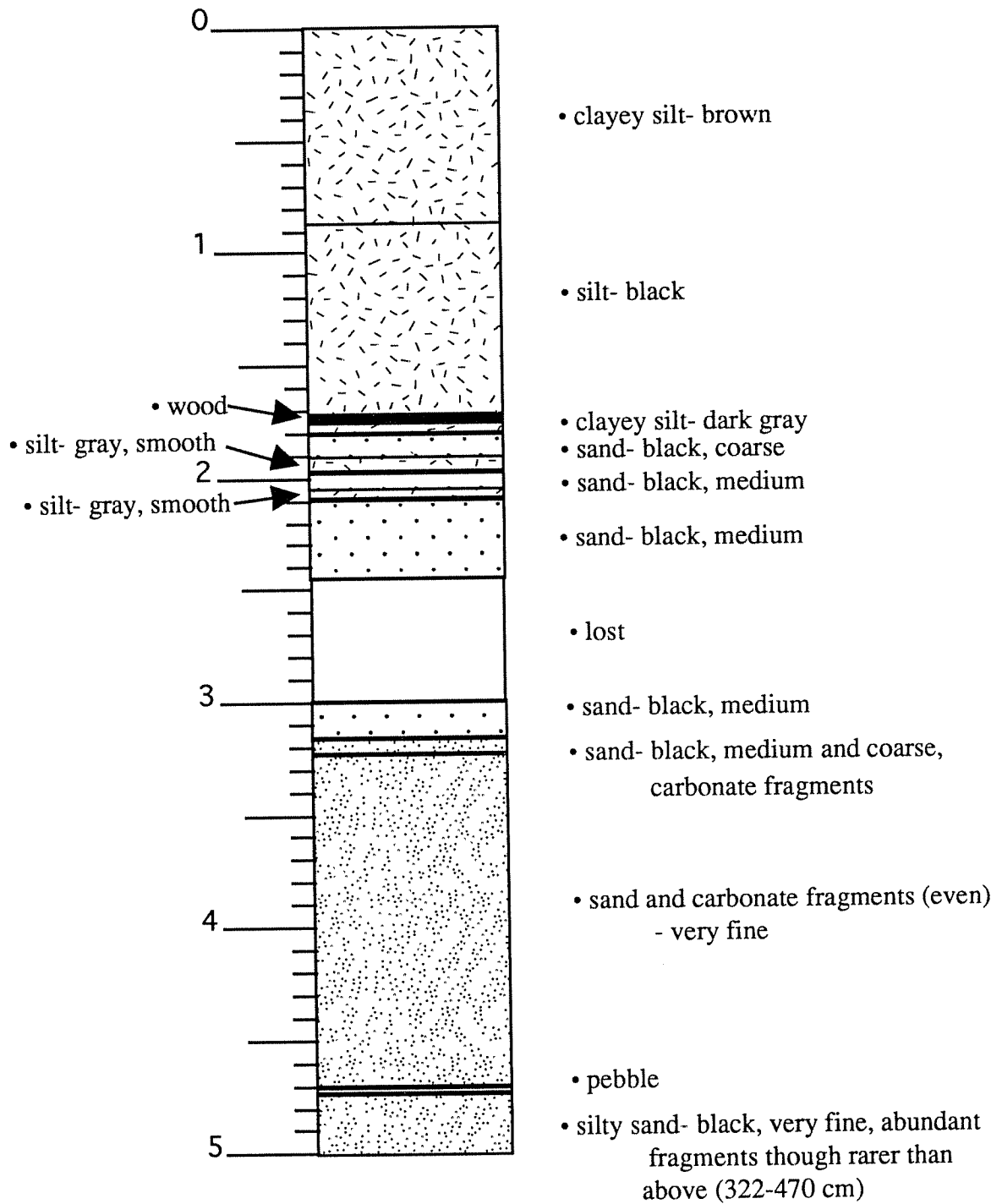
Core 2K - elevation: 1.5 m

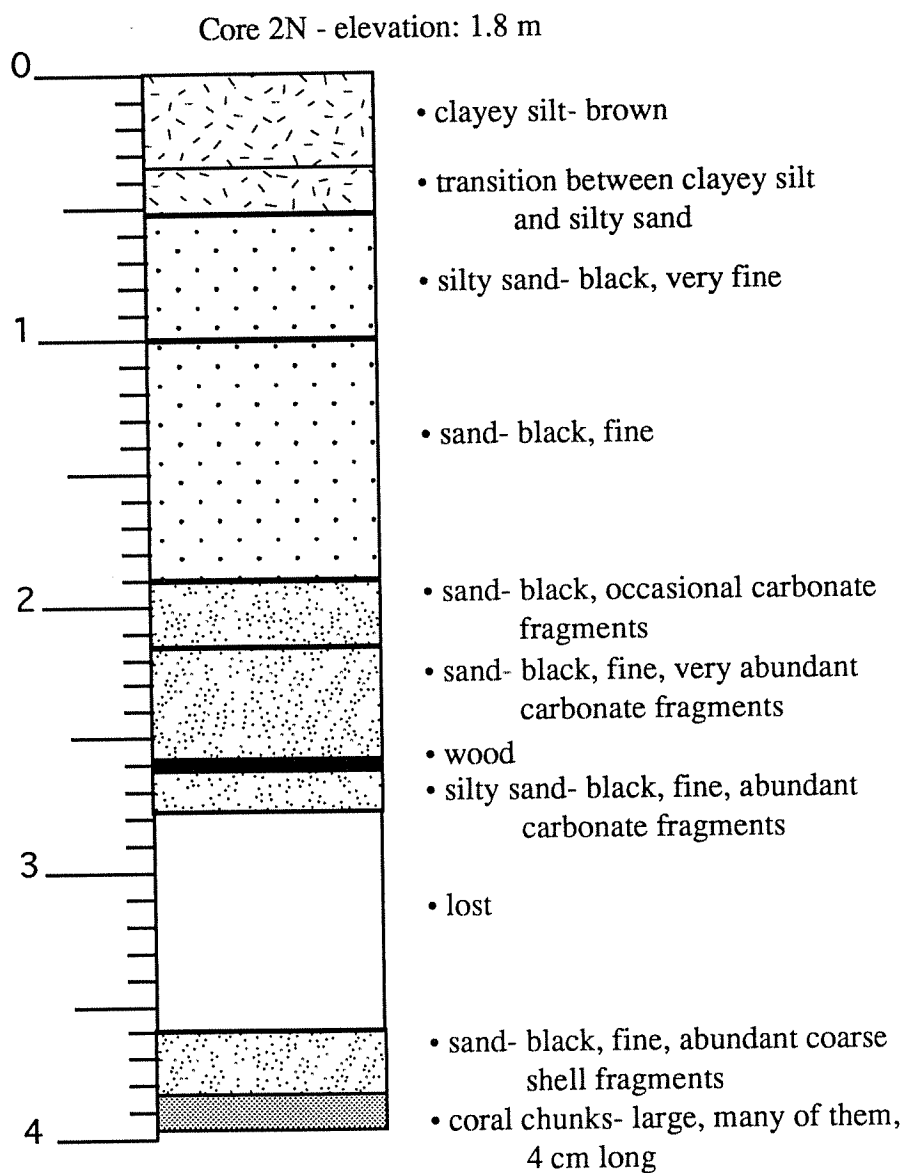


Core 2L - elevation: 1.7 m

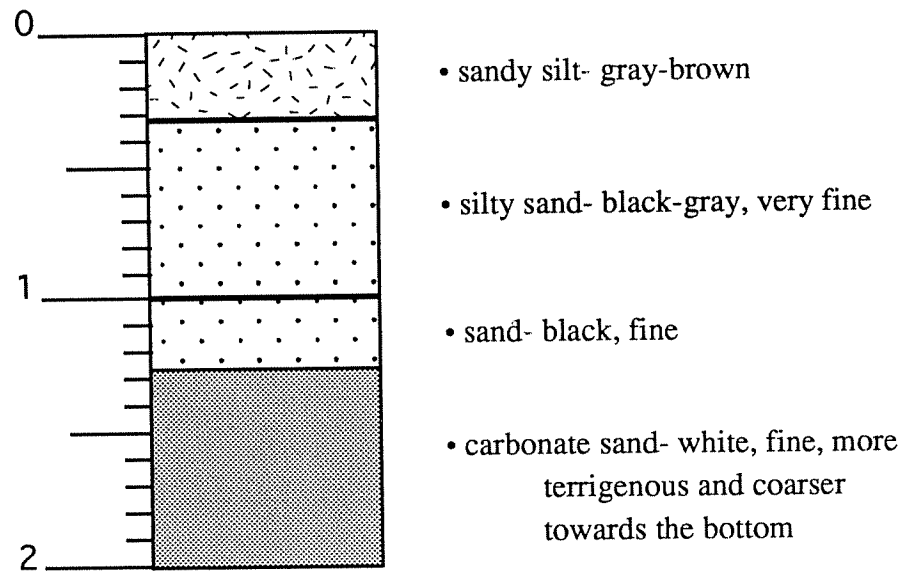


Core 2M - elevation: 1.1 m

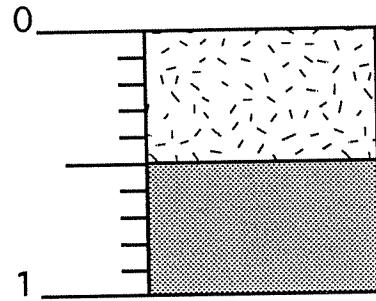




Core 20 - elevation: 2.3 m



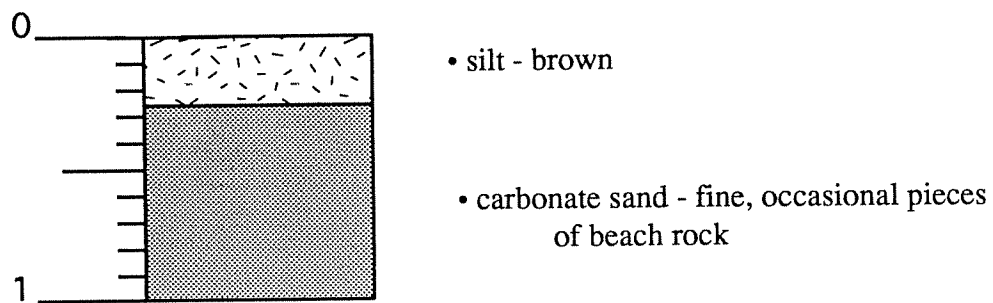
Core 2P - elevation: 2.9 m



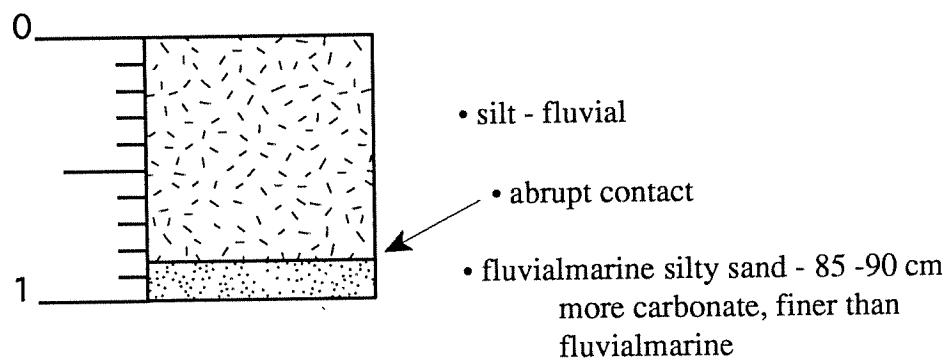
• silt- dark brown, rough (coarse)

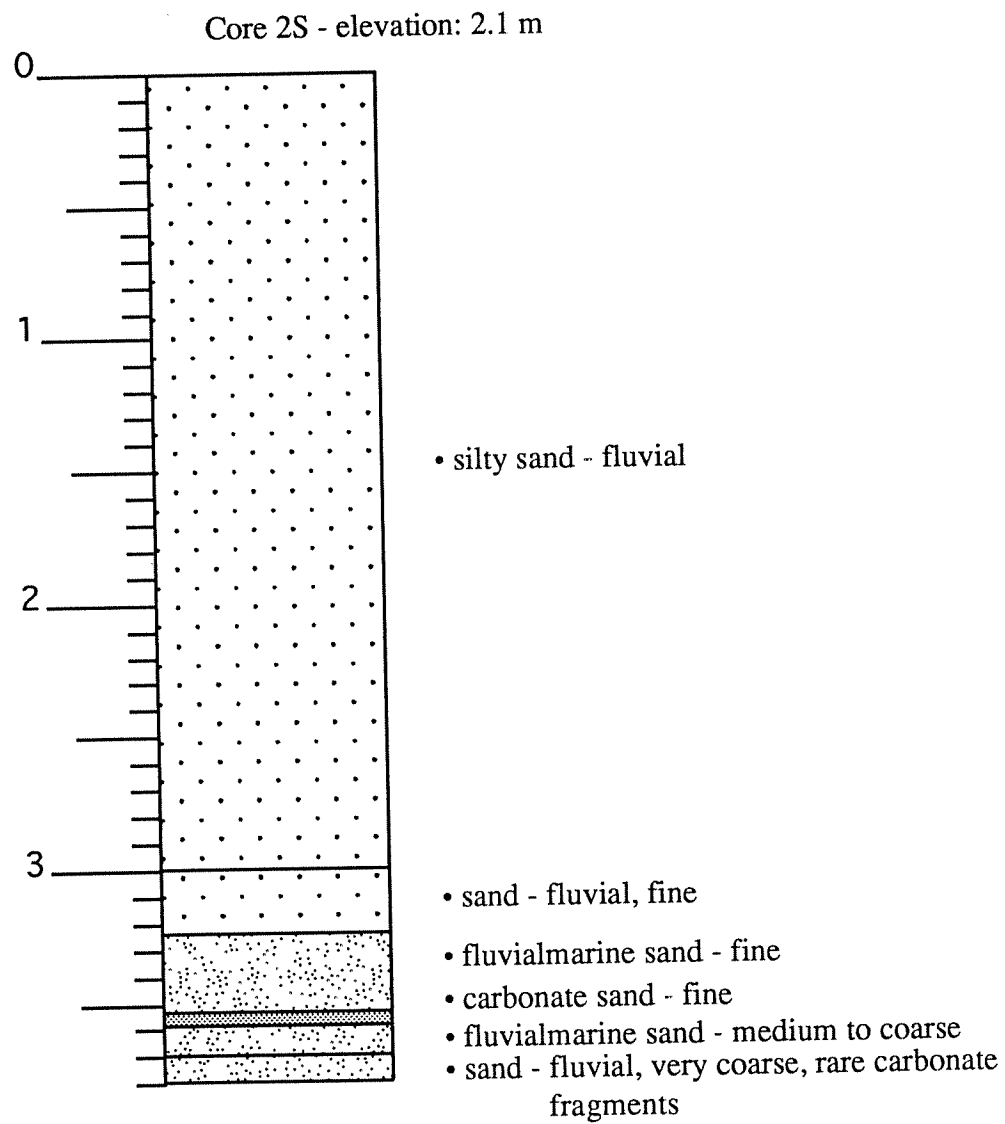
• carbonate sand- white-grey, fine

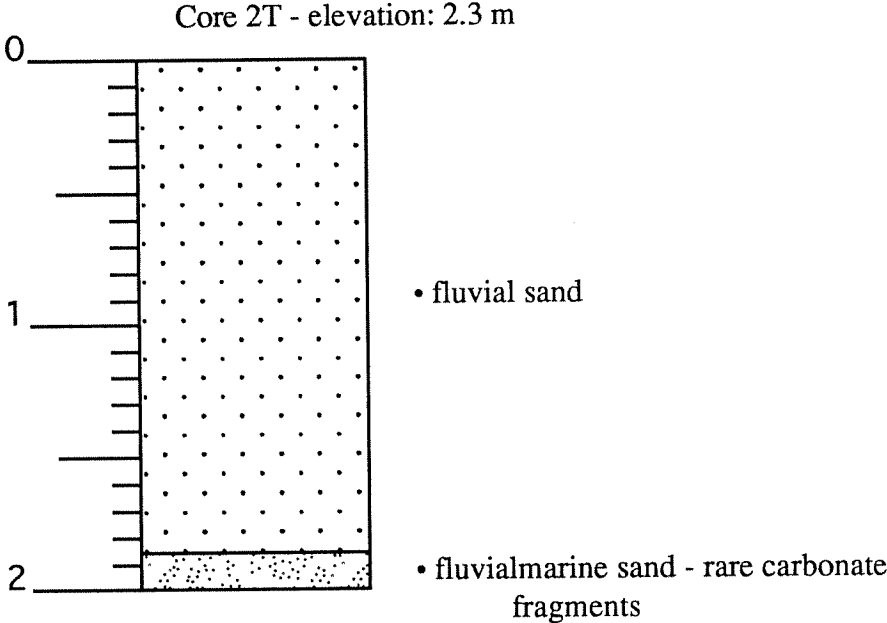
Core 2Q - elevation: 2.4 m

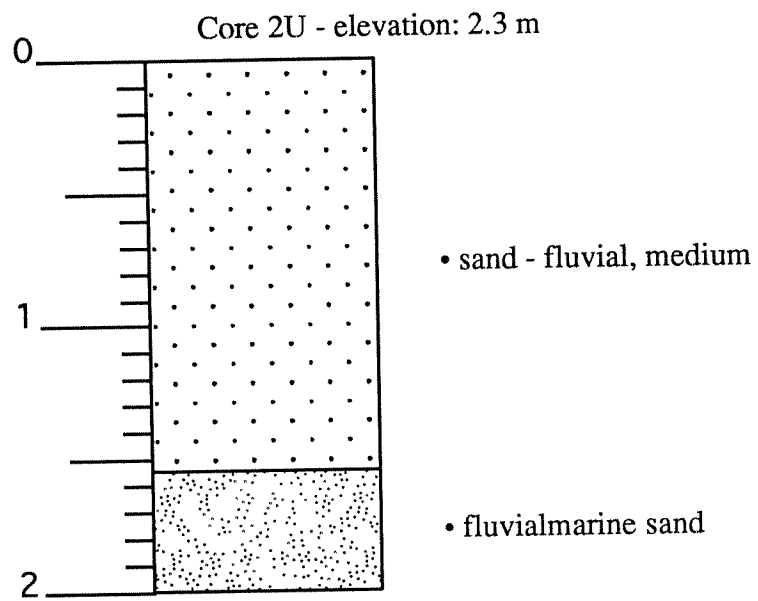


Core 2R - elevation: 1.8 m

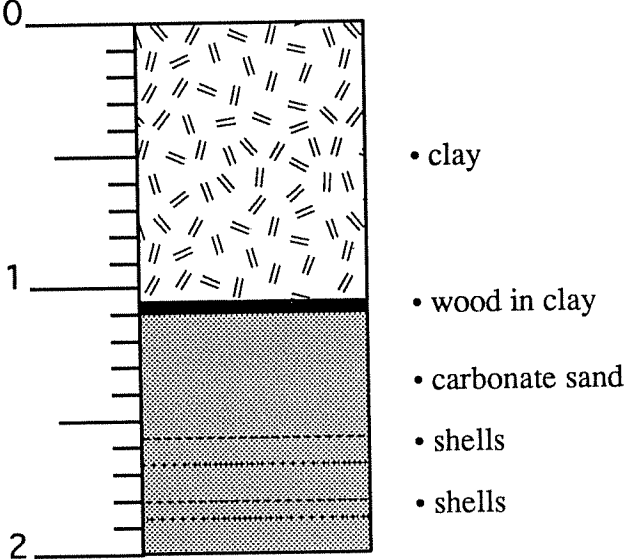


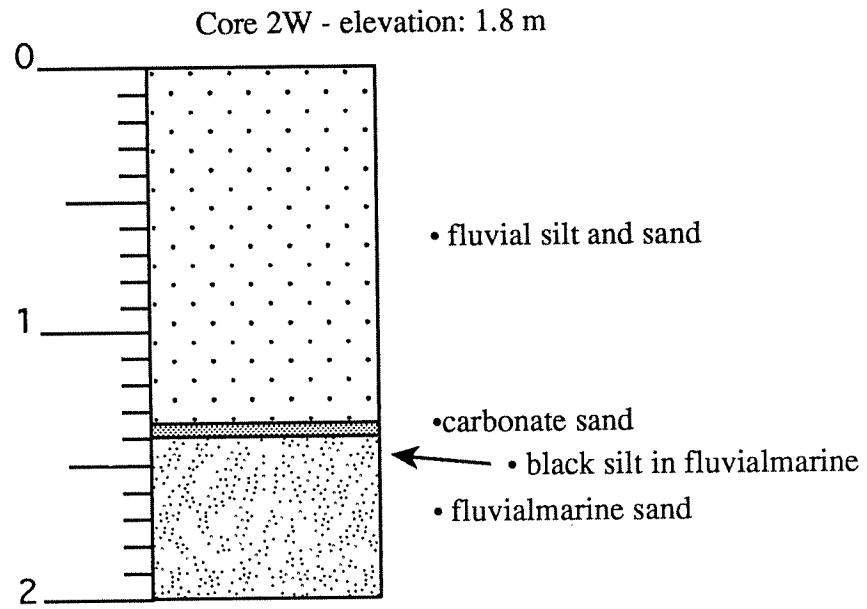


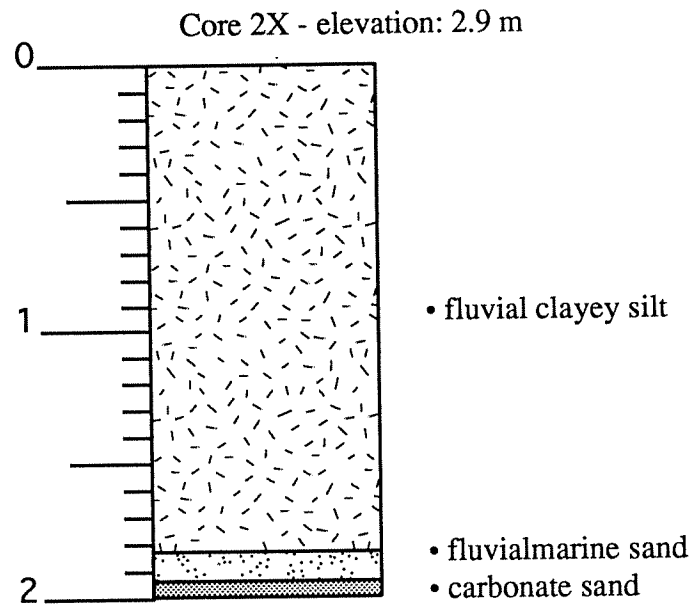


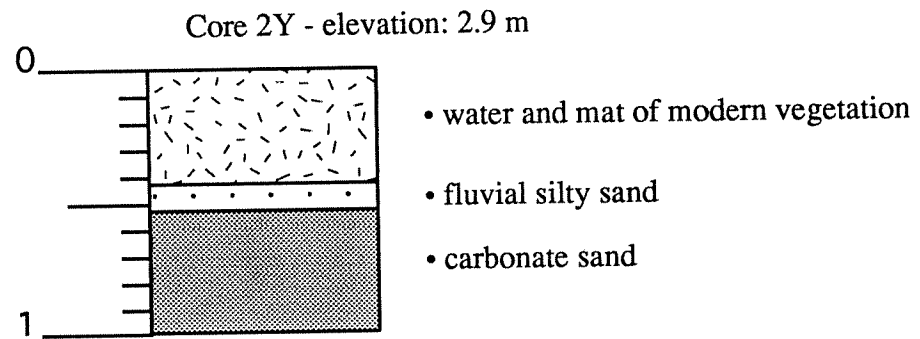


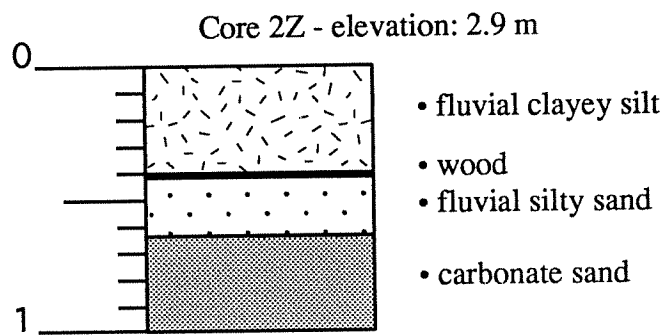
Core 2V - elevation: 2.1 m

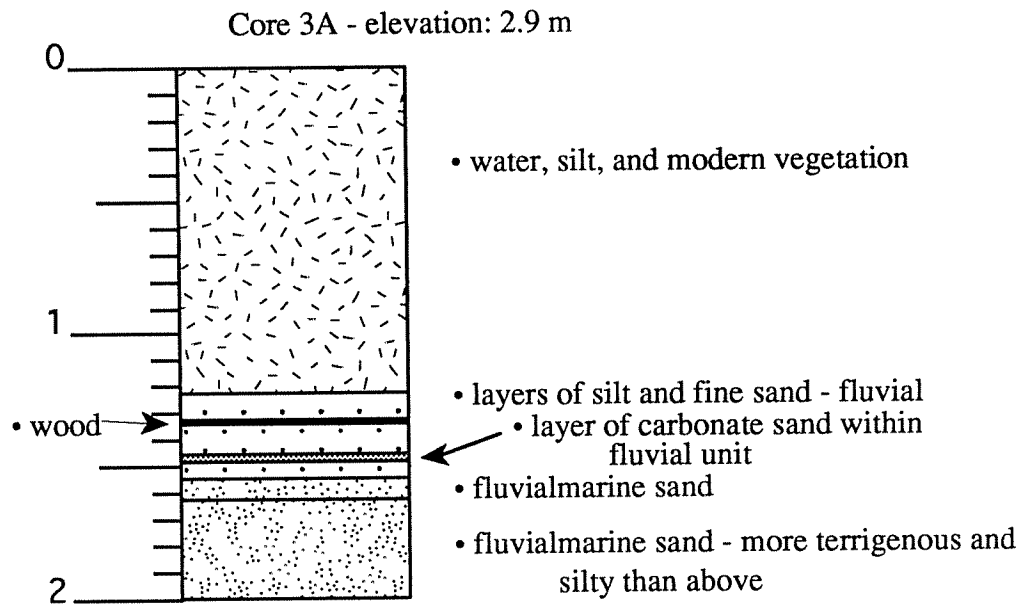












<u>Depth (cm)</u>	<u>Description</u>
0-6	• fine brown mud; contains plant stems, leaves, multiple rootlets; very wet.
6-15	• same as above, but drier; long rhizome (?) from 14-21 cm.
15-30	• plant remains becoming more oxidized; mud has splotches of rust colored oxidation and is more clayey in texture (sticks together more).
30-40	• remains still show oxidized character; long roots weave through entire section; sediment has taken on a dark clayey character, clay clumps together when prodded, very fine grained.
43	• contact , sediment becomes more oxidized and less clayey; small (3 mm) hard ball found, pebble? wood?
43-47	• strongly oxidized zone, only small rootlets.
47-58	• oxidized character slowly becomes less pronounced down section.
60-97	• dark mud with multiple small rootlets, less oxidation, very small amounts of sand.
fill	• larger rootlet at 68 cm; dark mud is coarse than previous muds, slightly gritty, but no coarse sand recovered (except for mentioned above).
100-125	• gritty dark brown mud, contains small nodules of harder, oxidized material, not rock (basalt?); splotches of oxidation, sparse organics.
125-147	• gradational contact ; much less oxidation; small wood fragments (136 cm); darker, finer, clayey mud.
147-162	• mud becomes slightly more gritty.
162-195	• dark gray, homogeneous clay with small fibrous organics.
195-200	• concentrated plant matter, removed for radiocarbon dating. 132-162 = gray-brown mud; 162-200 = dark gray mud.
200-228	• concentrated plant matter, leafy debris, very dense (200-213 cm), concentration declines down section.
229-283	• gradational contact ; dark brownish-gray mud, fine clayey, 252 cm and 258 cm have leafy plant remains; small fibrous, scattered organics; homogeneous matrix.
283-290	• abrupt contact ; peaty section, coarser, peat is finer texture than previous plug.
290-294	• dark brownish-gray clayey mud.
294-298	• abrupt contact ; coarser, darker, peatier
300-305	• peaty section continues from above.
305-309	• small clayey mud with thinly laminated peat layers.
309-337	• very peaty, crumbly with wood fragments.
337-367	• wet muddy fine sand, well sorted, no large clasts, no organic matter.
300-309	• second attempt: peaty section from previous core (200-300 cm).
309-312	• dense, woody remains (removed for radiocarbon dating).
312-326	• dark peaty section repeats
326-376	• same muddy fine sand as first attempt
400-412	• charcoal zone (2-3 cm removed for radiocarbon dating); black organic rich mud with black plant fragments of more charcoal.
412-458	• gradational contact ; well sorted muddy sand grades into poorly sorted pebble sand (thalweg?)
458-462	• major wood stalk (removed for radiocarbon dating).
462-491	• gradational contact ; grades into fine grained, well sorted sand; possible point bar?; possible channel migration shown by sand facies
end	

Core HAN 2 - elevation: 2.7 m

<u>Depth (cm)</u>	<u>Description</u>
0-25	• fibrous black, clay rich
25-75	• crumbly, silty, oxidized, red laterite soil.
100-150	• silty, crumbly, possible fill material, occasional charcoal.
150-200	• gradational mottled contact ; more clay rich, grading to dark gray.
200-210	• gray clay, stiff and compact with disseminated organics.
210-215	• full leaf fragments; occasional black layers (wood fragments?).
215-240	• continued disseminated organics.
240-285	• gradational contact ; muddy well-sorted medium/fine sand; sparse organics.
285-300	• abrupt contact ; dark gray clay; black organic chips; grades to darker gray at base.
306-309	• black organic rich reduced sediment.
309-310	• abrupt contact ; continued dark gray-black clay with occasional black banding.
310-316	• abrupt contact ; organics.
316-319.5	• abrupt contact ; black organic layer.
319.5-323	• abrupt contact ; clay rich, brown-gray.
323-325	• abrupt contact ; black layer.
325-327.5	• interlaminated contact with peat chip.
327.5-365	• black layer, (reduced?)
365-420	• well-sorted fine sand (carbonate?)
420-457	• abrupt contact ; coarse sand to gravel with small basalt pebbles.
457-462	• peat plug? charcoal? wood?
end	

Core HAN 3 - elevation: 2.7 m

<u>Depth (cm)</u>	<u>Description</u>
0-185	• fill, oxidized and red
185-206	• abrupt contact ; gray mud.
206-268	• contact ; more apparent fill
268-290	• contact ; clay-rich mud; organics, plant fragments.
290-304	• concentrated dense organics.
304-309	• gray-brown mud.
309-310	• thin organic layer, leaves and rootlets
310-312	• gray-brown mud, organic poor.
312.5-313	• abrupt contact ; black organic rich layer; compressed and laminated at base.
313-316.5	• flaser bedding of organics with gray-brown mud.
316.5-322	• end flaser bedding, start gray-brown silty featureless mud.
322-324	• abrupt contact ; black layer.
324-328.5	• abrupt contact ; featureless gray-brown mud with rare rootless.
328.5-330	• black layer.
330-335	• gray-brown mud.
335-365	• black layer.
365-372	• gray-brown mud (7 major black layers, 10 minor black layers).
372-375	• thick black layer with wood fragments (wood fragment taken for radiocarbon dating).
375	• black-gray mud
375-380	• wood fragments (include with previous wood for radiocarbon dating).
380-400	• interlaminated gray-brown mud with black organic layers.
400-427.5	• thick organic layer with stalks, wood fragments, reduced?, heavily compressed, layered fragments.
427.5	• finely laminated with clay and silt.
427.5-436	• single wood stalk (removed for radiocarbon dating).
436-470	• black, clay-rich mud with occasional wood fragments; compressed leaves and organics.
470-500	• gradual transition to more clay-rich; less organics, less peaty, dark gray/black.
500-520	• black, silty mud with occasional organics.
520-525	• fibrous wood fragment (small).
525-529	• sandy mud; well-sorted, abandoned meander ? oxbow? upper estuary? tidal?
530-535	• back into dark gray/black mud.
353	• wood fragment.
535-578	• organic-rich dark gray mud; occasional plant fragment, leaves; one lone basalt pebble.
578-600	• silty organic-rich soil (removed for radiocarbon dating).
end	

Core HAN 4 - elevation: 2.4 m

<u>Depth (cm)</u>	<u>Description</u>
0-368	• fill
368-405	• abrupt contact ; dark gray sand with mud matrix; sand is fine, mud increases down section.
405-435	• gradational contact ; gray-brown mud with black organic bands; clay-rich; occasional plant fragments.
435-465	• gradational contact ; fine-grained, dark gray sand.
465-475	• fine-grained sand, indicate a point bar deposit?
475-?	• gradational contact ; reddish, oxidized sand.
?-565	• gradational contact ; coarse sand, more poorly-sorted, reddish, no organics, mud matrix is red, thalweg? channel migration record?
end	

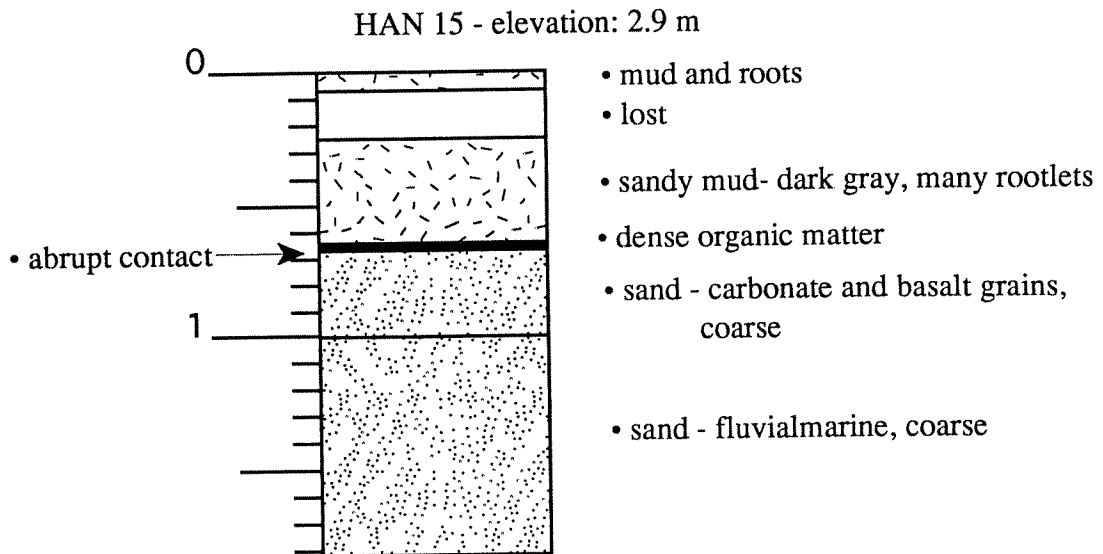
Core HAN 5 - elevation: 1.8 m: all fill, no *in situ* sediment found.

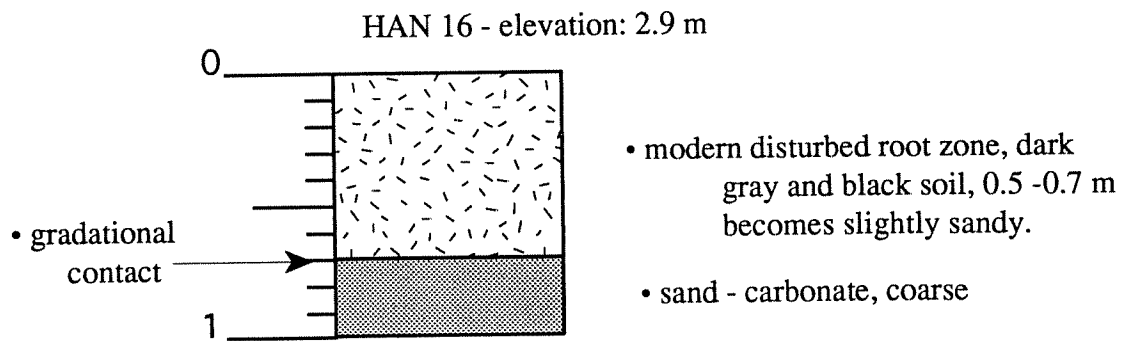
Core HAN 6 - elevation: 1.7 m

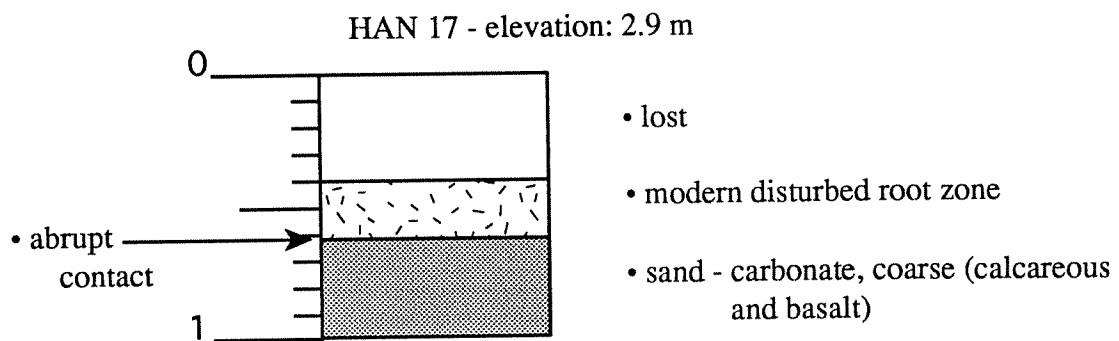
<u>Depth (cm)</u>	<u>Description</u>
0-65	• reddish silty fill with multiple plant fragments.
65-100	• gradational contact ; grayer, more reduced, more clayey.
100-200	• plant rich, more reduced, dark gray mud; occasional layer of concentrated wood fragments and plant detritus (possible oxbow?).
200-250	• dark gray mud (same as above).
250-300	• sandy mud grades to muddy sand.
end	base of column may be active channel grading up to oxbow.

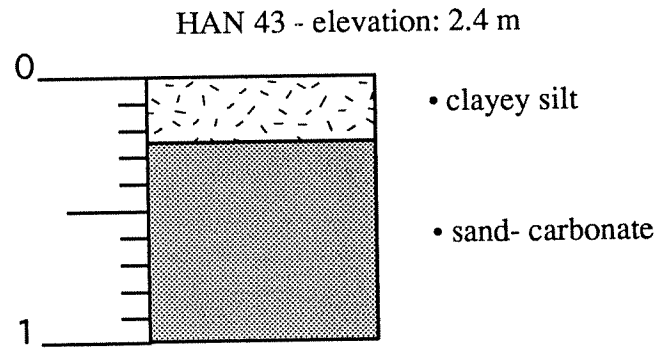
Core HAN 7 - elevation: 4.3 m

<u>Depth (cm)</u>	<u>Description</u>
0-100	• no recovery, all augered.
100-200	• red sandy soil with low organics; no plant fragments; interpreted as modern disturbed zone.
200-300	• red sandy soil continues; reduced roots probably from modern zone.
300-326	• continued organic-rich oxidized sandy soil.
326-337	• gradational contact ; darker, clay-rich, sandy mud; gray, well-sorted, fine sand.
337-368	• gradational contact ; extremely organic-rich gray mud with abundant plant fragments (stems, stalks, rhizomes, leaves, wood chips), plant fragments are not black (334-355 cm plant detritus removed for radiocarbon dating).
368-381	• plant fragments less abundant.
389-400	• wood fragments (removed for radiocarbon dating).
400-406	• wood fragments continue (also removed for radiocarbon dating).
406-428	• black silt-rich mud with plant fragments.
428-465	• black clay-rich mud; plant fragments are rare.
465-500	• higher sand content, black sandy mud; plant fragments are rare to absent.
500-600	• black muddy sand; no plant fragments; not clearly thalweg, could be floodplain, coarse sand could indicate levee or slide off slope.
600-649	• black muddy sand.
649-656	• wood fragment (removed).
656-700	• gradational contact ; orange-red sandy silty soil; crumbly; enigmatic origin, strongly resembles modern soil.
end	

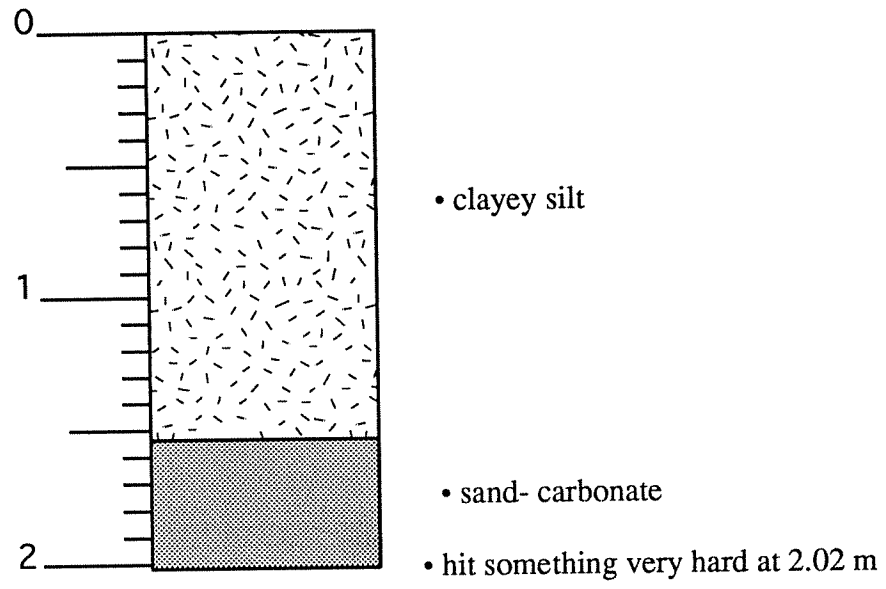


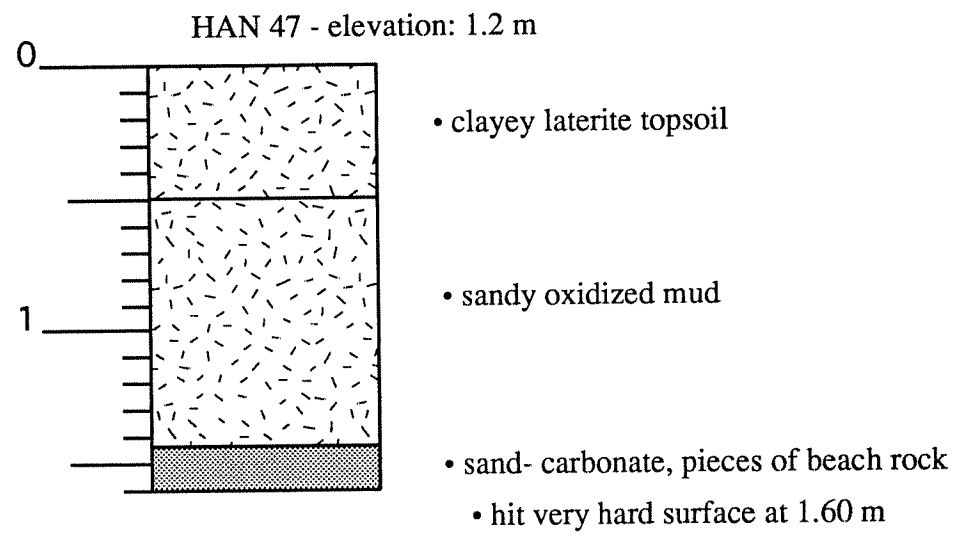


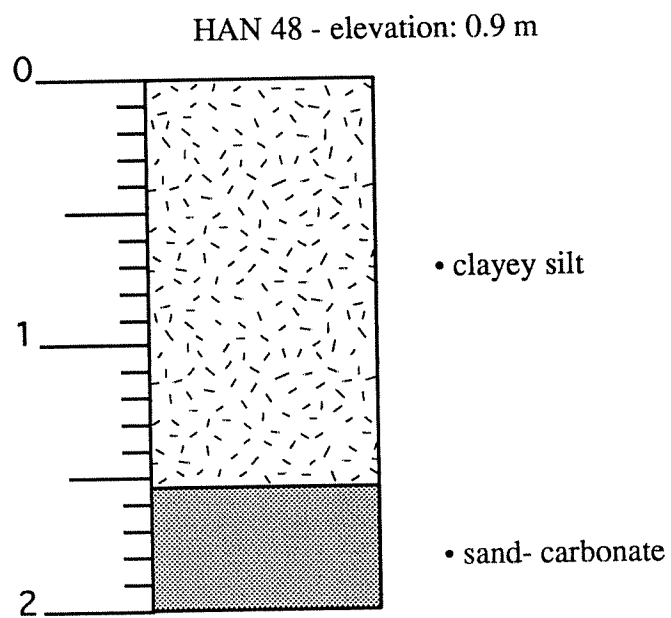


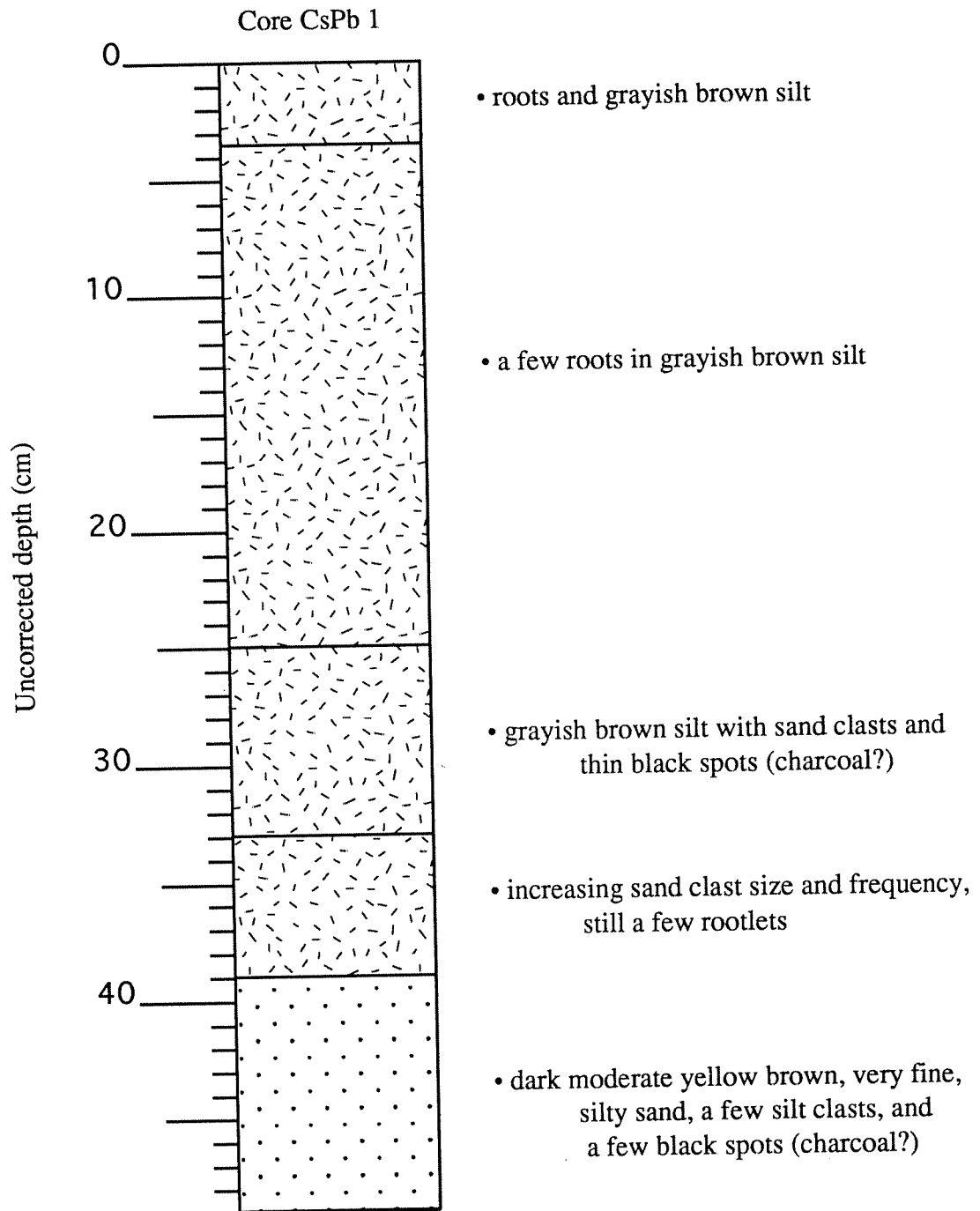


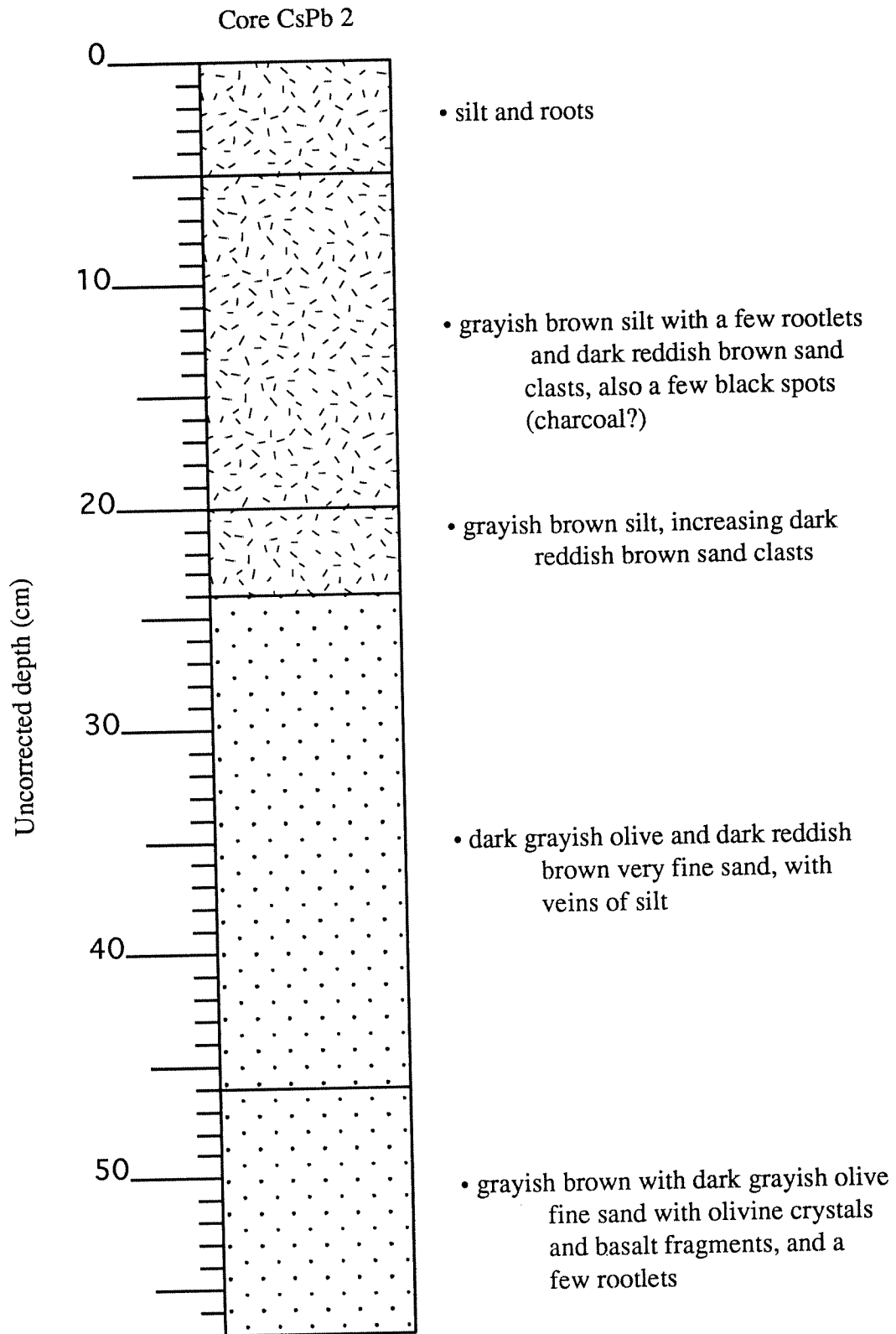
HAN 46 - elevation: 1.8 m

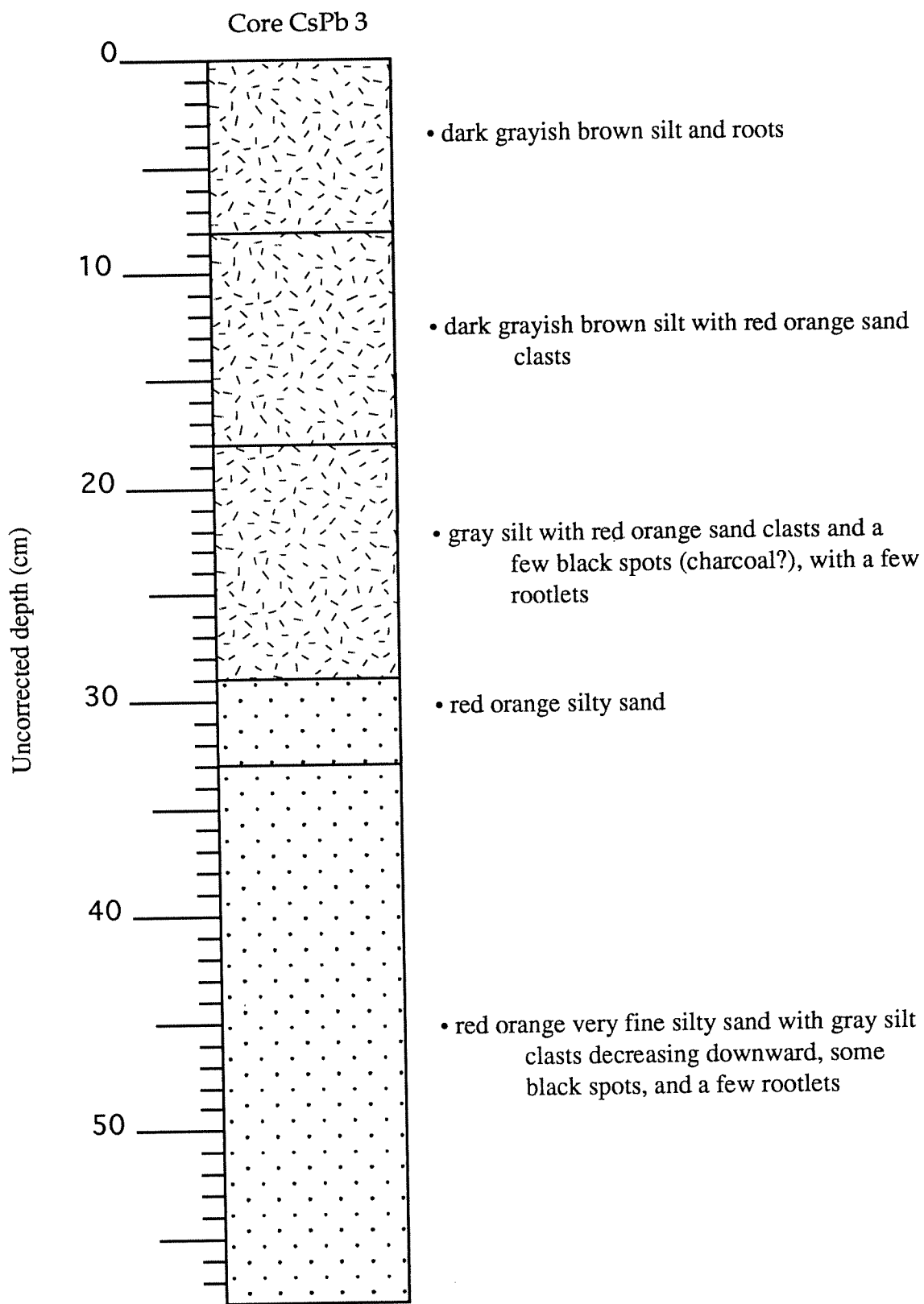












References

- Anderson, J.B. and M.A. Thomas. 1991. Marine ice-sheet decoupling as a mechanism for rapid, episodic sea-level change: the record of such events and their influence on sedimentation. *Sedimentary Geology*. 70: 87-104.
- Aston, S.R. and E.K. Duursma. 1973. Concentration effects on ^{137}Cs , ^{65}Zn , ^{60}Co , and ^{106}Ru sorption by marine sediments, with geochemical implication. *Netherlands Journal of Sea Research*. 6: 225-240.
- Athens, J.S. and J.V. Ward. 1991. *Paleoenvironmental and Archaeological Investigations, Kawaiinui Marsh Flood Control Project, Oahu*. U.S. Army Engineering Division, Pacific Ocean Environmental Section, Ft. Shafter, Hawaii. International Archaeological Research Institute, Inc. Honolulu, Hawaii.
- Baltzer, F. 1970. Datation absolue de la transgression holocène sur la côte ouest de Nouvelle-Calédonie sur des échantillons de toubes à palétuviers, interprétation néotectonique. *C.R. Acad. Sci. Paris, D*, 271:2251-2254.
- Bard, E., B. Hamelin, and R.G. Fairbanks. 1990a. U-Th ages obtained by mass spectrometry in corals from Barbados: Sea level during the past 130,000 years. *Nature*. 346:456-458.
- Bard, E., B. Hamelin, R.G. Fairbanks, and A. Zindler. 1990b. Calibration of the ^{14}C timescale over the past 30,000 years using mass spectrometric U-Th ages from Barbados corals. *Nature*. 345: 405-410.
- Beaman, R., P. Larcombe, and R.M. Carter. 1994. New evidence for the Holocene sea-level high from the inner Central Great Barrier Reef, Australia. *Journal of Sedimentary Research*. A64: 4, 881-885.
- Beasley, T.M. 1969. Lead-210 production by nuclear devices: 1946-1958. *Nature*. 224, 573.
- Bender, M., T. Sowers, M.L. Dickson, J. Orcharo, P. Grootes, P.A. Mayewski, and D.A. Meese. 1994. Climate correlations between Greenland and Antarctica. *Nature*. 372: 663-666.
- Berryman, K. 1979. Seismotectonic zoning study of the Fiji Islands. *New Zealand Geological Survey Earth Deformation Section Report*. 70: 1-48.
- Blanchon, P. and J. Shaw. 1995. Reef drowning during the last deglaciation: Evidence for catastrophic sea-level rise and ice-sheet collapse. *Geology*. 23: 4-8.
- Bloom, A.L. 1967. Pleistocene shorelines: A new test of isostasy. *Geological Society of America Bulletin*. 78:1477-1493.

- 1977. Atlas of Sea-Level Curves. New York: Cornell University.
- Bloom, A.L. and M. Stuiver. 1963. Submergence of the Connecticut coast. *Science*. 139:332-334.
- Bowman, G. and Harvey, N. 1986. Geomorphic evolution of a Holocene beach-ridge complex, South Australia. *Journal of Coastal Research*. 2 (3): 345-362.
- Bradley, R.S. 1985. Quaternary Paleoclimatology: Methods of Paleoclimatic Reconstruction. Boston; Unwin Hyman.
- Brisbin, I.L., Jr., R.J. Beyers, R.W. Dapson, R.A. Geiger, J.B. Gentry, J.W. Gibbons, M.H. Smith, and S.K. Woods. 1974. Patterns of radiocesium in the sediments of a stream channel contaminated by production reactor effluents. *Health Physics*. 27: 19-27.
- Bryan, W.B. and R.S. Stevens. 1993. Coastal bench formation at Hanauma Bay, Oahu, Hawaii. *Geological Society of America Bulletin*. 105:377-386.
- Buddmeier, R.W., S.V. Smith, and R.A. Kinzie. 1975. Holocene windward reef-flat history, Enewetok Atoll. *Geological Society of America Bulletin*. 86:1581-1584.
- Cabioch, G., B.A. Thomassin, and J.F. Lecolle. 1989. Age d'émersion des récifs frangeants holocènes autour de la Grande Terre de Nouvelle-Calédonie (SO Pacifique); nouvelle interprétation de la courbe des niveaux marins depuis 8000 ans. *C.R. Acad. Sci. Paris, II*. 308:419-425.
- Cambray, R.S., K. Playford, and N.J. Lewis. 1985. Radioactive fallout in air and rain: Results to the end of 1984. U.K. Atomic Energy Authority Rep. AERE-R-11915. U.K. AERE, Harwell, U.K.
- Campbell, B.L. 1982. Applications of environmental caesium-137 for the determination of sedimentation rates in reservoirs and lakes and related catchment studies in developing countries. AAEC Research Establishment, Lucas Heights Research Laboratories, PMB Sutherland, 3322, N.S.W., Australia.
- Carter, M.W., and A.A. Moghissi. 1977. Three decades of nuclear testing. *Health Physics*. 33: 55-71.
- Carter, R.W.G. 1988. Coastal Environments: An Introduction to the Physical, Ecological and Cultural Systems of Coastlines. Academic Press, Inc. San Diego.
- Chappell, J. 1974. Late-Quaternary glacio- and hydro-isostasy, on a layered earth. *Quaternary Research*. 4:429-440.

- Chappell, J. and H.A. Polach. 1991. Post-glacial sea-level rise from a coral record at Huon Peninsula, Papua New Guinea. *Nature*. 349:147-149.
- Chrastowski, M.J. and T.A. Thompson. 1992. Late Wisconsinan and Holocene coastal evolution of the southern shore of Lake Michigan. In Quaternary Coasts of the United States: Marine and Lacustrine Systems C.H. Fletcher and J.F. Wehmiller (Eds.), pp. 397-413. SEPM Special Publication No. 48.
- Clark, J.A., W.E. Farrell, and W.R. Peltier. 1978. Global changes in post-glacial sea level: A numerical calculation. *Quaternary Research*. 9:265-287.
- COHMAP, 1988. Climatic changes of the last 18,000 years: Observations and model simulations. *Science*. 241: 1043-1052.
- Coudray, J. and G. Delibrias. 1972. Variations du niveau marin au-dessus de l'actuel en Nouvelle-Calédonie depuis 6000 ans. *C.R. Acad. Sci. Paris, D*, 375:2623-2626.
- Crozaz, G., E. Picciotto, and W. De Breuck. 1964. Antarctic snow chronology with ^{210}Pb . *Journal of Geophysical Research*. 69: 2597-2604.
- Dahlman, R.C., C.W. Francis, and T. Tamura. 1975. Radiocesium cycling in vegetation and soil. p. 462-481. In Mineral Cycling in Southeastern Ecosystems. F.G. Howell, J.B. Gentry, and M.H. Smith (Eds.). ERDA Symp. Ser. CONF-740513. US ERDA, Washington, DC.
- Daly, R.A. 1920. A general sinking of the sea in recent times. *Proceedings of the National Academy of Science*. 6 (5):246-250.
- 1934. The Changing World of the Ice Age. New Haven, Connecticut: Yale University Press.
- Davies, P.J. and D. Hopley. 1983. Growth facies and growth rates of Holocene reefs in the Great Barrier Reef. *Bureau of Mineral Resources Journal of Australian Geology and Geophysics*. 8 (3):237-251.
- Davis, J.J. 1963. Cesium and its relationship to potassium in ecology. p. 539-556. In Radioecology. V. Schultz and A.W. Klement, Jr. (Eds.). Reinhold, New York.
- Davis, R.B., C.T. Hess, C.T. Hess, S.A. Norton, D.W. Hanson, K.D. Hoagland, and D.S. Anderson. 1984. ^{137}Cs and ^{210}Pb dating of sediments from soft-water lakes in New England (U.S.A.) and Scandinavia, a failure of ^{137}Cs dating. *Chemical Geology*. 44: 151-181.
- Dawson, A.G. 1994. Geomorphological effects of tsunami run-up and backwash. *Geomorphology*. 10: 1-12.

- Devoy, R.J.N. (Ed.) 1987. Sea Surface Studies. New York: Croom Helm.
- Dickinson, W.R., D.V. Burley, and R. Shutler Jr. 1994. Impact of hydro-isostatic Holocene sea-level change on the geologic context of island archaeological sites, Northern Ha'apai Group, Kingdom of Tonga. *Geoarchaeology*. 9(2):85-111.
- Dominguez, J.M.L., Martin, L., and Bittencourt, A.C.S.P. 1987. Sea-level history and Quaternary evolution of river mouth-associated beach-ridge plains along the east-southeast Brazillian coast: A summary. *In Sea-level Fluctuation and Coastal Evolution*. D. Nummedal, O.H. Pilkey, and J.D. Howard (Eds.). pp.115-127. SEPM Special Publication No. 41.
- Donoghue, J.F. and W.F. Tanner. 1992. Quaternary terraces and shorelines of the panhandle Florida region. *In Quaternary Coasts of the United States: Marine and Lacustrine Systems* (C.H. Fletcher and J.F. Wehmler, Eds.), pp. 233-241. SEPM Special Publication No. 48.
- Dye, T. 1994. Apparent ages of marine shells: Implications for archaeological dating in Hawaii. *Radiocarbon*. 36: 51-57.
- Easton, W.H. and E.A. Olson. 1976. Radiocarbon profile of Hanauma Reef, Oahu, Hawaii. *Geological Society of America Bulletin*. 87:711-719.
- Ebisemiju, F.S. 1990. Sediment delivery ratio prediction equations for short catchment slopes in a humid tropical environment. *Journal of Hydrology*. 114: 191-208.
- Edwards, R.L., J.W. Beck, G.S. Burr, D.J. Donahue, J.M.A. Chappell, A.L. Bloom, E.R.M. Druffel, and F.W. Taylor. 1993. A large drop in atmospheric $^{14}\text{C}/^{12}\text{C}$ and reduced melting in the Younger Dryas, documented with ^{230}Th ages of corals. *Science*. 260: 962-968.
- Ehlers, J., K. Nagorny, P. Schmidt, B. Stieve, and K. Zietlow. 1993. Storm surge deposits in North Sea marshes dated by ^{134}Cs and ^{137}Cs determination. *Journal of Coastal Research*. 9 (3): 698-701.
- Ellison, J.C. 1994. Paleo-lake and swamp stratigraphic records of Holocene vegetation and sea-level changes, Mangaia, Cook Islands. *Pacific Science*. 48(1): 1-15.
- Evans, D.W., J.J. Alberts, and R.A. Clark III. 1983. Reversible ion exchange fixation of cesium-137 leading to mobilization from reservoir sediments. *Geochimica et Cosmochimica Acta*. 47: 1041-1049.
- Eyman, L.D. and N.R. Kevern. 1975. Cesium-137 and stable cesium in a hypereutrophic lake. *Health Physics*. 28: 549-555.

- Fairbanks, R.G. 1989. A 17,000-year glacio-eustatic sea level record: influence of glacial melting rates on the Younger Dryas event and deep-ocean circulation. *Nature*. 342:637-642.
- Fairbridge, R.W. 1961. Eustatic changes in sea level. *Physics and Chemistry of the Earth*. 5:99-185.
- Farrell, W.E. and J.A. Clark. 1976. On postglacial sea level. *Geophysical Journal*. 46:647-667.
- Feng, X. and S. Epstein. 1994. Climatic implications of an 8000-year hydrogen isotope time series from bristlecone pine trees. *Science*. 265: 1079-1081.
- Fisk, H.N. 1951. Loess and Quaternary geology of the Lower Mississippi Valley. *Journal of Geology*. 59:333-356.
- Fletcher, C.H. and A.T. Jones. (in press). Sea-level highstand recorded in Holocene shoreline deposits on Oahu, Hawaii. *Journal of Sedimentary Research*.
- Fletcher, C.H., B.M. Richmond, G.M. Barnes, and T.A. Schroeder. 1995. Marine flooding on the coast of Kauai during Hurricane Iniki: Hindcasting inundation components and delineating washover. *Journal of Coastal Research*. 11: 188-204.
- Friedlander, G., J.W. Kennedy, and J.M. Miller. 1964. Nuclear and Radiochemistry. New York, John Wiley and Sons, Inc. pp. 10-14.
- Furumoto, A.S., E. Herrero-Bervera, and W.M. Adams. 1990. Earthquake risk and hazard potential of the Hawaiian Islands. Technical report to the State Department of Civil Defense. Hawaii Institute of Geophysics, University of Hawaii, p.37.
- Godwin, H., R.P. Suggate, and E.H. Willis. 1958. Radiocarbon dating of the eustatic rise in ocean-level. *Nature*. 181:1518-1519.
- Hallock, P. 1981. Production of carbonate sediments by selected large benthic foraminifera on two Pacific coral reefs. *Journal of Sedimentary Petrology*. 51 (2): 467-474.
- Houghton, J.T., G.J. Jenkins, and J.J. Ephraums, (Eds.) 1990. *Climate Change: The IPCC Scientific Assessment*. Cambridge: Cambridge University Press.
- Jelgersma, S. 1966. Sea-level changes during the last 10,000 years. *Royal Meteorological Society Proceedings of Symposium on World Climate 8000-0 B.C.*, Imperial College, London. Royal Metallurgical Society, London, pp. 54-71.
- Jones, A.T. 1992. Holocene coral reef on Kauai, Hawaii: Evidence for a sea-level highstand in the central Pacific. In Quaternary Coasts of the United States: Marine

- and Lacustrine Systems C.H. Fletcher and J.F. Wehmiller (Eds.). pp. 267-271. SEPM Special Publication No. 48.
- Kayanne, H., T. Ishii, E. Matsumoto, and N. Yonekura. 1993. Late Holocene sea-level change on Rota and Guam, Mariana Islands, and its constraint on geophysical predictions. *Quaternary Research*. 40:189-200.
- Kidson, C. 1982. Sea-level changes in the Holocene. *Quaternary Science Reviews*. 1: 121-151.
- Kidson, C. and A. Heyworth. 1973. The Flandrian sea-level rise in the Bristol Channel. *Proceedings of the Ussher Society*. 2: 565-584.
- Koide, M., A. Soutar, and E.D. Goldberg. 1972. Marine geochronology with ^{210}Pb . *Earth and Planetary Science Letters*. 14: 442-446.
- Krishnaswami, S., D. Lal, J.M. Martin, and M. Meybeck. 1971. Geochronology of lake sediments. *Earth Planetary Science Letters*. 11: 407-414.
- LaMarche, V.C. Jr. 1973. Holocene climatic variations inferred from treeline fluctuations in the White Mountains, California. *Quaternary Research*. 3: 632-660.
- Lambeck, K. 1990. Glacial rebound, sea-level change and mantle viscosity. *Quarterly Journal of the Royal Astronomical Society*. 31: 1-30.
- Lomenick, T.F., and T. Tamura. 1965. Naturally occurring fixation of cesium-137 on sediments of lacustrine origin. *Soil Science Society of America Proceedings*. 29: 383-386.
- Longmore, M.E. 1982. The caesium-137 dating technique and associated applications in Australia- a review. *In Archaeometry: An Australian Perspective*. W. Ambrose and P. Duerden (Eds.). p. 310-321. Australian National Univ. Press, Canberra, Australia.
- Lowe, J.J. and M.J.C. Walker. 1984. Reconstructing Quaternary Environments. New York; Longman Scientific & Technical.
- Luckman, B.H. 1988. 8,000 year old wood from the Athabasca Glacier, Alberta. *Canadian Journal of Earth Science*. 25: 148-151.
- Matsumoto, E. 1990. Carbon dating results for samples from HIPAC Project in 1988-1989. *In Sea-level Changes and Tectonics in the Middle Pacific. Report of HIPAC Project in 1988 and 1989*. N. Yonekura (Ed.). pp. 7-8. Univ. of Tokyo, Japan.
- Matsumoto, E., Matsushima, Y., Miyata, T., and Maeda, Y. 1988. Holocene high sea-level stand on Kauai, Hawaii. *In Sea-level Changes and Tectonics in the Middle*

- Pacific. Report of HIPAC Project in 1986 and 1987. N. Yonekura (Ed.). pp. 91-99. Univ. of Tokyo, Japan.
- McCredie, S. 1994. When nightmare waves appear out of nowhere to smash the land. *Smithsonian*. 24 (12): 28-39.
- McFarlan, E. 1961. Radiocarbon dating of Late Quaternary deposits, South Louisiana. *Geological Society of America Bulletin*. 72:129-158.
- McMormick, C.L. 1973. Probable causes of shoreline recession and advance on the south shore of eastern Long Island. In Coastal Geomorphology. D.R. Coates (Ed.). Proceedings of Third Annual Geomorphology Symposia Series. SUNY, Binghamton.
- Menard, H.W. 1964. Marine Geology of the Pacific. New York: McGraw Hill, pps. 271.
- Milan, C.S., E.M. Swenson, R.E. Turner, and J.M. Lee. 1995. Assessment of the ^{137}Cs method for estimating sediment accumulation rates: Louisiana salt marshes. *Journal of Coastal Research*. 11 (2): 296-307.
- Mitrovica, J.X. and W.R. Peltier. 1991. On postglacial geoid subsidence over the equatorial oceans. *Journal of Geophysical Research*. 96(B12):20,053-20,071.
- Miyata, T., Y. Maeda, E. Matsumoto, Y. Matsushima, P. Rodda, and A. Sugimura. 1988. Emerged notches and microatolls on Vanua Levu, Fiji. Sea-level Changes and Tectonics in the Middle Pacific. Report of HIPAC Project in 1986 and 1987. N. Yonekura (Ed.) Univ. of Tokyo, Japan. 67-76.
- Moberly, R., Jr. 1968. Loss of Hawaiian littoral sand. *Journal of Sedimentary Petrology*. 38: 17-34.
- Moberly, R., Jr. and T. Chamberlain. 1964. Hawaiian beach systems: Final report, Appendices A and B. Prepared for Harbors Division, Department of Transportation, State of Hawaii.
- Moberly, R., Jr., Baver, L.D., Jr., and Morrison, A. 1965. Source and variation of Hawaiian littoral sand. *Journal of Sedimentary Petrology*. 35: 589-598.
- Moore, J.G. and G.W. Moore. 1984. Deposit from a giant wave on the island of Lanai, Hawaii. *Science*. 226: 1312-1315.
- Moore, J.G., W.B. Bryan, and K.R. Ludwig. 1994. Chaotic deposition by a giant wave, Molokai, Hawaii. *Geological Society of America Bulletin*. 106: 962-967.
- Mörner, N.A. 1976. Eustasy and geoid changes. *Journal of Geology*. 84:123-151.
- 1980. The Northwest European 'sea-level laboratory' and regional Holocene eustasy. *Paleogeography, Paleoclimatology, Paleoecology*. 29:281-300.

- Nakada, M. 1986. Holocene sea levels in oceanic islands: Implications for the rheological structure of the earth's mantle. *Tectonophysics*. 121:263-276.
- Nakada, M. and K. Lambeck. 1989. Late Pleistocene and Holocene sea-level change in the Australian region and mantle rheology. *Geophysical Journal*. 96:497-517.
- Nerem, R.S. 1995. Global mean sea level variations from TOPEX/POSEIDON altimeter data. *Science*. 268: 708-710.
- Neumann, A.C. and I. Macintyre. 1985. Reef response to sea-level rise: Keep-up, catch-up or give-up. *Proceedings of the Fifth International Coral Reef Congress, Tahiti*. 3:105-110.
- Nunn, P. D. 1990. Coastal processes and landforms of Fiji: Their bearing on Holocene sea-level changes in the south and west Pacific. *Journal of Coastal Research*. 6(2):279-310.
- Olsson, I.U. 1968. Modern aspects of radiocarbon dating. *Earth Science Review*. 4: 203-218.
- Otvos, E.G. 1992. Quaternary evolution of the Apalachicola coast, northeastern Gulf of Mexico. *In Quaternary Coasts of the United States: Marine and Lacustrine Systems*. C.H. Fletcher and J.F. Wehmiller (Eds.). pp. 221-232. SEPM Special Publication No. 48.
- Paterson, W.S.B., R.M. Koerner, D. Fisher, S.J. Johnsen, H.B. Clausen, W. Dansgaard, P. Bucher, and H. Oeschger. 1977. An oxygen-isotope climatic record from the Devon Island ice cap, arctic Canada. *Nature*. 266: 508-511.
- Peltier, W.R. and A.M. Tushingham. 1989. Global sea level rise and the greenhouse effect: Might they be connected? *Science*. 244: 806-810.
- Peltier, W.R., W.E. Farrell, and J.A. Clark. 1978. Glacial isostasy and relative sea level: A global finite element model. *Tectonophysics*. 50:81-110.
- Pennington, W., R.S. Cambray, and E.M. Fisher. 1973. Observations on lake sediments using fallout ^{137}Cs as a tracer. *Nature*. 242: 324-326.
- Pennington, W., R.S. Cambray, J.D. Eakins, and D.D. Harkness. 1976. Radionuclide dating of the recent sediments of Blelham Tarn. *Freshwater Biology*. 6: 317-331.
- Perkins, R.W. and C.W. Thomas. 1980. Worldwide fallout. p. 53-82. *In Transuranic Elements in the Environment*. W.C. Hanson (Ed.) USDO/TIC-22800. US DOE, Washington, DC.

- Pirazzoli, P.A. 1991. World Atlas of Holocene Sea-Level Changes. New York: Elsevier. pp 300.
- Pirazzoli, P.A. and L.F. Montaggioni. 1988. Holocene sea-Level changes in French Polynesia. *Paleogeography, Paleoclimatology, Paleoecology*. 68:153-175.
- Ritchie, J.C. and J.R. McHenry. 1990. Application of radioactive fallout cesium-137 for measuring soil erosion and sediment accumulation rates and patterns: A review. *Journal of Environmental Quality*. 19: 215-233.
- Ritchie, J.C., J.R. McHenry, and A.C. Gill. 1973. Dating recent reservoir sediments. *Limnology and Oceanography*. 18: 245-263.
- Robbins, J.A. and D.N. Edgington. 1975. Determination of recent sedimentation rates in Lake Michigan using Pb-210 and Cs-137. *Geochimica et Cosmochimica Acta*. 39: 285-304.
- Rodda, P. 1988. Visit to western Samoa with the HIPAC Team. Sea-level Changes and Tectonics in the Middle Pacific. Report of the HIPAC Project in 1986 and 1987. N. Yonekura (Ed.). Univ. of Tokyo, Japan. 85-90.
- Scholl, D.W. and M. Stuiver. 1967. Recent submergence of Southern Florida: A comparison with adjacent coasts of other eustatic data. *Geological Society of America Bulletin*. 78:437-454.
- Schulz, R.K. 1965. Soil chemistry of radionuclides. *Health Physics*. 11: 1317-1324.
- Schulz, R.K., R. Overstreet, and I. Barshad. 1960. On the soil chemistry of cesium 137. *Soil Science*. 89: 19-27.
- Scoffin, T.P., D.R. Stoddart, A.W. Tudhope, and C.D. Woodroffe. 1985. Exposed limestones of Suvarrow Atoll. *Proceedings of the Fifth International Coral Reef Congress, Tahiti*. 3:137-140.
- Shackleton, N.J. 1987. Oxygen isotopes, ice volumes, and sea level. *Quaternary Science Reviews*. 6: 183-190.
- Shepard, F.P. 1963. Thirty-five thousand years of sea level. pp 1-10 In Essays in Marine Geology in Honor of K.O. Emery. T. Clements (Ed.) Los Angeles: University of Southern California Press.
- 1964. Sea-level changes in the past 6000 years: possible archaeological significance. *Science*. 143: 574-576.
- Soil Conservation Service. 1972. "Soil Survey of Islands of Kauai, Oahu, Maui, Molokai, and Lanai, State of Hawaii." U.S. Department of Agriculture and the University of Hawaii Agricultural Experiment Station.

- Stapor, F.W., Jr., T.D. Mathews, and F.E. Lindfors-Kearns. 1991. Barrier-island progradation and Holocene sea-level history in southwest Florida. *Journal of Coastal Research*. 7 (3): 815-838.
- Stearns, H.T. 1935. Shore benches on the island of Oahu. *Geological Society of America Bulletin*. 46: 1467-1482.
- Stearns, H.T. 1977. Radiocarbon profile of Hanauma Reef, Oahu, Hawaii: A Discussion. *Geological Society of America Bulletin*. 88: 1535.
- Stearns, H.T. 1978. Quaternary shorelines in the Hawaiian Islands. *Bernice P. Bishop Museum Bulletin*. 237: 1-57.
- Stuiver, M. 1993. Editorial Comment. *Radiocarbon*. 35 (1): iii.
- Stuiver, M. and B. Becker. 1993. High-precision decadal calibration of the radiocarbon time scale, AD 1950-6000 BC. *Radiocarbon*. 35 (1): 35-65.
- Stuiver, M. and P.J. Reimer. 1987. User's Guide to the Programs CALIB and DISPLAY2.1. Quaternary Isotope Laboratory, University of Washington.
- Stuiver, M., P.D. Quay, and H.G. Ostlund. 1983. Abyssal water carbon-14 distribution and the age of the world oceans. *Science*. 219: 849-851.
- Sugimura, A., Y. Maeda, Y. Matsuhima, and P. Rodda. 1988. Further report on sea-level investigation in Western Samoa. Sea-level Changes and Tectonics in the Middle Pacific. Report of the HIPAC Project in 1986 and 1987. N. Yonekura (Ed.). Univ. of Tokyo, Japan. 77-84.
- Talma, A.S. and J.C. Vogel. 1993. A simplified approach to calibrating ^{14}C Dates. *Radiocarbon*. 35: 317-322.
- Tamura, T. 1964a. Reaction of cesium-137 and strontium-90 with soil minerals and sesquioxides. p. 465-478. *In* 8th International Congress of Soil Science, Buchrest, Romania. 31 August-9 September. International Society of Soil Science, Wageningen, Netherlands.
- Tamura, T. 1964b. Selective sorption reaction of caesium with mineral soils. *Nuclear Safety* 5: 262-268.
- Tamura, T. and D.G. Jacobs. 1960. Structural implications in cesium sorption. *Health Physics*. 2: 391-398.
- Thom, B.G., J.R. Hails, and A.R.H. Martin. 1969. Radiocarbon evidence against higher post-glacial sea levels in eastern Australia. *Marine Geology*. 7: 161-168.

- Torgenson, T. and M.E. Longmore. 1984. ^{137}Cs diffusion in highly organic sediment of Hidden Lake, Fraser Island, Queensland, Australia. *Journal of Marine and Freshwater Research*. 35: 537-548.
- Tucker, M.E. and V.P. Wright. 1990. Carbonate Sedimentology. Blackwell Scientific Publications, London.
- Tudhope, A.W. and T.P. Scoffin. 1994. Growth and structure of fringing reefs in a muddy environment, South Thailand. *Journal of Sedimentary Research*. A64: 752-764.
- Tushingham, A.M. and W.R. Peltier. 1991. Ice-3G: A new global model of late Pleistocene deglaciation based upon geophysical predictions of post-glacial relative sea-level change. *Journal of Geophysical Research*. 96 (B3):4497-4523.
- Tushingham, A.M., and W.R. Peltier. (1992). Ice-3G: Validation of the ICE-3G model of Wurm-Wisconsin deglaciation using a global data base of relative sea-level histories. *Journal of Geophysical Research*. 97 (B3): 3285-3304.
- van de Plassche, O., (Ed.) 1986. Sea-level Research. Norwich: Geo Books.
- van de Plassche, O. 1991. Late Holocene sea-level fluctuations on the shore of Connecticut inferred from transgressive and regressive overlap boundaries in salt-marsh deposits. *Journal of Coastal Research*. Special Issue #11. 159-179.
- Walcott, R.I. 1972. Past sea levels, eustasy and deformation of the earth. *Quaternary Research*. 2:1-14.
- Watts, A.B. and U.S. ten Brink. 1989. Crustal structure, flexure, and subsidence history of the Hawaiian Islands. *Journal of Geophysical Research*. 94(B8):10,473-10,500.
- Wigley, T.M.L. and S.C.B. Raper. 1987. Thermal expansion of sea water associated with global warming. *Nature*. 330: 127-131.
- Williams, M.A.J., D.L. Dunkerley, P. DeDeckker, A.P. Kershaw, and T.J. Stokes. 1993. Quaternary Environments. London; Hodder & Stoughton.
- Wise, S.M. 1980. Caesium-137 and lead-210: A review of technique and some applications in geomorphology. p. 109-127. In Timescales in Geomorphology. R.A. Cullingford, D.A. Davidson, and J. Lewin (Eds.). John Wiley & Sons, New York.
- Woodroffe, C.D., R. McLean, H. Polach, and E. Wallensky. 1990. Sea level and coral atolls: Late Holocene emergence in the Indian Ocean. *Geology*. 18: 62-66.
- Yonekura, N. (Ed.) 1988. Sea-level changes and tectonics in the middle Pacific. *Report of the HIPAC Project in 1986 and 1987*. Univ. of Tokyo, Japan.

Zhang, J., W.W. Huang, and M.C. Shi. 1990. Huanghe (Yellow River) and its estuary: Sediment origin, transport, and deposition. *Journal of Hydrology*. 120: 203-223.